Aus der Klinik für Neurochirurgie
der Medizinischen Fakultät Charité – Universitätsmedizin Berlin

Dissertation

Die Rolle des ephrinB2-EphB4 Signalweges bei der Vermittlung vaskulärer Resistenzmechanismen unter antiangiogener Therapie

zur Erlangung des akademischen Grades
Doctor medicinae (Dr. med.)

vorgelegt der Medizinischen Fakultät der
Charité – Universitätsmedizin Berlin

von

Christian Uhl

aus München

Datum der Promotion:
06.09.2019

Vorwort

Teilergebnisse dieser Arbeit wurden am 10. Juli 2018 im Journal *Angiogenesis* unter dem Titel „EphB4 mediates resistance to antiangiogenic therapy in experimental glioma“ publiziert.

In der oben genannten Publikation wurden die Daten der orthotopen Tumorimplantationen sowie der Schädelfensteroperationen, namentlich der Figures 1B, C sowie 3 und 4C, D, G, H, K, L, aus Daten erstellt, welche im Rahmen dieser Monographie erneut veröffentlicht werden.

Table of Contents

I Abstract in English Language

Introduction

Glioblastoma multiforme is the most frequent malignant brain tumor. Despite all medical efforts, the 5 year-survival rate is still only 5%. Antiangiogenic therapies, which primarily target the vascular endothelial growth factor (VEGF), have demonstrated a positive impact on other tumor entities, yet they have not improved the overall survival of patients with glioblastoma multiforme so far. Increased activation of parallel angiogenic pathways, such as the receptor tyrosine kinase EphB4 and its ligand ephrinB2, probably take part in mediating antiangiogenic resistance.

Methods

To assess the role of EphB4 in mediating resistance towards antiangiogenic treatment in glioblastoma, we coimplanted EphB4-overexpressing reporter cells ($EphB4^{OE}$) or control reporter cells without effect (pLXSN) together with glioma cells orthotopically into nude mice. Subsequently, tumor growth was measured by means of small animal MRI on postoperative days 14, 21, 25 and 29. PLXSN and EphB4-overexpressing reporter cells were treated antiangiogenically with the VEGF-receptor 2 inhibitor Sunitinib or a placebo respectively for four days, starting on day 25 postoperatively. Thus, 4 groups emerged: control (pLXSN), treated control (pLXSN+Sun), EphB4-overexpression ($EphB4^{OE}$) and treated EphB4-overexpression ($EphB4^{OE}$+Sun). Immediately after the last MRI, the brains of the animals were harvested and immunohistochemically stained to determine vessel density, pericyte-endothelial interaction, tumor cell proliferation and apoptosis. In additional experiments, chronic cranial window operations were performed to subsequently conduct intravital microscopy. Thus vessel network characteristics such as total vessel density, functional vessel density, blood flow, vessel diameter and vessel permeability were examined to detect potential EphB4-mediated resistance mechanisms. Intravital microscopy was performed on days 12, 14 and 16 postoperatively. Again both control and EphB4-overexpressing tumors were either treated with Sunitinib or a placebo for four days, starting on postoperative day 12.

Results

EphB4^{OE}- tumors proved to grow significantly slower than the control group. Antiangiogenic treatment did not significantly inhibit tumor growth in EphB4^{OE}-tumors compared to the untreated EphB4^{OE}-tumors. On the contrary, tumor growth was significantly inhibited in treated pLXSN tumors compared to untreated pLXSN ones. While treated pLXSN tumors experienced significant reductions in vessel densities, the amount of proliferating cells and increased apopotic cell numbers, these parameters remained stable in the treated EphB4^{OE}-tumors. Intravital microscopy revealed sustained functioning vessel networks in treated EphB4^{OE}-tumors, while treated pLXSN tumors displayed reduced amounts of functioning vessels.

Conclusion

EphB4 takes part in mediating antiangiogenic resistance by maintenance of functioning vascular networks, however it also acts as a tumor suppressive by decelerating tumor growth.

II Abstrakt in deutscher Sprache

Einführung

Das Glioblastoma multiforme ist der häufigste bösartige Gehirntumor. Trotz medizinischer Fortschritte beträgt die 5-Jahres-Überlebensrate noch immer nur 5%. Antiangiogene Therapien, die hauptsächlich den vaskulären endothelialen Wachstumsfaktor (VEGF) inhibieren, haben positive Auswirkungen auf die Behandlung anderer Tumorentitäten gezeigt, allerdings verbesserten sie bislang nicht die Überlebenszeit bei Patienten mit Glioblastoma multiforme. Man nimmt eine verstärkte Aktivierung von parallelen angiogenen Signalwegen an, wie dem der Rezeptor Tyrosinkinase EphB4 und ihres Liganden ephrinB2, welche daraufhin antiangiogene Resistenzen vermitteln.

Methodik

Um die Rolle von EphB4 in der Resistenzvermittlung bei der antiangiogenen Therapie von Glioblastomen zu untersuchen, implantierten wir entweder EphB4-überexprimierende- ($EphB4^{OE}$) oder Kontroll-Reporterzellen (pLXSN), die keine Wirkung auf die Zielzellen haben, zusammen mit Gliomzellen orthotop in Nacktmäuse. Anschließend wurde das Tumorwachstum mittels Kleintier-MRT an den postoperativen Tagen 14, 21, 25 und 29 gemessen. Kontroll- und EphB4-überexprimierende Tumoren wurden ab dem 25. postoperativen Tag für vier Tage entweder antiangiogen mit VEGF-Rezeptor 2-Blocker Sunitinib oder einem Placebo behandelt. Dadurch entstanden vier Gruppen: Kontrolle (pLXSN), behandelte Kontrolle (pLXSN+Sun), EphB4-Überexpression ($EphB4^{OE}$) und behandelte EphB4-Überexpression ($EphB4^{OE}$+Sun). Direkt im Anschluss an das letzte MRT wurden die Gehirne entnommen und immunhistochemisch gefärbt, um Gefäßdichte, Perizyten-Endothelzellinteraktion, Tumorzellproliferation und -apoptose zu ermitteln. In weiteren Experimenten wurden Schädelfensteroperationen durchgeführt, um anschließend intravitalmikroskopische Aufnahmen zu machen. Mit dieser Messmethode wurden verschiedene Parameter des Gefäßnetzwerks wie die totale Gefäßdichte, die funktionelle Gefäßdichte, der Blutfluss, Gefäßdurchmesser und die Gefäßpermeabilität analysiert, die durch mögliche Resistenzmechanismen unter EphB4-Überexpression beeinflusst werden könnten. Die Intravitalmikroskopie wurde an den postoperativen Tagen 12, 14 und 16 durchgeführt.

Wieder wurden sowohl Kontroll- als auch EphB4-überexprimierende Tumoren entweder mit einem Placebo oder mit Sunitinib ab dem 12. Tag postoperativ für 4 Tage behandelt.

Ergebnisse

Unbehandelte EphB4^{OE}-Tumoren wuchsen deutlich langsamer als die unbehandelten pLXSN-Tumoren. Die antiangiogene Therapie hatte keinen signifikanten Einfluss auf das Wachstum der behandelten EphB4^{OE}-Tumoren im Vergleich zu den unbehandelten EphB4^{OE}-Tumoren. Hingegen bewirkte die antiangiogene Therapie eine signifikante Verminderung des Tumorwachstums von behandelten pLXSN-Tumoren im Vergleich zu den unbehandelten pLXSN-Tumoren. Während behandelte pLXSN-Tumore eine deutlich verminderte Gefäßdichte und weniger proliferierenden Zellen aufwiesen sowie eine erhöhte Anzahl an apoptotischen Zellen, waren diese Parameter in behandelten EphB4^{OE}-Tumoren konstant. Die Intravitalmikroskopie zeigte, dass sich behandelte EphB4^{OE}-Tumoren ein funktionierendes Gefäßnetzwerk erhielten, während behandelte Kontrollen eine verminderte Anzahl an funktionierenden Gefäßen aufwiesen.

Fazit

EphB4 vermittelt antiangiogene Resistenzen durch den Erhalt funktionierender Gefäßnetzwerke, wirkt jedoch gleichzeitig auch tumorsupprimierend durch die Verlangsamung von Tumorwachstum.

1 Introduction

1.1 Glioblastoma Multiforme

Glioblastoma multiforme (GBM) is the most frequent malignant brain tumor among adults, accounting for almost half of all malignant brain-originating tumors [1]. Featuring an incidence of approximately 3.2 per 100,000 individuals, GBM occurs mainly in patients older than 50 years [1]. Women are less affected than men [1]. Its median survival time amounts to less than a year; only 5% of diagnosed patients survive longer than five years [1]. Reflecting the poor prognosis, the WHO has continuously rated it as a grade IV tumor, the highest possible ranking among neoplasms in the central nervous system [2, 3].

Historically, the name of the GBM derives on the one hand from its origin within glial cells, specifically astrocytes, on the other the term multiforme is intended to describe the various impressions of the tumor featuring necrosis, hemorrhages, multinuclear cells in a variety of forms and size as well as microvascular proliferation [4, 5].

Distinguished for the first time by Scherer in 1940 into a rapidly developing primary GBM and a slowly developing secondary GBM, based on whether the tumor originated *de novo* or emerged from an already existing astrocytoma respectively, gradually more differentiations came along [6].

Following the new grading of the WHO (status: 2016), GBM are now considered a subgroup of diffuse glioma (previously astrocytoma), a term used for tumors with infiltrative properties and high likelihood of recurrence after surgery [3, 7]. Diffuse glioma are further subdivided into isocitrate dehydrogenase (IDH)-wildtype (corresponding to primary GBM), IDH-mutant (corresponding to secondary GBM) and not otherwise specified (NOS; in case of unfeasible IDH-determination) [3]. IDH-wildtype GBM now further involves giant cell GBM as well as epitheloid GBM and gliosarcoma [3].

IDH-mutation, present in about 10% of GBMs, is a crucial factor for survival time [3]. On an average patients exhibiting an IDH-mutation survive more than twice as long as patients having an IDH-wildtype GBM in population based studies [3, 8-10]. IDH-wildtype GBMs further tend to occur in older patients (62 vs. 44 years) and to display a more distinct necrosis as well as differing gene mutations compared to IDH-mutant tumors [9-11].

Associated for the first time with the differentiation of primary and secondary GBM via next generation sequencing in 2008 by Parsons *et al.*, testing for an IDH-mutation proved to be the only reliable method to differentiate the previously histologically indistinguishable tumor subtypes [9]. The mutation takes place at the beginning of tumor development of the secondary GBM, since already its predecessors, diffuse astrocytoma (WHO grade II) and anaplastic astrocytoma (WHO grade III) frequently display the mutation [12, 13]. The main effect of the mutation of IDH, which is at molecular level physiologically involved in the Krebs cycle, is still unclear [14].
So far the discovery of IDH-mutation correlation with GBM subtype solely forms a prognostic achievement; therapeutical advantages will have to be exploited in the future.

At present the standard treatment of GBM consists of combined radiotherapy, surgery and chemotherapy [15]. Surgery is either performed diagnostically to obtain a biopsy, or curative with the goal to maximally resect the tumor. Subsequently radiation (60Gy) combined with administration of temozolomide (TMZ) is being implemented over 6 weeks, ensued by a closing conservation therapy with TMZ over 6 months [15].
Patients who are older than 65 are treated either with radiation or chemotherapy, depending on their promoter methylaton status of O6-methylguanine DNA methyltransferase (MGMT), as an epigenetic silencing via methylation of the gene promoter was shown to enhance the effect of TMZ and to significantly prolong overall survival (OS) [16, 17]. MGMT is a DNA-repair enzyme, which is capable of preventing alkylating substances to establish cross links within the DNA double-strands of cancerougenous cells, thereby posing a resistance mechanism towards alkylating antineoplastic agents such as TMZ [18, 19].

As the combination of TMZ and lomustine in 2017 was the last successful approach in the treatment of GBM, by significantly prolonging OS in MGMT-methylated GBM, other possible treatments are intensively researched [20].
Antiangiogenic therapies, which had been shown to exert positive impacts on other tumor entities, were naturally considered to be effective in targeting the highly vascularized GBM.

1.2 Antiangiogenic Therapy

The history of antiangiogenic therapy dates back more than 40 years to 1971, when Folkman hypothesized that all tumors depend on angiogenesis [21]. Subsequently he concluded that if creation of new tumor vessels was impaired, the cancer would not be able to survive [21]. However, it took 33 years until the first antiangiogenic drug, VEGF-inhibitor bevacizumab (Avastin®), was accepted by the Food and Drug Administration (FDA) to be administered in the treatment of advanced colorectal carcinoma (CRC) [22]. The concept behind targeting tumor angiogenesis is based on the assumption that tumors use signaling molecules to establish their vascular network by acquisition of physiological vessels [23]. Primarily members of the VEGF-family and its receptor tyrosine kinases (RTKs), but also pathways such as the tie2-pathway or notch-delta like ligand 4 signaling pathway have been identified to take part in these processes [24-26]. Especially, VEGF-factors are increasingly released due to hypoxic stress within the frequently oxygen depleted tumor tissues [27]. Consequently antiangiogenic therapy aims at inhibiting these molecules or their receptors, whereby the tumor is cut off from its supply of oxygen and nutrition [23].

In the USA thirteen drugs have been approved so far, which either directly target VEGF and its receptors or exhibit antiangiogenic activities by blocking related pathways [28]. Yet only two drugs are used to target neoplasms within the brain, namely bevacizumab as a second line therapy in GBM following TMZ failure and everolimus (Afinitor®) in subependymal giant cell astrocytoma when curative surgery is not an option [28]. Causes for the still low numbers of antiangiogenic drugs are various, primarily because overall benefits of antiangiogenic therapy have been quite modest so far. On the one hand, survival time in most tumor entities has only been increased slightly, on the other treatments are costly and have toxic side effects [23, 29, 30].

Several Phase III studies of antiangiogenic drugs in addition to standard therapy in GBM, have been carried out so far. The AVAglio study for example, evaluated the impact of bevacizumab in newly diagnosed GBM [31]. Bevacizumab was applied during combined radio-chemotherapy as well as during the following TMZ-maintenance therapy and finally as a monotherapy until progressive disease (PD) or death occurred [31]. Addition of bevacizumab did not prolong OS and had higher adverse events than the placebo group [31]. However progression-free survival (PFS), determined by means

of Karnofsky Performance Score and Global Health Index, was significantly improved [31]. Since the study design provided for the investigators to decide on how to proceed with patients after PD, it is difficult to evaluate a possible positive effect of bevacizumab subsequent to patient worsening.

An explorative study by Chinot *et al.*, following the publication of the AVAglio study, compared the outcome of patients receiving solely bevacizumab and those who received other additive treatments after PD [32]. In contrast to the AVAglio study, Chinot *et al.* showed a possible positive effect of bevacizumab by means of prolonged OS and PFS when used as a monotherapy [32]. It was proposed that crossover effects might be responsible for the significantly improved PFS, while OS was not prolonged in the AVAglio study [33].

Another Phase III study examined the effect of enzastaurin, an inhibitor of Protein kinase C β, which mediates VEGF-induced angiogenesis in recurrent GBM [34]. Despite promising Phase II studies, administration of enzastaurin neither resulted in prolonged OS, nor in prolonged PFS compared to standard therapy with lomustine, an alkylating agent [34].

Also cilengitide, inhibiting the integrins αvβ3 and αvβ5, which are assumed to play a pivotal part in the interaction of tumor and brain tissue, and are overexpressed on tumor cells as well as its vessels, failed to improve OS and PFS in a Phase III study concerning patients with newly diagnosed GBM [35].

Furthermore, a Phase III study with cediranib, a drug targeting multiple factors such as VEGF-receptors 1-3 as well as platelet derived growth factor receptors and c-kit was conducted in recurrent GBM [36]. Similar to bevacizumab, results in preceeding Phase II studies were promising, yet cediranib neither improved PFS as a monotherapy nor in combination with lomustine [36].

Rearrangement of chaotic tumor networks following the reduction of exuberant VEGF-secretion, and the subsequent balance of pro- and antiangiogenic factors as well as development of resistances during treatment, is supposed to be responsible for the often poor impact of antiangiogenic drugs [37]. Possible mechanisms of resistance are the acquisition of non-tumoral vessels (“vessel co-option”), and forming of vessel-like structures by tumoral cells (“vascular mimicry”), as well as increased activation of other angiogenic systems and alteration in stromal cells such as pericytes [38]. Pericytes are

perivascular cells responsible for vessel stabilization, modulating their tone and morphology, which have been suspected to mediate antiangiogenic resistance [38].

One of the signaling pathways which has demonstrated its significance in mediating angiogenesis and to further promote enhanced interaction between endothelial cells (ECs) and pericytes, is the Eph-ephrin signaling pathway, thus the purpose of this study was to evaluate its role in mediating resistance towards antiangiogenic therapy [39].

1.3 Eph-ephrin System

The Eph-ephrin system comprises receptors, so called Ephs (differentiated into EphA counting from 1-9 and EphB from 1-5) and their ligands, named ephrins (ephrinA counting from 1-5 and ephrinB from 1-3) [40, 41]. Ephs are RTK, featuring multiple extracellular ectodomains, which are the docking stations for the ephrins, a transmembrane segment and an intracellular domain, consisting of the tyrosine kinase and therefore responsible for signal transduction within the cell [42]. Ephrins possess an Eph-binding domain and are connected to the cell membrane either by means of a glycosylphosphatidylinositol (GPI) anchor in case of ephrinAs, or appear as a transmembrane segment with a short cytoplasmatic region in case of ephrinBs [40, 43]. EphA will promiscuously bind to the different ephrinA- ligands, as EphB will do to the different ephrinBs, except for EphA4, which can also bind ephrinBs, EphB2 which can bind ephrinA2 and EphB4, which almost exclusively binds ephrinB2 [40, 41]. In the majority of cases receptor and ligand are both bound to the cell membrane, thus interaction usually occurs by cell-to-cell interaction [40, 41, 43]. Ephs are expressed by almost all cell types, but have been described most precisely in developing and adult neural cells and developing vascular cells [39, 44-48].

Pathway activation is triggered by connection of receptor and ligand, resulting in a bidirectional signaling, on the one hand in the ligand cell ("reverse signaling"), on the other in the receptor cell ("forward signaling") [40, 43].
Forward signaling in the Eph-expressing cell is mediated by activation of the RTK, which thereupon causes autophosphorylation processes within the cell, whereas

reverse signaling in the ephrin-expressing cell is triggered by means of Src family kinases and PDZ-domains [43, 49].
The activated pathways cause alterations of the actin cytoskeleton of the cells, thereby influencing cell motility, morphology, adhesion and invasiveness, but also regulating actions necessary for survival, like proliferation, differentiation and self-renewal [40, 43, 45]. These pathways not only play a role in physiological processes, but also in cancers, where the Eph-ephrin system has been proven to play various roles, at times enhancing or also decelerating tumor progression. For instance the EphA2-receptor has been shown to be increasingly expressed in malignant breast cancer and prostate cancer as well as EphB4, which has been found upregulated in many cancers such as breast cancer, mesothelioma, bladder cancer, prostate cancer and CRC [39, 44, 50-55]. In contrast, the EphA1-receptor is usually exclusively expressed in the epidermis, and has been found to be significantly reduced in basal cell carcinomas and squamous cell carcinomas, or has been demonstrated to be less expressed, the more degenerated a tumor presented in prostate or breast cancer is [51, 56, 57].

Activation of pathways in the interacting cells effects opposing reactions, either reinforcing repulsion (in the receptor-presenting cell) or adhesion (in the ligand-carrying cell) via forward and reverse signaling respectively, thereby prohibiting intermingling of cells [41, 47, 58]. This fact has been found to be pivotal for angiogenesis, where especially the interaction of receptor EphB4 and its ligand ephrinB2 has demonstrated their significance in preventing uncontrolled blending of arterial and venous ECs [47, 48, 59].

While next to neural cells, EphB4-receptors are predominantly expressed on venous ECs, ephrinB2s appear mainly on the membranes of arterial ECs [48, 59, 60]. The decisive role of the EphB4-ephrinB2 system in steering and mediating vasculogenesis has been demonstrated in knock-down experiments, where depletion of ephrinB2 or EphB4 resulted in failed formation of vessel networks in embryonic mice and the subsequent death of the animals [46, 48, 59, 60]. Overexpression of EphB4 or ephrinB2 has been shown to cause increased sprouting of ECs and improved formation of vascular networks by interacting with other angiogenic systems such as VEGF-receptors or the angiopoietin system *in vitro* and *in vivo* [39, 47, 49]. The EphB4-

ephrinB2 system has been shown to promote tumor angiogenesis and thereby tumor progression in various types of cancer [39, 61, 62].

As stated previously, the purpose of this study was to evaluate the role of EphB4-ephrinB2 signaling in mediating antiangiogenic resistance in GBM. Previous studies have demonstrated on the one hand significantly increased EphB4-levels in glioma, on the other, alteration of tumor vessels exposed to EphB4-overexpression, revealing vascular morphologies similar to ones resistant to antiangiogenic therapy [39, 63, 64].
Earlier studies had already picked out increased vessel size as the functional mechanism of tumors to regain and maintain blood flow in the often poorly perfused tumor centers [65-67]. Moreover, increase of blood flow and red blood cell velocity were described as major angiogenic mechanisms to compensate for vessel loss due to antiangiogenic therapy [68]. All these changes in vascular characteristics have been demonstrated in glioma cells under the circumstances of endothelial EphB4-overexpression [39].

As a proof of principle, screening experiments from our study group depicted endothelial EphB4 overexpression in subcutaneously implanted glioma cells to result in increased resistance towards antiangiogenic therapy, mediated via sustained pericyte-endothelial cell connections [69].
Since these results may not be transferred to orthotopically growing glioma, the present study was targeted to investigate the role of EphB4 on vascular resistance mechanisms in an orthotopic glioma model, in order to identify its relevance for translation into clinical application.

1.4 Hypothesis

EphB4-ephrinB2 interaction has been shown to take part in regulating angiogenesis in physiological and carcinogenic processes. Furthermore, tumor vessels exposed to an EphB4-overexpression displayed morphological characteristics similar to vessels resistant to antiangiogenic treatment, thus the thesis reads as follows:

EphB4-ephrinB2 signaling takes part in mediating vascular resistance towards antiangiogenic treatment in glioma.

2 Material and Methods

2.1 Cell Lines

Human glioma cells (SF126 cells, Tokyo Metropolitan Institute of Gerontology, Tokyo, Japan) as well as reporter cells (Phoenix-ECO cells, Martinsried, Germany) were used, which were co-implanted into the experimental animals.

The highly transfectable Phoenix-ECO cells are a producer cell-line created from human embryonic kidney cells (HEK, 293T cell line) and transformed by Adenovirus E1a, carrying a temperature sensitive T antigen co-selected with neomycin [70]. The objective of a producer cell-line is high-titer production of retroviral particles, subsequent to introduction of viral vectors into the cells. The task of the producer cell-line is thereby to provide for the infectivity of the retroviral particles by production and equipment of viral proteins, concerning their structure and their surface [71]. Episomes of the Epstein Barr virus (EBV) have shown here to be the most effective in serving as installation constructs for the viral vectors, by enabling fast and long-lasting as well as stable production of retroviral particles [72].

We used Phoenix-ECO cells that had been transfected with a so called pLXSN-vector, which contained elements of Moloney murine leukemia virus (MoMuLV) and Moloney murine sarcoma virus (MoMuSV) [73]. The pLXSN vector was an empty plasmid-vector, whose RNA had been packaged into the EBV episomes inside of the reporter cells. Subsequent to implantation, the retroviral particles were released, infected the target cells and by this means transported the gene information of the pLXSN-vector into the DNA of mice and rat cells (ECOTROPIC packaging system). Thereupon the target cells initiated an increased production and overexpression of the (empty) pLXSN gene.
Since the pLXSN-vectors lacked necessary structural genes (gag, pol, and env) they were not capable of replication. However Phoenix-ECO cells were able to produce gag-pol and envelope proteins to provide the necessary requirements for the infectiousness of the ecotropic virus. Therefore, the retroviral particles were able to infiltrate target cells but not to replicate within them. The gag-pol and the envelope proteins were selected with hygromycin and diptheria-toxin resistance as coselectable markers, respectively.

To establish an overexpression of EphB4 on ECs we used Phoenix-ECO cells, which carried a pLXSN vector that had undergone cloning of the genetic code of the EphB4-receptor (2992 bp). Thereby, the Phoenix-ECO cell was capable of producing a retrovirus that transfected ECs, and by installing the EphB4-gene into cellular DNA, caused an increased expression of the receptor on the cell's surface. For control tumors non-modified pLXSN vectors were used, which did not produce an effect in the target cells.

Since the reporter cells were implanted together with human glioma cells we expected the retroviral particles to exclusively infect ECs of the murine vessels acquired by the tumor, not the human tumor tissue itself. This fact was pivotal for the experiments, as the objective was to determine solely the effect of EphB4 on tumor angiogenesis and subsequent antiangiogenic resistance development.

2.2 Cell Culture

All cell lines were cultivated with 4.5 g/l in Dulbecco's Modified Eagle's Medium (DMEM, Gibco™, Karlsruhe, Germany), which was supplied with 10% fetal bovine serum (FBS, ScienCell, San Diego, USA) and 1% penicillin-streptomycin-solution (ScienCell, San Diego, USA) at 37^{o} C at 5% CO_2. Furthermore, geneticindisulfat (G-418, Roth, Karlsruhe, Germany) 800 µg/ml was added to test the Phoenix-ECO cells for neomycin resistance.

Before the start of the experiments, the Phoenix-ECO cells underwent increased selection by means of addition of hygromycin (Thermo Scientific, Dreieich, Germany) (300 µg/ml) and diphteria-toxine (EMD Millipore Corporation, San Diego, USA) (1 µg/ml), to reduce risk of recombination and to secure the exclusive use of functioning cells.

The cells were split after reaching confluency of 70 to 80%. For splitting, the cells were washed with phosphate buffered saline (PBS, Gibco™, Karlsruhe, Germany), followed by application of trypsin (Thermo Scientific, Dreieich, Germany), which served the purpose of detaching the cells of the culture flask ground. The cells were placed in the incubator for five minutes to be exposed to the trypsin. Using the microscope it was verified subsequently that all cells had been detached. Following that, the cells were centrifuged for 5 minutes at a velocity of 1300 rcf. The consequentially formed cell pellet was resuspended, and the cells were seeded out at a concentration of about 10^6 per cell culture flask.

For storage the cells were frozen in FBS with 10%Dimethylsulfoxid (DMSO, SIGMA-ALDRICH CHEMIE GmbH, Steinheim, Germany) in a nitrogen tank at -80°C.

2.3 Experimental Animals

For the *in vivo* experiments NU/NU Nude Mice (Charles River Laboratories, Sulzfeld, Germany) were used. Since the mice lack a thymus, they are not capable of producing T-cells and are therefore considered immune-deficient. This fact was pivotal for the experimental setup, since the concept required the implantation of xenogenetic material into the animals. Immune-competent mice would have been able to suppress the growth of the human Phoenix-ECO cells and SF126 cells, preventing the xenograft implantation.

All mice were of female sex and with a body weight between 20 and 28g. The mice were operated on when they had reached an age of 6 to 8 weeks. During the experiments, they were kept in the animal stables of the NeuroCure Clinical Research Center at Charité Campus Mitte. At all times, the mice had unlimited access to dry food and water. The litter was exchanged once a week. For enrichment purposes (modification of living environment to improve behaviour and state of the animals) the mice were always kept in groups of at least two, and the cages were supplied with material for nest construction and modifications of cage environment. The animals underwent a day-night circle of 12 hours at a temperature of around 22.5 ºC. Animals losing more than 30% of their bodyweight or showing significant neurological deficits (limb paresis, vertigo) were removed from the experiments and euthanized in narcosis by decapitation.

2.4 Study Design

Two main studies were designed, with four different groups, respectively. In the first study, tumor growth using magnetic resonance imaging (MRI) after implantation of orthotopic xenografts was performed. In the other study, the development of the vascular network of 3D tumor spheres was analysed using the chronic cranial window technique and intravital microscopy.

In each study animals were randomly assigned to one of four groups: EphB4-overexpression (EphB4^{OE}), control (pLXSN), treated EphB4-overexpression (EphB4^{OE}+Sun), and treated control (pLXSN+Sun).

A total number of 68 animals were included in the experiments. There were 23 drop-outs, mainly due to exitus during high dose treatment and non-sufficient growth of implanted tumor cells. The final number of animals which were analysed is presented in tables 1 and 2.

2.4.1 Orthotopic Xenografts

In this series of experiments 6 animals were assigned to each of the four groups, respectively. Animals were treated with Sunitinib or a sham substance for four consecutive days, beginning on the 25th day after implantation of the tumor cells. Tumor growth was documented on the 14th, 21st, 25th and 29th day postoperatively by means of small-animal MRI imaging (Fig. 1). After the last MRI examination the mice were reanesthetized for perfusion fixation with PBS and PFA and their brains harvested for immunohistological staining.

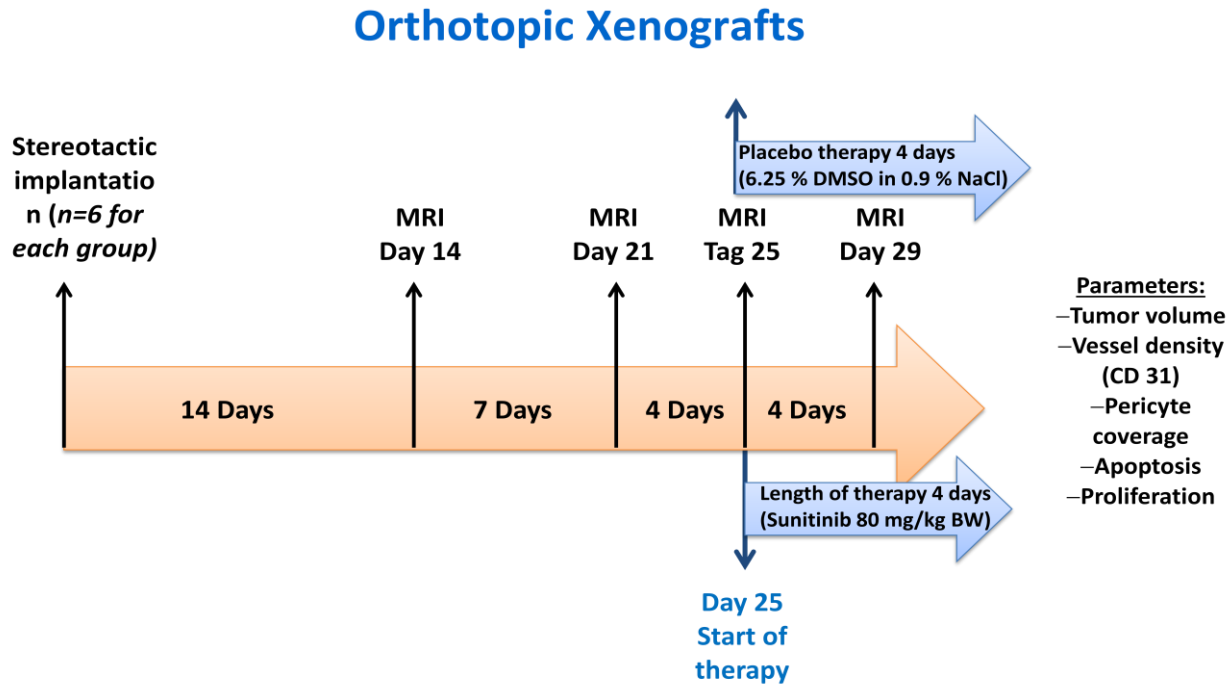

Figure 1: Experimental protocol: Implantation of orthotopic xenografts.

2.4.2 Intravital Microscopy

In this study 5 animals were assigned to the four groups described above, respectively. Animals were treated with Sunitimib or a sham substance for four consecutive days, beginning on the 12th day after implantation of the tumor spheres and preparation of the chronic cranial window. Intravital microscopy was performed on postoperative days 12, 14 and 16 (Fig. 2).

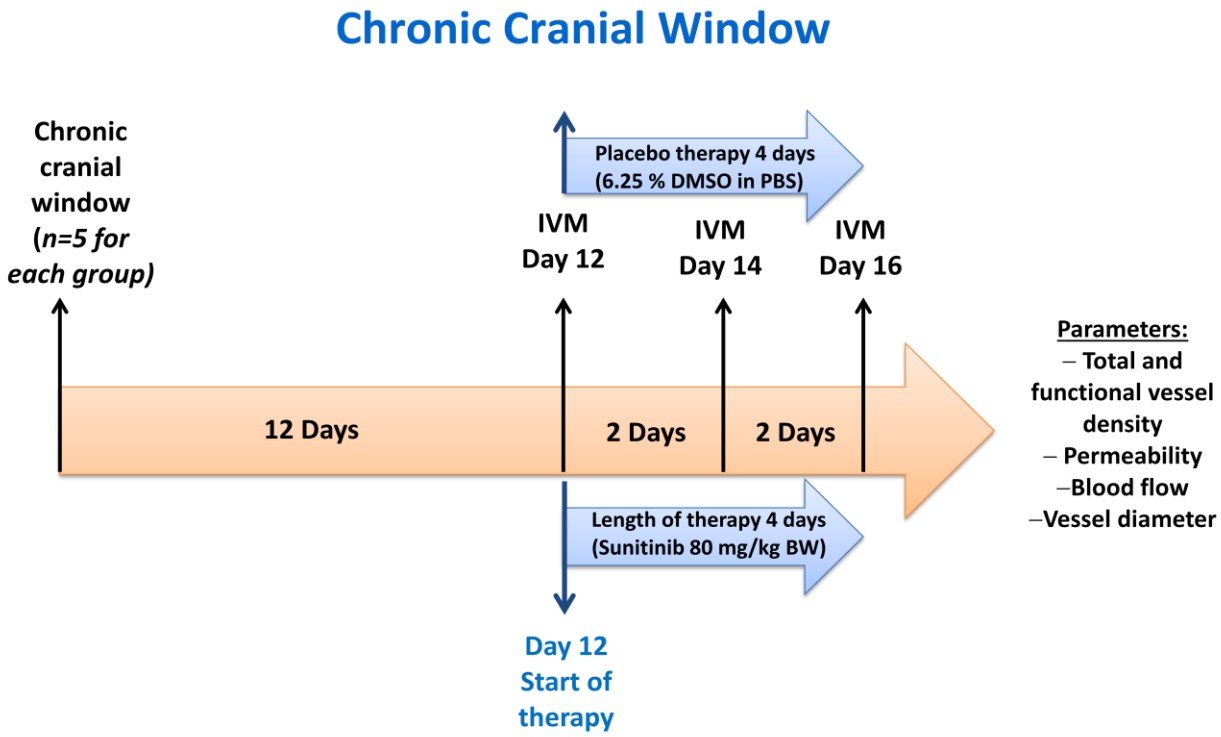

Figure 2: Experimental protocol: Chronic cranial window and intravital microscopy.

	DAY 14	DAY 21	DAY 25	DAY 29
PLXSN	6	6	6	6
PLXSN + SUN	6	6	6	6
EPHB4^{OE}	3	6	6	6
EPHB4^{OE} + SUN	4	7	7	7

Table 1: Final number of mice used for orthotopic xenografts.

	DAY 12	DAY 14	DAY 16
PLXSN	5	5	5
PLXSN + SUN	5	5	5
EPHB4^{OE}	5	5	5
EPHB4^{OE} + SUN	5	5	5

Table 2: Final number of mice used for chronic cranial window operations.

2.5 Anesthesia and Analgesia

For implantation of the orthotopic xenografts, preparation of the chronic cranial window and during IVM, the mice were anesthetized with a mix of esketaminhydrochlorid (Ketanest®, Pfizer Pharma, Berlin) (7.5mg/kg bodyweight) and xylacin (Rompun®, Bayer, Leverkusen) (2.5mg/kg BW), as well as aqua ad iniectabilia (Aqua, B Braun Melsungen AG, Melsungen) via intraperitoneal injection [65].
MRI-scans were performed under inhalation anesthesia, using a mix of oxygen (0.2l/min), nitrogen (0.8l/min) and isoflurane (1-1.5 l/min) (Dräger Vapor® 2000, Drägerwerk AG & Co., Lübeck, Germany).

2.6 Orthotopic Xenograft Implantation

Phoenix-ECO cells and glioma cells were defrosted six days before implantation and split at least once at a ratio of 1:5, 1:10 and 1:20 respectively. Cell culture flasks with a confluency of 80 to 90 percent were selected for implantation. Only SF126 cells reaching a maximum passage of 5, and Phoenix-ECO cells reaching a maximum passage of 9, were utilized.
A total of 1 x 10^4 SF126 cells were implanted together with 1 x 10^4 Phoenix-ECO cells, which either carried the EphB4-vector or an empty pLXSN-vector for control, respectively. The cell number was acquired using CASY® cell counting technology (Casy® Model TT, Roche Diagnostics, Mannheim, Germany). The cells were split and resuspended in PBS at concentrations of 2 x 10^4/µl, and subsequently 100 µl of the Sf126 glioma cells and 100 µl of the Phoenix-ECO cells were merged and stored on ice.
For implantation, the mice were anesthetized and the scalp disinfected adequately. After a midline incision, the skin margins were reflected by means of 6-0 sutures (ETHICON®, Johnson & Johnson International, Norderstedt, Germany) and the skull

bone exposed. The site of the implantation was determined as a point being two millimeters rostrally and one millimetre right laterally of the bregma. A hole in the frontal bone was created with a 23-gauge needle (Sterican® Gr. 16, B Braun Melsungen AG, Melsungen, Germany). 1µl of the combined tumor and Phoenix-ECO cells was thereupon injected using a Hamilton®-syringe (Hamilton Bonaduz AG, Bonaduz, Switzerland). The needle was placed 3 millimetres deep within the brain, followed by a subsequent waiting period of one minute. Then the tumor cells were injected for 5 minutes, followed by another waiting period of 5 minutes. At the end, the needle was slowly removed for another period of five minutes. The operative field was cleaned and the skin incision sewed up.

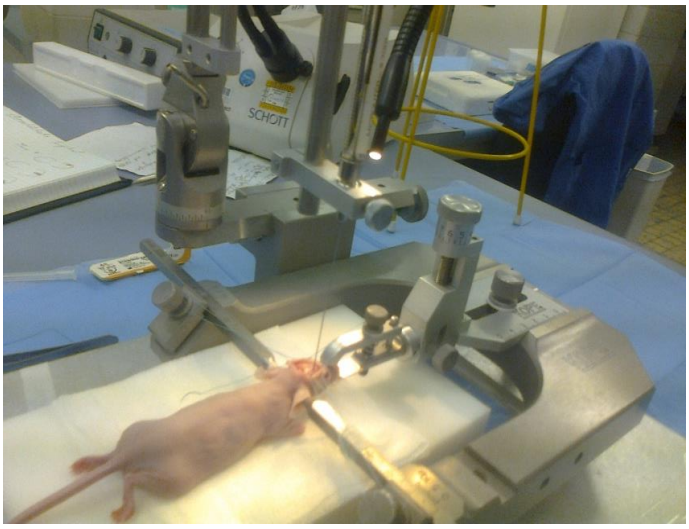

Figure 3: Implantation of an orthotopic xenograft.

2.7 Antiangiogenic Treatment

For antiangiogenic treatment, the mice received Sunitinib (Sutent malate, BIOZOL Diagnostica, Eching, Germany) 80 mg/kg/BW for four days from day 25 until day 29 p.o. in the orthotopic xenograft implantation, and from day 12 to 16 p.o. in the chronic cranial window, respectively. The treatment was applied every 24 hours.

Sunitinib is a multi-tyrosine kinase inhibitor, which is primarily used as a first line therapy in metastasizing renal cell carcinoma (RCC), and as second-line drug in non-operable gastro-intestinal stromal tumors (in case of non-response towards Imatinib) [74]. Furthermore, it has shown to significantly prolong progression-free survival in

unresectable or metastasized well-differentiated pancreatic neuroendocrine tumors [75]. Sunitinib has also shown antitumor effects in thyroid, lung, pancreatic, oesophageal and bladder carcinomas as well as sarcoma and glioma [76].

Its main targets are receptors of signaling molecules such as VEGF-receptor 2, platelet-derived growth factor receptor (PDGF)-β, both involved in promoting angiogenesis, and proto-oncogene cKit, which plays a pivotal part in tumor progression [77-79]. By using Sunitinib, our goal was to inhibit the main receptors responsible for tumor angiogenesis, and thereby to be able to evaluate the significance of the EphB4-receptor in mediating resistance towards antiangiogenic therapy.

Control groups were treated with NaCl 0.9% and 6.25% cell-toxic DMSO to effect cell stress, imitating the application of Sunitinib.

2.8 Magnetic Resonance Imaging

Tumor growth was documented on the 14th, 21st, 25th and 29th day p.o. by means of small-animal MRI (PharmaScan 70/16 US, NeuroCure Clinical Research Center, Charité Campus Mitte) in T1- and T2-weighted sequences. For T1-weighted images, the mice received 100 µl retroorbital injections of contrast agent, consisting of a mix of 20% Magnevist® ((0,05mmol/ml) Bayer Vital, Leverkusen, Germany) and 80% sodium chloride 0.9% (B. Braun Melsungen AG, Melsungen, Germany). The scans were performed using Bruker Software Paravision 5.1. MRI data was evaluated using AnalyzeDirect.

2.9 Immunohistochemistry

2.9.1 Desmin-Pecam Staining

After the last MRI-scans had been performed the mice were perfused with 20 ml of PBS and 10 ml of paraformaldehyde by intracardial transfusion with a 23-gauge needle (Sterican® Gr. 16, B Braun Melsungen AG, Melsungen, Germany). Following that, the brains were extracted from the cranium and placed for three consecutive days in 10, 20 and 30 percent glucose respectively, and subsequently briefly placed in isopentane.

By means of a cryostat, 20-µm thick tissue samples were produced. The tissue samples were fixated with methanol for 5 minutes at -20ºC. Afterwards, the tissue samples were

circled with a wax pencil and washed in PBS three times for 5 minutes respectively. Subsequently, non-specific antibodies in the tissue samples were blocked by means of Casein 1% in PBS for half an hour and incubated with primary antibodies versus Desmin (Abcam®, Cambridge, UK) (detects pericytes) and Pecam (BD Biosciences, Heidelberg, Germany) (detects endothelial specific marker CD31) overnight at 4ºC at concentrations of 1:200 and 1:50, respectively. The next day, the tissue samples were washed again three times for five minutes with 0.9
5% Casein in PBS. Then the secondary antibodies were applied, FITC-conjugated donkey anti-rabbit IgG (Jackson Immuno-Research, Baltimore, USA) and Cy3-conjugated donkey anti-rat IgG (Jackson Immuno-Research, Baltimore, USA), at a concentration of 1:200. Also DAPI (Jackson Immuno-Research, Baltimore, USA) was applied at a concentration of 1:100 for ten minutes to counterstain the nuclei of the cells. At the end, the tissue samples were washed again three times with PBS and subsequently covered with IS mounting medium.

By means of a fluorescence microscope (Axiotech Observer, Zeiss, Göttingen, Germany) equipped with a camera images of the tumor margins and of the tumor center were taken. The amount of vessels was determined by manually counting the CD31-positive ECs in each region of interest (ROI; 1.93mmx1.51mm) [n/ROI]. Pericyte coverage was determined by forming an index of Desmin-positive vessels over the total number of vessels multiplied by 100 [%]. The images were evaluated with the image editing program ImageJ.
For each group at least *n*=5 tumors were histologically examined in each staining. 10 pictures of each tumor were taken at 20x and evaluated.

2.9.2 Ki67 Staining

For the Ki67 staining, we used the same protocol as described for the Desmin-Pecam costaining, using, however, a primary antibody versus Ki67 (Thermo-Scientific, Fremont, USA) instead of a primary antibody versus Desmin. Using Image J it was possible to single select the green fluorescent Ki67 channel, whose images were converted into 8-bit format and subsequently made binary to display all Ki67-positive

cells as black pixels on a white background. These spots were counted automatically to determine the proliferating cells for each region of interest [n/ROI].
For each group at least *n*=5 tumors were histologically examined in each staining. Of each tumor 5 pictures at 20x were taken and evaluated.

2.9.3 TUNEL Staining

For detection of apoptotic cell nuclei by means of terminal deoxynucleotidyl transferase dUTP nick end labeling (TUNEL)-assay, the S7165 | ApopTag® Red In Situ Apoptosis Detection Kit (Merck Millipore, Darmstadt, Germany) was utilized. Samples were washed with PBS two times for 5 minutes before being placed in a precooled ethanol-acetic acid composition (2:1) at -20ºC for 5 minutes, and afterwards were washed again with PBS two times for 5 minutes. Then the equilibration buffer was applied for 10 seconds at room temperature, before the working strength enzyme was applied for 1 hour of incubation at 37 ºC. Afterwards the enzyme was blocked with the strength stop/wash buffer, agitated for 15 seconds, and incubated for another 10 minutes. Finally the samples were washed another 3 times for 1 minute with PBS before being incubated with the Working Strength anti-digoxigenin conjugate at 37 ºC. Following that, CD31 staining was added, following the same protocol as described before, but using FITC-conjugated donkey anti-rat as a secondary antibody for CD 31.

Similar to evaluating the images stained by means of Ki67, the red channel detecting rhodamine staining was singled out, and the picture converted into an 8-bit and made binary. Following that, it was possible to analyze the now black apoptotic cell nuclei on the white background and to automatically count the particles, and therefore the apoptotic cell nuclei per ROI [n/ROI].
For each group at least *n*=5 tumors were histologically examined in each staining. Of each tumor, 5 pictures at 20x were taken and evaluated.

2.10 Chronic Cranial Window

Phoenix-ECO and glioma cells were defrosted 3 to 4 days before implantation, and were used for operation when confluency amounted to 80 to 90%. To visualize the cells

during IVM, 1,1′-Dioctadecyl-3,3,3′,3′-tetramethylindocarbocyanine perchlorate (DiI) (Molecular Probes®, Eugene, USA) was added to the medium at a ratio of 1:133 (fluorescence spectra 550-567 nm).

For the chronic cranial window operation, a 3D spheroid assay as described by Laib *et al.* was performed the night before the implantation [80]. For this purpose, Methocel consisting of Endothelial Cell Basal Medium (PromoCell, Heidelberg, Germany) and carboxymethylcellulose (SIGMA-ALDRICH CHEMIE GmbH, Steinheim, Germany), as well as culture medium, which contained the amount of 50,000 Phoenix-ECO cells and SF126 cells altogether, were intermingled at a ratio of 1:4, and pipetted into 96 round-well plates, where they formed 3D-spheroids overnight (Fig. 4).

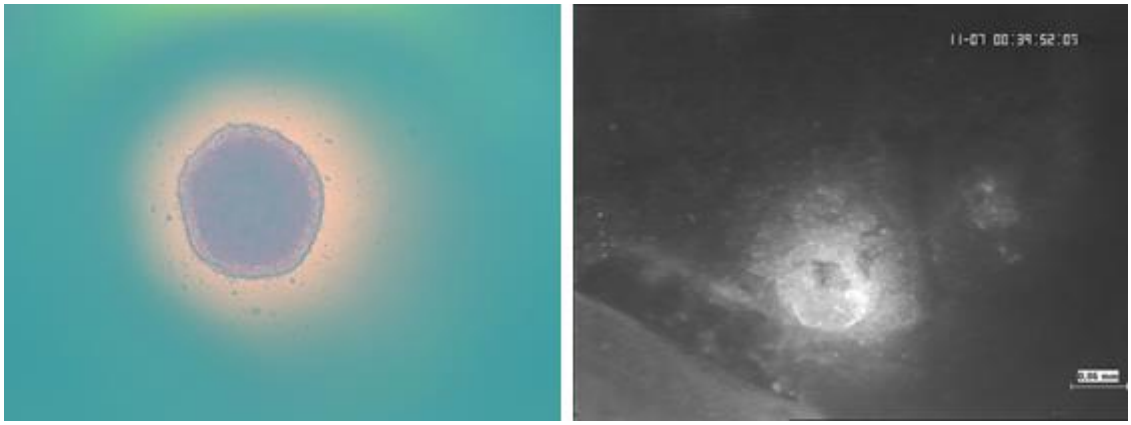

Figure 4: 3D-Spheroid in 5x-magnification under white light on the left and in 5x-magnification under green light during IVM on the right.

For the operation, the mice were anesthetized as described before and disinfected appropriately. The skin was incised in the midline and the calvaria was exposed. Under the operating microscope a circular window with a diameter of 1.5 cm was trephined over the right hemisphere. Using two surgical micro pipettes, the circular bone flap was lifted smoothly, and by means of a 26-gauge needle the superior sagittal sinus was detached from the tabula interna of the bone flap. After craniotomy, the dura mater was removed in an area without superficial vessels, using two 26-gauge needles. Subsequently one of the 3D-spheroids, which had been stored on ice, was collected and placed on the

prepared area. Immediately after that, the dental cement, consisting of a fluid component and a powder component (CYANO VENEER®, Hager & Werke, Duisburg, Germany), was stirred up and dispensed around the operative window with a 27-gauge

needle (Sterican® Gr. 20, B Braun Melsungen AG, Melsungen, Germany). As long as the dental cement was still plastic, an autoclaved 7 µm thick glass plate was placed on the mass creating a closed window. Subsequently the window was sealed hermetically with the dental cement, the operative field was cleaned and the skin incision was sewed up. Then the mice received local anaesthesia by application of lidocainhydrochloride (Xylocain® 2%, AstraZeneca GmbH, Wedel) on the operative wound, as well as tramadolhydrochlorid (2,5mg/100 ml drinking water) (Tramal®, Grünenthal GmbH, Aachen, Germany) for the remaining 16 days of the experiment for general analgesia.

Figure 5: Operative site during the chronic cranial window operation after removal of the circular bone flap. The sagittal sinus is located in the center of the image, dividing the two hemispheres.

2.11 Intravital Microscopy

On day 12, 14 and 16 p.o. the mice underwent intravital microscopy (IVM). For this Purpose, the mice were anaesthetized as described before and disinfected appropriately. Then 100 µl Fluoriso-5-thiocyanat-conjugated Dextran (FITC-Dextran, SIGMA-ALDRICH GmbH, Steinheim, Germany) with a molecular weight of 150 kDa dissolved in 2% of aqua were applied retroorbitally (fluorescence spectra 492-518nm). The operative wound was reopened and the chronic cranial window exposed. After cleaning the window with 0.9% NaCl, the mice were placed under the intravital microscope (Axiotech Vario Microscope). The microscope was equipped with a 100W-Mercury lamp attached to a Ploema-Pak illuminator with a blue (450-490nm) and a green (520-570nm) filter block (Zeiss, Oberkochen, Germany) [65]. Objectives with a magnification of x5 and x10 “long-distance“, and x20 “water-immersion“ objectives (Zeiss, Oberkochen, Germany) were used. Subsequent to checking the position of the 3D-Spheroid by using green light to detect the DiI-stained cells at x5 magnification, 5

different regions of interest (ROI) of the tumor were examined under blue light in x20 magnification, showing the vessels perfused by FITC-Dextran. Each ROI was recorded for 20 seconds, using a low-light charged-coupled device video camera (Cohu, FK 6990, Pieper, Schwerte, Germany) and stored on video tape using a S-VHS-recorder (Panasonic, Munich, Germany) [65]. The videos were evaluated off-line using a television monitor on a specialized computer in a darkroom. After intravital microscopy, the wound was sutured and coated with Xylocain® 2 %.

2.12 Evaluation of Intravital Microscopy

Intravital microscopic parameters were evaluated using a computer assisted microcirculation analysis system (CapImage, Zeintl Software Engineering, Heidelberg, Germany). The analysis of microcirculatory parameters included the total vascular density (TVD), the functional vessel density (FVD), the perfusion index (PI), vessel diameters (VD), the volumetrical blood flow (Qv) and vessel permeability indicated by calculation of the permeability index (PI).

2.12.1 Total Vascular Density

TVD was defined as the length of all vessels per ROI (0.06cmx0.05cm) [cm/cm^2] [39, 63, 65]. This included all vessels perfused by FITC-Dextran as well as vessels that were non-functional and thereby did not contain any fluorescence dye or demonstrated motionless blood flow (static erythrocytes).

2.12.2 Functional Vascular Density

FVD was defined as the length of all vessels that were perfused by FITC-Dextran or displayed moving erythrocytes per ROI [cm/cm^2] [39, 63, 65].

2.12.3 Perfusion Index

The PI was calculated by dividing FVD over TVD, multiplying the result by 100 [63, 65].

$$\mathbf{PI = (FVD/TVD) \times 100}$$

2.12.4 Vessel Diameter

Vessel diameter was examined by drawing a diagonal line through the ROI, and by evaluating all vessels that were cut by the diagonal at the point of intersection. The diameter was determined as the length of one vessel wall to another [µm].

2.12.5 Volumetrical Blood Flow

Blood flow was measured by randomly choosing three vessels and automatically determining the velocity of erythrocytes that passed by in ten seconds (Red blood cell velocity [mm/s]). Subsequently, the result was calculated with the VD in the following formula:

$$\mathbf{Qv = \pi \times (D/2)^2 \times RBCV / K.}$$

K represents the Baker-Wyland-Factor (=1.3) which takes into account the parabole behaviour of blood flow in capillary vessels [63, 65, 81]. The unit of the blood flow was [nL/s].

2.12.6 Vessel Permeability

To determine vessel permeability the efflux of FITC-Dextran next to three different vessels was measured. The fluorescence intensity of the intravascular vessel segments next to these efflux areas and the extravascular fluorescence intensity were determined to form a ratio, which defined a permeability index between 1 and 2 [39]. The higher the permeability index was, the less a vessel was losing FITC-Dextran, extravasating through the vessel wall. The formula for the permeability index was as follows:

Permeability Index = Intravascular/extravascular fluorescence

2.13 Statistical Analysis

The data from the tissue samples as well as the MRI images and the intravital microscopic parameters were evaluated using GraphPad Prism 5 (GraphPad Software, San Diego, USA). The comparison of size and edema of the orthotopic xenografts was

evaluated using *Two-way ANOVA* with Sidak correction. Vessel density, pericyte coverage, proliferating and apoptotic cell nuclei were analyzed using the *student's t-test* with Welch's correction. The intravital microscopic parameters were compared by means of Two-way ANOVA with Sidak correction. Statistical significance was considered at a p-value ≤ 0.05.

All results are presented as mean ± standard deviation.

3 Results

3.1 Orthotopic Xenografts

3.1.1 MRI-Data

Fig.7 represents tumor growth of all groups over time. PLXSN-tumors displayed faster tumor progression than EphB4^{OE}-tumors. Also the effect of Sunitinib treatment is apparent, as treated pLXSN tumors were gradually reduced in volume. Tumor growth was slightly impaired in treated EphB4^{OE}-tumors.

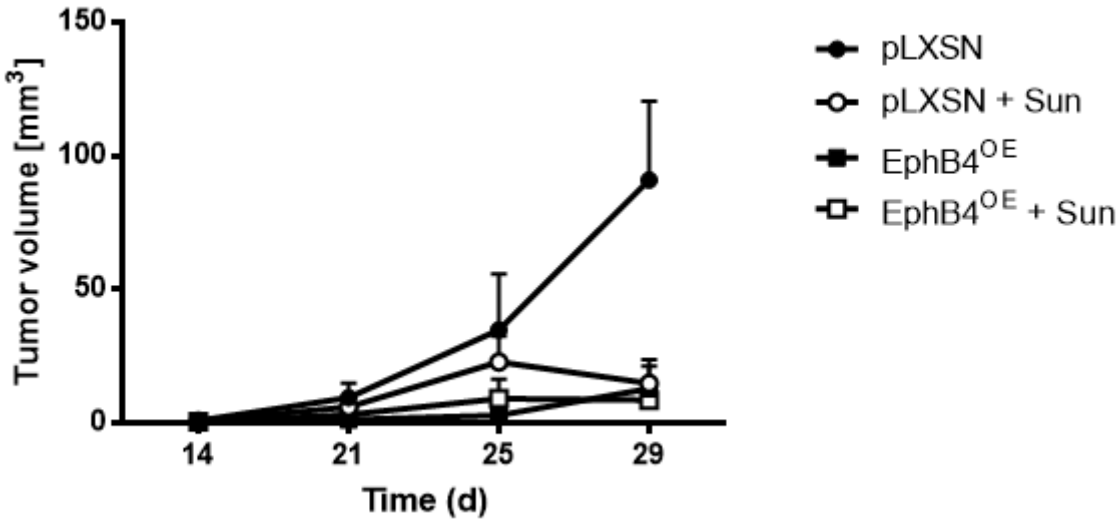

Figure 6: Tumor growth in mm^3 over time. All groups. Mean±SD.

The growth of untreated control and EphB4^{OE}-tumors is presented in figures 8 and 9. While on the first two MRI-examinations on days 14 and 21 p.o. no differences were detected, pLXSN tumors experienced rapid volume increase thereafter until day 29 p.o. On the contrary EphB4^{OE}-tumors took time to become visible, in many cases showing the first perceptible growth on day 25.
(pLXSN: 0.8 mm^3 on day 14, 9.4 mm^3 on day 21, 34.8 mm^3 on day 25, 91.0 mm^3 on day 29; EphB4^{OE}: 0.1 mm^3 on day 14, 1.2 mm^3 on day 21 , 2.8 mm^3 on day 25, 12.9 mm^3 on day 29; $p<0.01$ on day 25 p.o., $p<0.0001$ on day 29 p.o.).

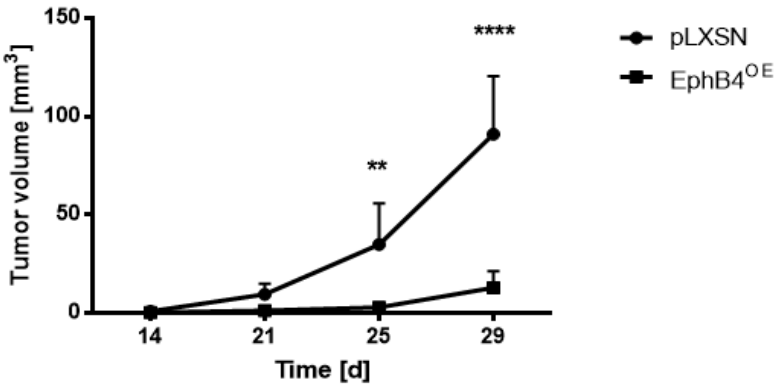

Figure 7: **T**umor growth in mm^3 over time. plXSN- vs. $EphB4^{OE}$-tumors. Mean±SD. Two-way ANOVA with Sidak correction. **p<0.01, ****p<0.0001

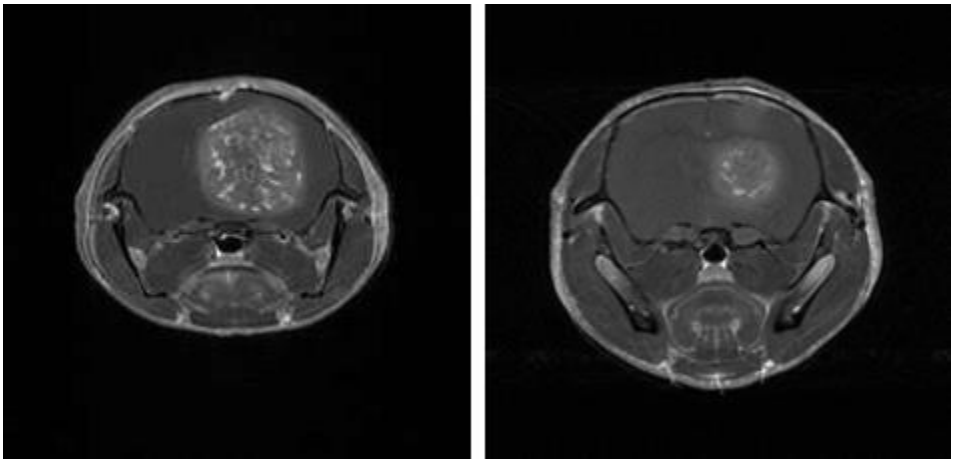

Figure 8: T1-weighted MRI-scans with contrast medium on day 29 p.o., showing an untreated pLXSN-tumor on the left and an untreated $EphB4^{OE}$ -tumor on the right. Untreated pLXSN-tumors displayed clearly bigger tumor volumes than untreated $EphB4^{OE}$-tumors.

Fig. 9 shows the effect of Sunitinib on pLXSN-tumors. Sunitinib significantly (p<0.0001) inhibited tumor growth, with a reduction of tumor volume on day 29 p.o. to about 20% of untreated pLXSN-tumors.

(pLXSN: 0.8 mm^3 on day 14, 9.4 mm^3 on day 21, 34.8 mm^3 on day 25, 91.0 mm^3 on day 29; pLXSN + Sun: 0.7 mm^3 on day 14, 5.9 mm^3 on day 21, 22.8 mm^3 on day 25, 14.9 mm^3 on day 29).

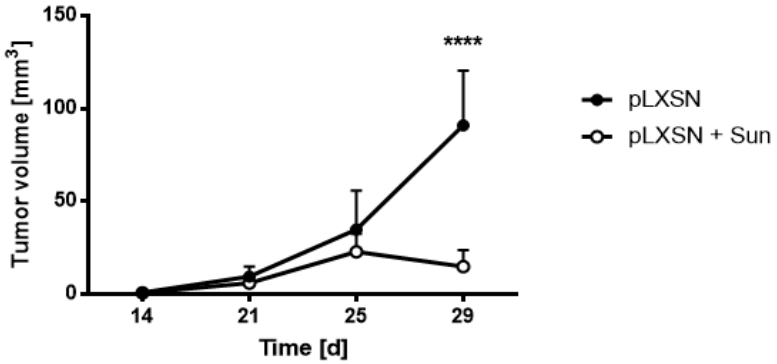

Figure 9: Tumor growth in mm^3 over time. Comparing pLXSN vs. pLXSN+Sun tumors. Mean±SD. Two-way ANOVA with Sidak correction, ****p<0.0001

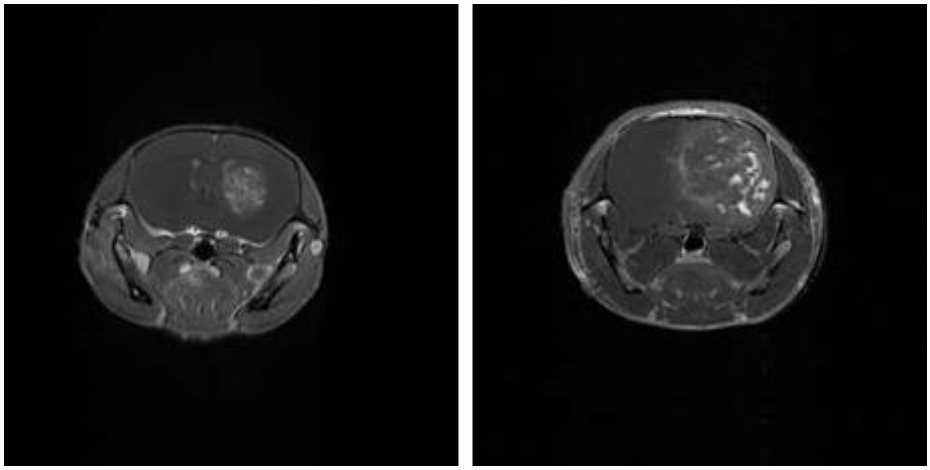

Figure 10: T2-weighted MRI-scans without contrast medium on day 29 p.o., showing a treated pLXSN-tumor on the left and an untreated pLXSN-tumor on the right. Antiangiogenic treatment caused a significant reduction in tumor volume in treated pLXSN-tumors compared to the untreated pLXSN-tumors.

Comparison of tumor growth in $EphB4^{OE}$-tumors is presented in Fig. 11. Sunitinib treatment also resulted in suppression of tumor growth in $EphB4^{OE}$-tumors, however the difference to the untreated $EphB4^{OE}$-tumors was not statistically significant.
($EphB4^{OE}$: 0.1 mm^3 on day 14, 1.2 mm^3 on day 21, 2.8 mm^3 on day 25, 12.9 mm^3 on day 29; $EphB4^{OE}$+Sun: 0.4 mm^3 on day 14, 3.0 mm^3 on day 21, 9.1 mm^3 on day 25, 8.9 mm^3 on day 29)

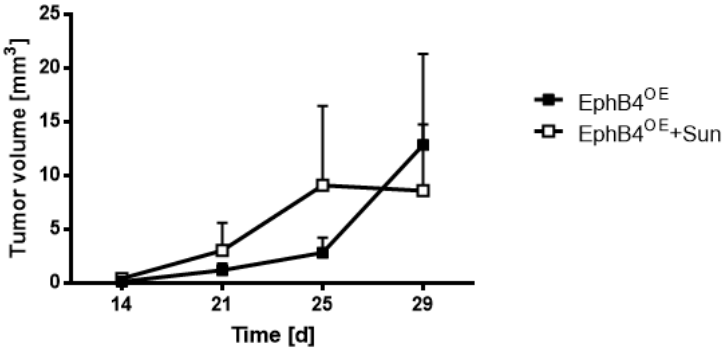

Figure 11: Tumor growth in mm^3 over time. Comparing $EphB4^{OE}$ vs. $EphB4^{OE}$ +Sun tumors. Mean±SD.

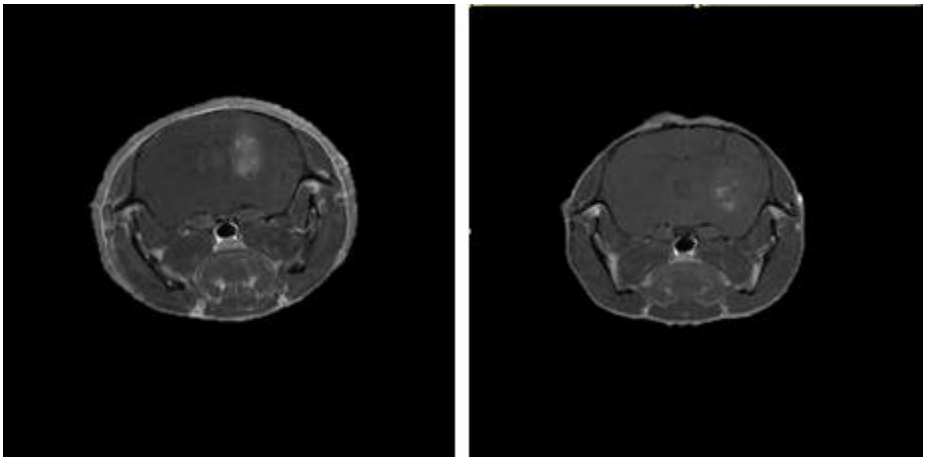

Figure 12: T1-weighted MRI-scans with contrast medium on day 29 p.o., showing an untreated $EphB4^{OE}$-tumor on the left and a treated $EphB4^{OE}$-tumor on the right. Antiangiogenic treatment inhibited tumor growth of $EphB4^{OE}$-tumors, yet the difference to the untreated $EphB4^{OE}$- tumors was not pronounced.

3.2 Immunohistochemical Stainings

3.2.1 CD31-Staining

Fig. 13 gives an overview of the number of CD31-positive cells of all groups. The figure shows the reduced number of vessels, reflecting the antiangiogenic effect of Sunitinib treatment by clearly reducing the vessel quantity of treated pLXSN-tumors, whereas treated $EphB4^{OE}$-tumors were not affected.

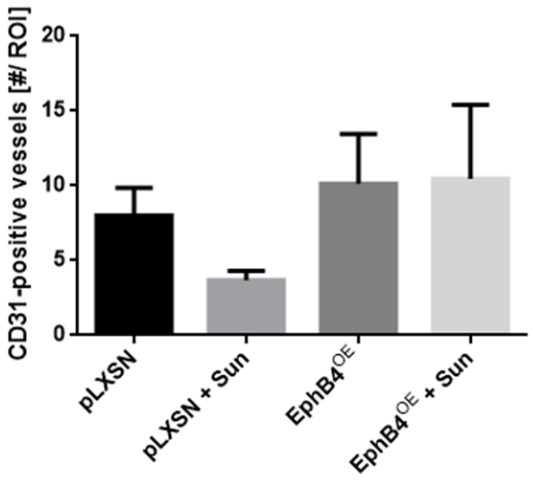

Figure 13: Number of CD31-positive vessels per ROI. All groups. Mean±SD.

Treatment of pLXSN-tumors with Sunitinib resulted in a significant ($p<0.001$) reduction of vessels compared to the untreated pLXSN-tumors.
(pLXSN: 8.0/ROI; pLXSN + Sun: 3.7/ROI)

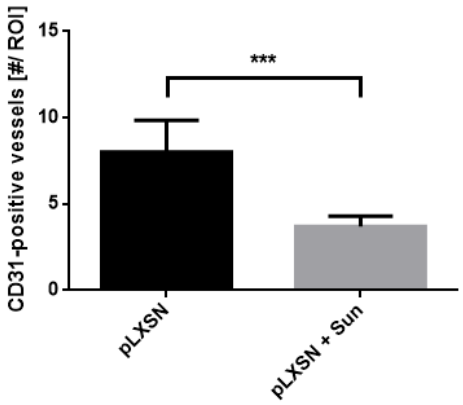

Figure 14: Number of CD31-positive vessels per ROI. pLXSN vs. pLXSN+Sun. Mean±SD.
Student's t-test with Welch's correction. ***p<0.001

Fig. 15 shows the number of vessels in treated and untreated EphB4^{OE}-tumors, displaying no reduction of vessel numbers during treatment.
(EphB4^{OE}: 10.1/ROI; EphB4^{OE}+Sun: 10.5/ROI).

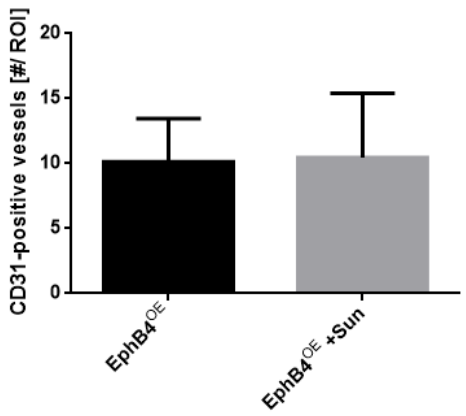

Figure 15: Number of vessels per ROI. EphB4^{OE} vs. EphB4^{OE} + Sun. Mean±SD.

Untreated groups are compared in Fig. 17, however, no significant difference was found. (pLXSN: 8.0#/ROI; EphB4^{OE}: 10.1 #/ROI)

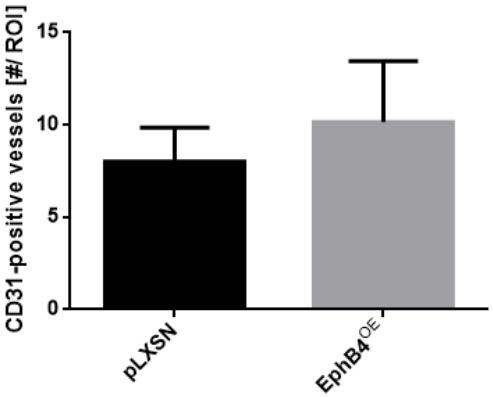

Figure 16: Number of vessels per ROI. pLXSN vs. EphB4^{OE}. Mean±SD.

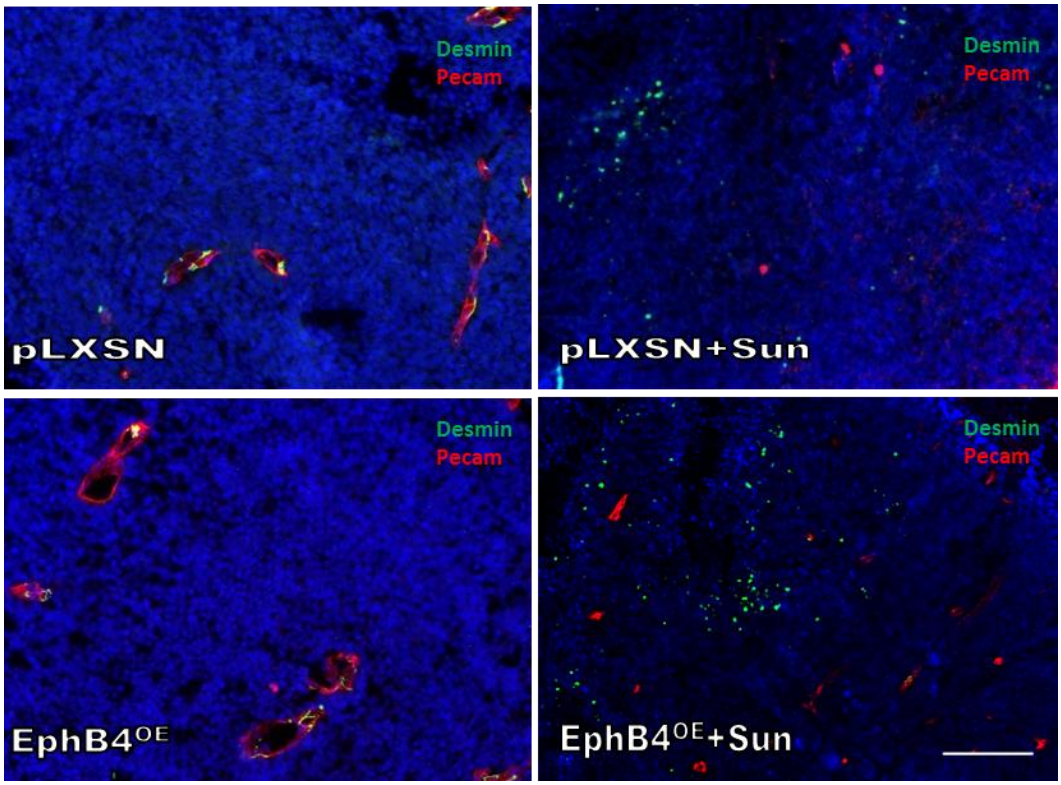

Figure 17: Pecam (red)-, Desmin (green)-, DAPI- (blue) costaining of the orthotopic xenografts, showing significant reduction of vessels in the treated pLXSN-tumors and notable alterations of vessel morphology in both treated groups. Treated antiangiogenic tumors presented a destruction of vascular structures and vessel continuity. Bar indicates 50 µm.

3.2.2 Pericyte Coverage

Fig. 18 represents the determined pericyte coverage in all groups. Sunitinib treatment reduced the proportion of pericyte-covered vessels to all vessels in both pLXSN- and EphB4^{OE}-tumors at least by half.

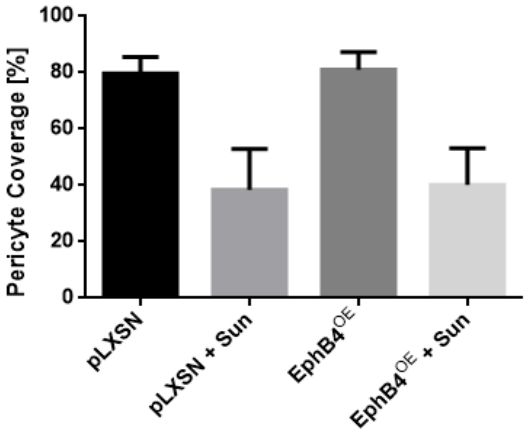

Figure 18: Pericyte coverage in %. All groups. Mean±SD.

Fig. 19 demonstrates the difference between treated and untreated pLXSN-tumors, showing a significant ($p<0.01$) reduction of pericyte covered vessels after antiangiogenic treatment.
(pLXSN: 79.6%; pLXSN + Sun: 38.4%)

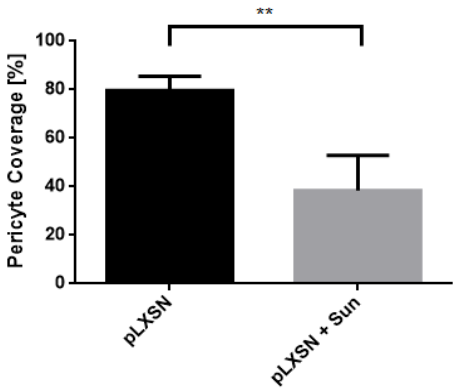

Figure 19: Pericyte coverage in %. Comparing pLXSN and pLXSN + Sun. Mean±SD.
Student's t-test with Welch's correction. ** $p<0.01$

Pericyte coverage also dropped in treated EphB4^{OE}-tumors by more than 40% compared to the untreated EphB4^{OE}-tumors, as shown in Fig. 20. No significant differences were revealed comparing the untreated groups.
(EphB4^{OE}: 81%; EphB4^{OE}+Sun: 40.2%; $p<0.001$)

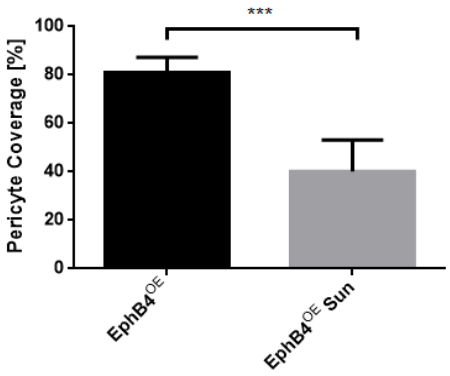

Figure 20: Pericyte coverage in %. Comparing EphB4^{OE} and EphB4^{OE}+Sun. Mean±SD. Student's t-test with Welch's correction. ***p<0.001

In Fig. 21 the effect of Sunitinib on pericyte coverage is shown in the Pecam-Desmin-costaining. While almost all vessels in the placebo groups were tightly covered by pericytes, most of them had been detached from the perished vessels in the treated groups and were spread all over the tumor.

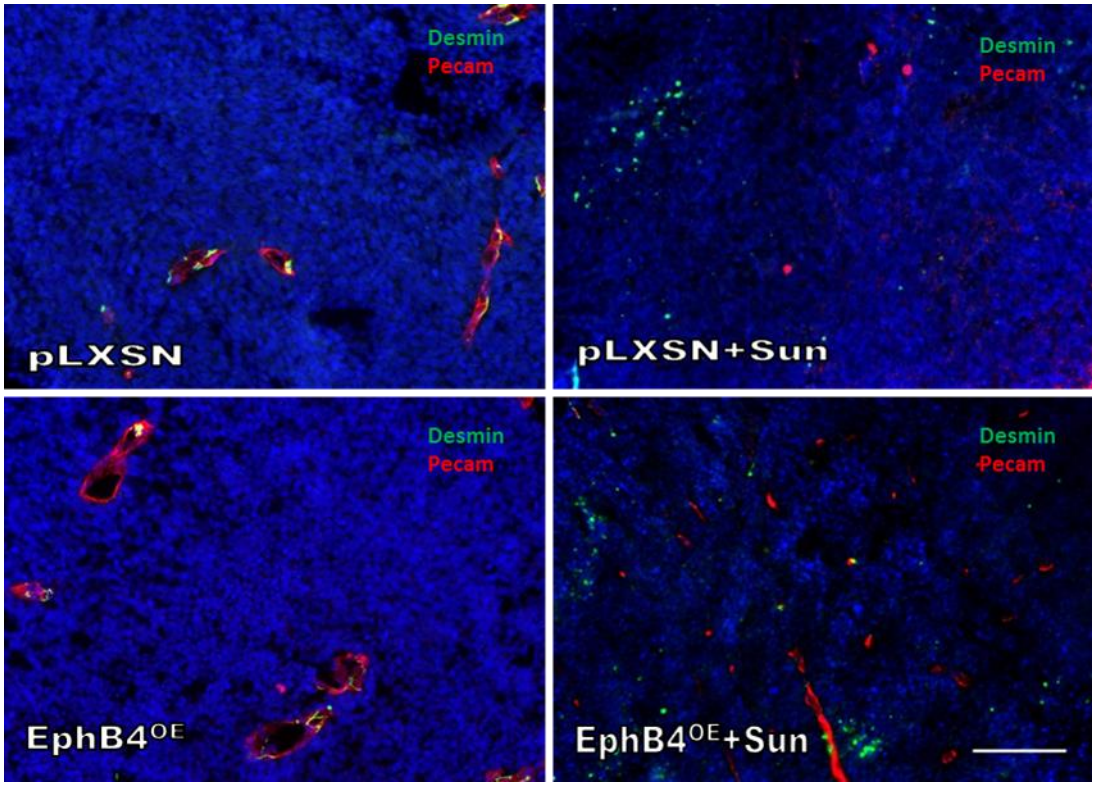

Figure 21: Pecam (red)-, Desmin (green)-, DAPI- (blue) costaining of the orthotopic xenografts, showing significant reduction of pericyte-vessel interaction in both treated groups, while vessels in the placebo groups are extensively covered. Bar indicates 50 µm.

3.2.3 Ki67-staining

To assess cell proliferation, Ki67-stainings were performed. The untreated pLXSN-tumors revealed the highest results of Ki67, while proliferating cells were hardly to be found in treated pLXSN-tumors. EphB4^{OE}-tumors displayed a lower number of proliferating cells and the reduction following antiangiogenic therapy was less pronounced (overview of all groups in Fig. 22).

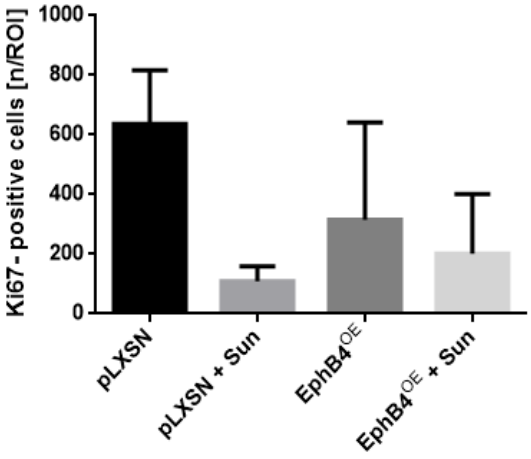

Figure 22: Ki67-positive cells per ROI. All groups. Mean±SD.

Sunitinib treatment caused a significant ($p<0.01$) reduction of proliferating cells in treated pLXSN-tumors, reducing their number to one-sixth of the untreated pLXSN-tumors (Fig. 23).
(pLXSN: 637.3 /ROI; pLXSN+Sun: 109.9/ROI)

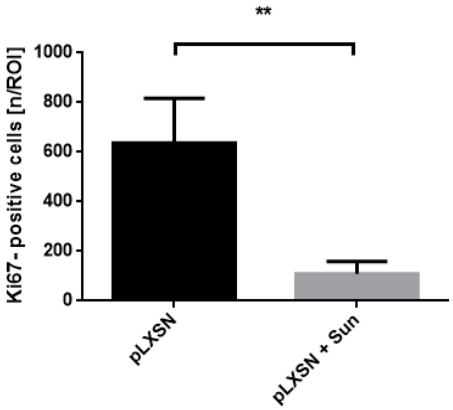

Figure 23: Ki67-positive cells per ROI. Comparing pLXSN and pLXSN+Sun. Mean±SD.
Student's t-test with Welch's correction. **p<0.01

Furthermore, a reduction of proliferating cells in treated EphB4^{OE}-tumors was observed, however not enough to be statistically significant (Fig. 24).
(EphB4^{OE}: 298.3 n/ROI; EphB4^{OE}+Sun: 213.2 n/ROI)

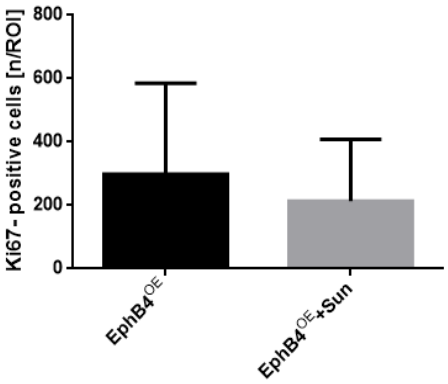

Figure 24: Ki67-positive cells per ROI. Comparing EphB4^{OE} and EphB4^{OE}+Sun. Mean±SD.

Comparison of untreated EphB4^{OE}- and pLXSN-tumors revealed a significant ($p<0.05$) reduction of Ki67-positive cells in the EphB4^{OE}-tumors, amassing only half of proliferating cells of the pLXSN-tumors (Fig. 25).
(pLXSN: 637.3 n/ROI; EphB4^{OE}: 298.3 n/ROI)

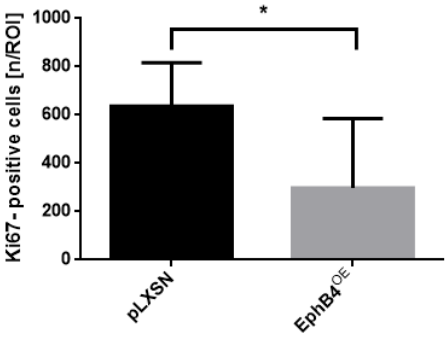

Figure 25: Ki67-positive cells per ROI. Comparing pLXSN and EphB4^{OE}. Mean±SD.
Student's t-test with Welch's correction. *$p<0.05$

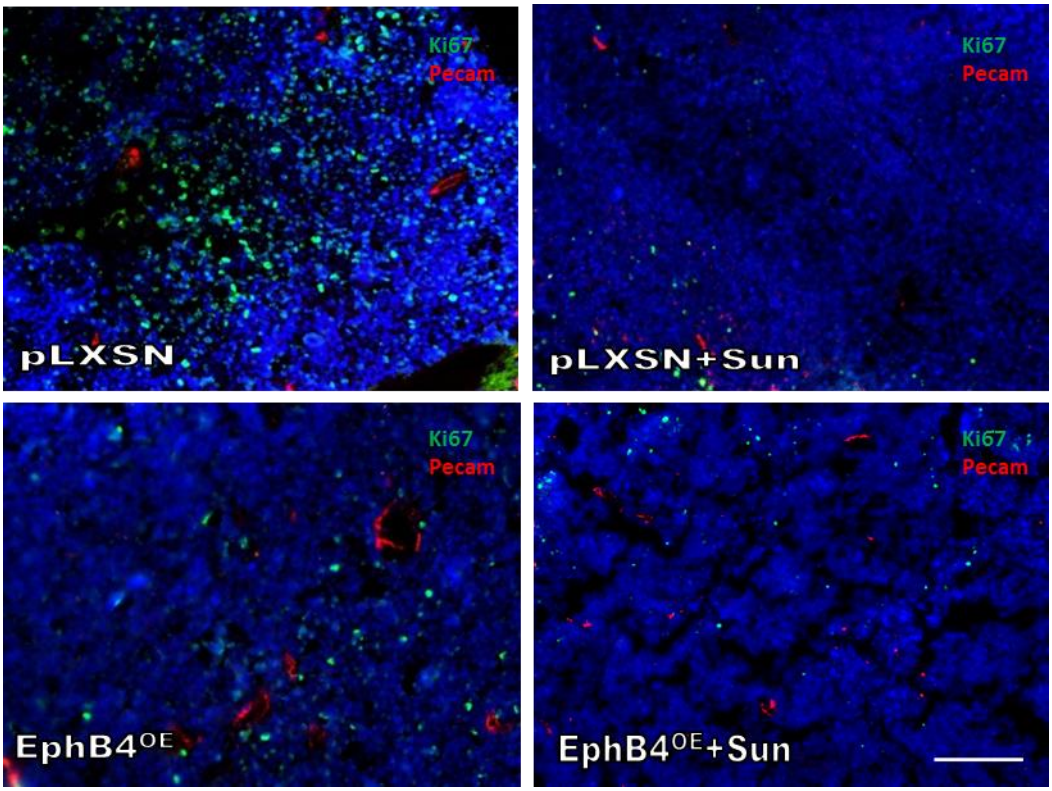

Figure 26: Pecam (red)-, Ki67(green)-, DAPI- (blue) costaining of the orthotopic xenografts, showing clear reduction of proliferating cells in both treated groups and in general few proliferating cells in the untreated EphB4^{OE}- tumors. High amounts of Ki67-positive cells in the untreated pLXSN-tumors. Bar indicates 50 µm.

3.2.3 Apoptosis

TUNEL-staining for apoptotic cell nuclei detected elevated amounts of apoptotic nuclei in treated pLXSN-tumors, while EphB4^{OE}-tumors proved to be less affected by the treatment (overview Fig. 27).

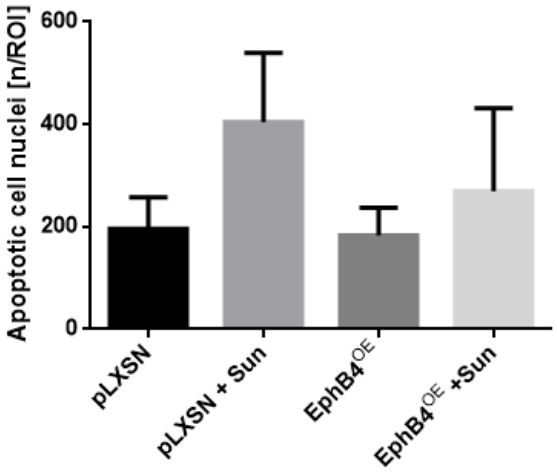

Figure 27: Number of apoptotic cell nuclei per ROI. All groups. Mean±SD.

Treatment of pLXSN-tumors clearly increased the number of apoptotic cell nuclei, as shown in Fig. 28.
(pLXSN: 196.1/ROI pLXSN + Sun: 404/ROI; $p<0.05$)

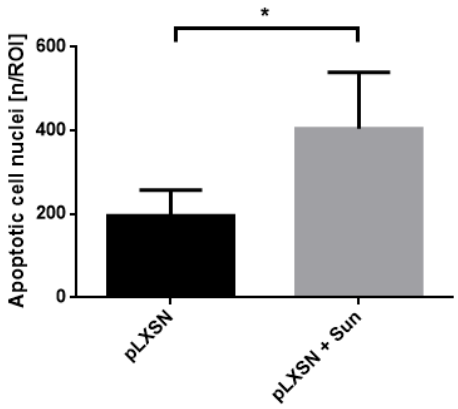

Figure 28: Number of Apoptotic cell nuclei per ROI. pLXSN vs. pLXSN+Sun. Mean±SD.
Student's t-test with Welch's correction. *$p<0.05$

In contrast to the control groups a slight, but not significant increase in apoptotic cell nuclei was detected in the EphB4^{OE} groups following treatment (Fig. 29).
(EphB4^{OE}: 183.2/ROI; EphB4^{OE}+Sun: 269.7/ROI)

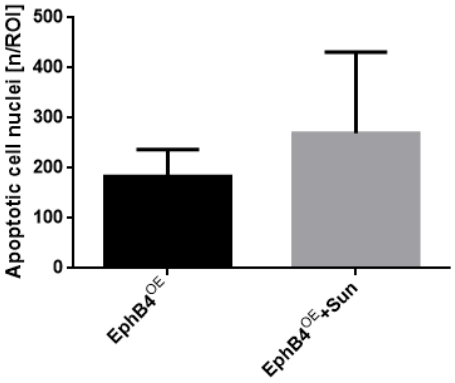

Figure 29: Number of apoptotic cell nuclei per ROI. EphB4 vs. EphB4+Sun. Mean±SD.

Comparing the untreated pLXSN- and EphB4^{OE}-tumors, no significant differences were detected.

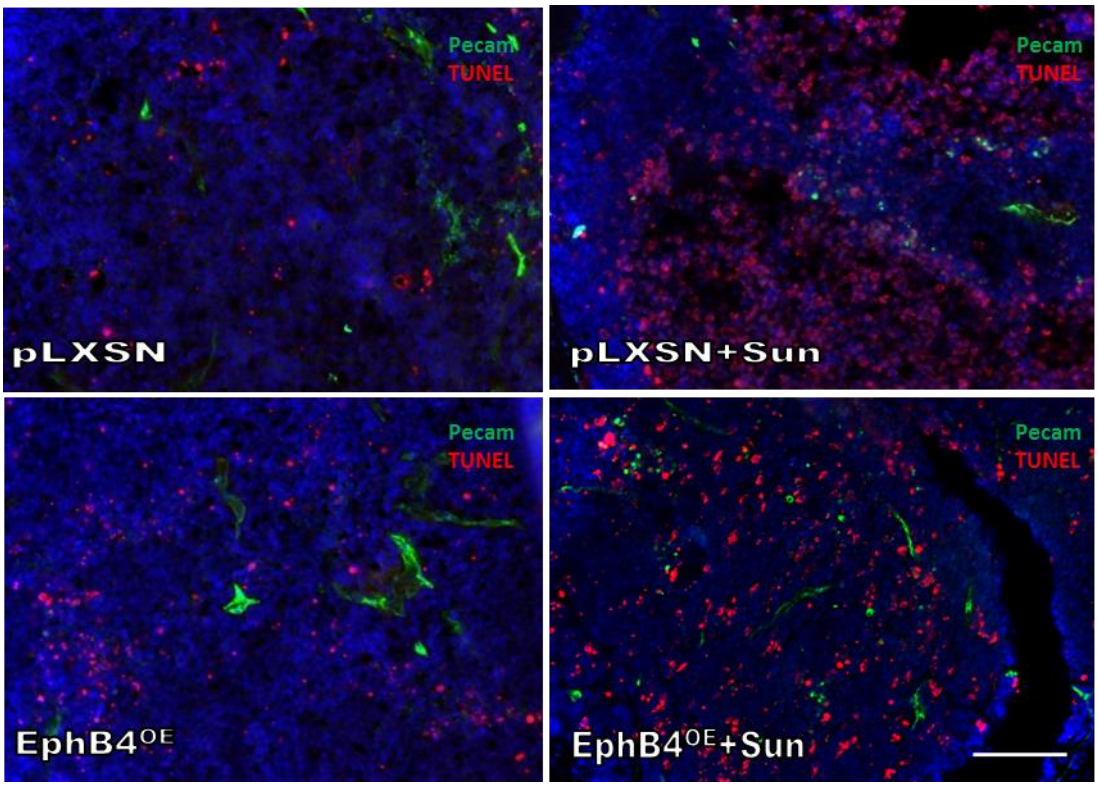

Figure 30: Pecam (green)-, TUNEL (red)-, DAPI- (blue) costaining of the orthotopic xenografts, showing no visible differences concerning quantities of apoptotic cell nuclei between untreated pLXSN and EphB4^{OE}-tumors, in contrast to the large areas of apoptotic cell nuclei characterizing treated pLXSN-tumors. Treated EphB4^{OE}-tumors displayed less increase in apoptotic cell nuclei numbers. Bar indicates 50 µm.

3.3 Chronic Cranial Window

3.1.2 Total Vascular Density

As represented in the overview of all groups, pLXSN-tumors demonstrated the highest amount of vessels, whereas treated pLXSN and EphB4^{OE} groups exhibited the least vascular density. PLXSN-tumors presented a maximum on day 14 p.o., while the amount of vessels in the other groups declined over the course of time (Fig. 31).

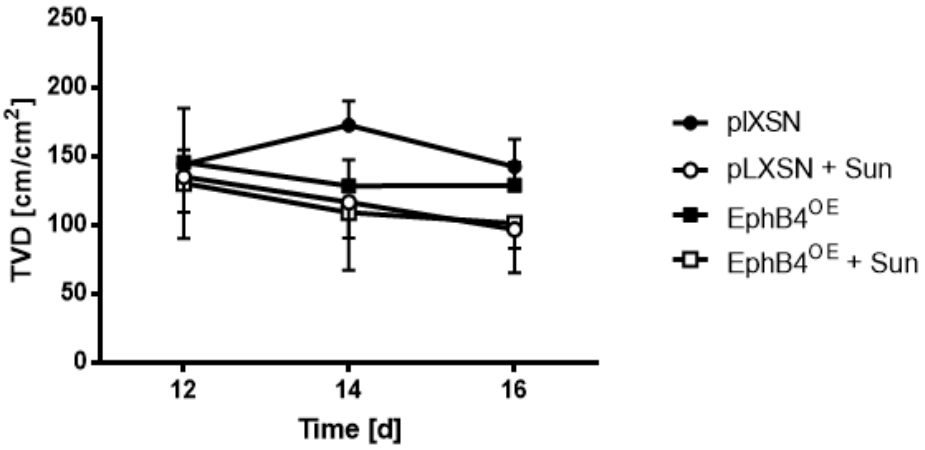

Figure 31: Total vascular density in cm/cm^2 over time in days. All groups. Mean±SD.

Sunitinib application resulted in a decline of vessel density in the treated pLXSN-tumors, effecting a significant reduction on postoperative days 14 ($p<0.001$) and 16 ($p<0.01$) (Fig. 32).

(pLXSN: 144.3 cm/cm^2 on day 12, 172.9 cm/cm^2 on day 14, 142.6 cm/cm^2 on day 16; pLXSN+Sun: 135.4 cm/cm^2 on day 12, 116.8 cm/cm^2 on day 14, 96.9 cm/cm^2 on day 16).

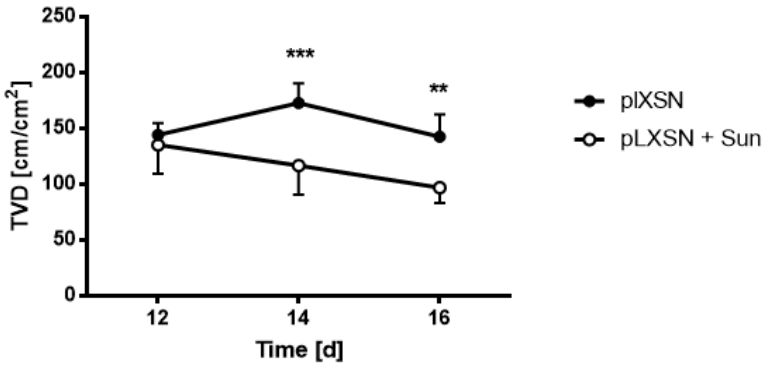

Figure 32: Total vascular density in cm/cm^2 over time in days. pLXSN vs. pLXSN+Sun. Mean±SD. Two-way Anova with Sidak correction. ***p<0.001, **p<0.01

Untreated pLXSN-tumors revealed a significantly (p<0.05) increased TVD compared to untreated EphB4^{OE}-tumors on day 14 p.o. (Fig. 33).
(pLXSN: 144.3 cm/cm^2 on day 12, 172.9 cm/cm^2 on day 14, 142.6 cm/cm^2 on day 16; EphB4^{OE}: 145.4 cm/cm^2 on day 12, 128.6 cm/cm^2 on day 14, 129.1 cm/cm^2 on day 16).

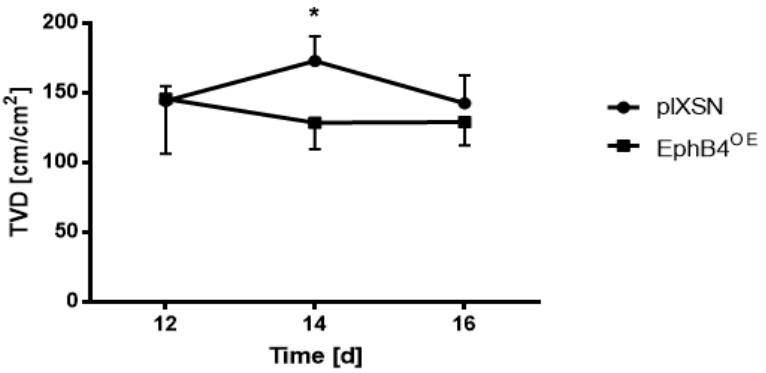

Figure 33: Total vascular density in cm/cm^2 over time in days. pLXSN vs. EphB4^{OE}. Mean±SD. Two-way Anova with Sidak correction. *p<0.05.

Antiangiogenic treatment did not result in a significant reduction of vascular density in EphB4^{OE}-tumors (Fig. 34).
(EphB4^{OE}: 145.4 cm/cm^2 on day 12, 128.6 cm/cm^2 on day 14, 129.1 cm/cm^2 on day 16; EphB4^{OE}+Sun: 130.5 cm/cm^2 on day 12, 109.2, cm/cm^2 on day 14, 101.4 cm/cm^2 on day 16).

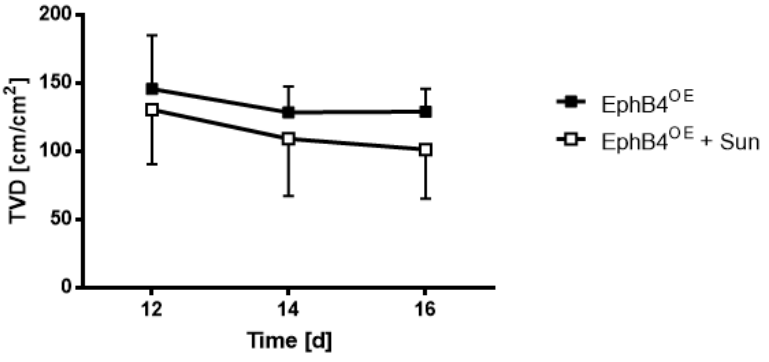

Figure 34: Total vascular density in cm/cm^2 over time in days. EphB4^{OE} vs. EphB4^{OE}+Sun. Mean±SD.

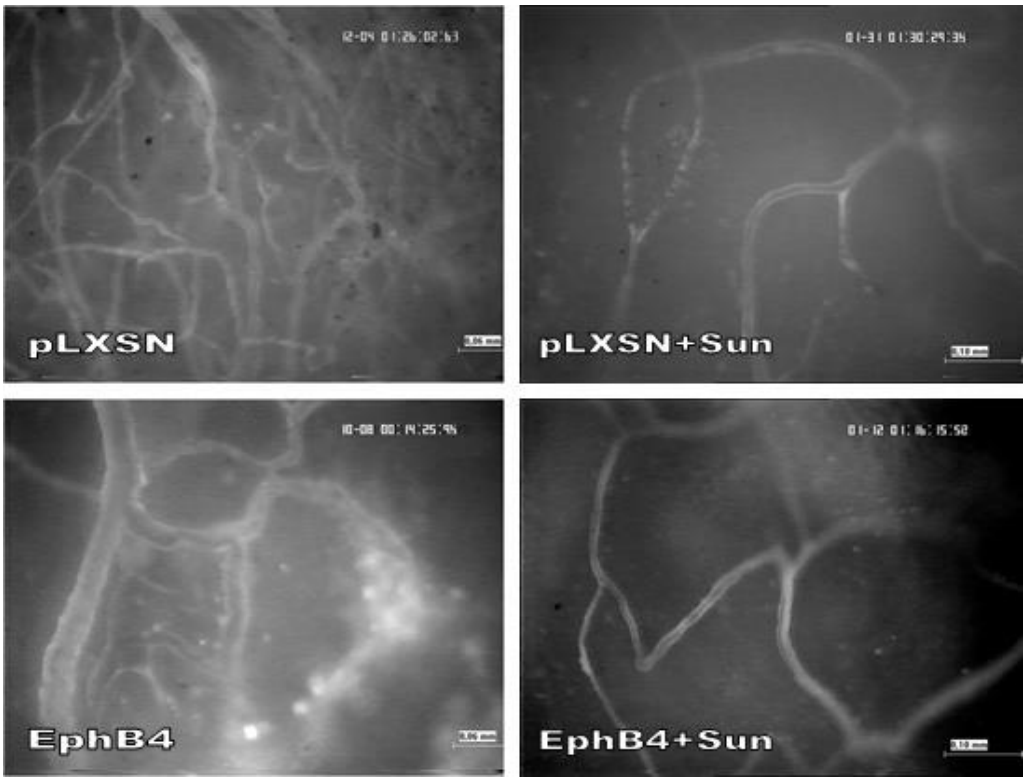

Figure 35: IVM-Images of the different groups on day 14 p.o. after retro-orbital injection of 100µl 2% FITC-Dextran 150 kD. Untreated pLXSN-tumors displayed increased vascularisation compared to untreated EphB4^{OE}-tumors and both treated groups.

3.2.2 Functional Vascular Density

Untreated pLXSN-tumors exhibited the highest FVD, while both treated groups displayed a gradually reduced FVD (overview Fig. 36).

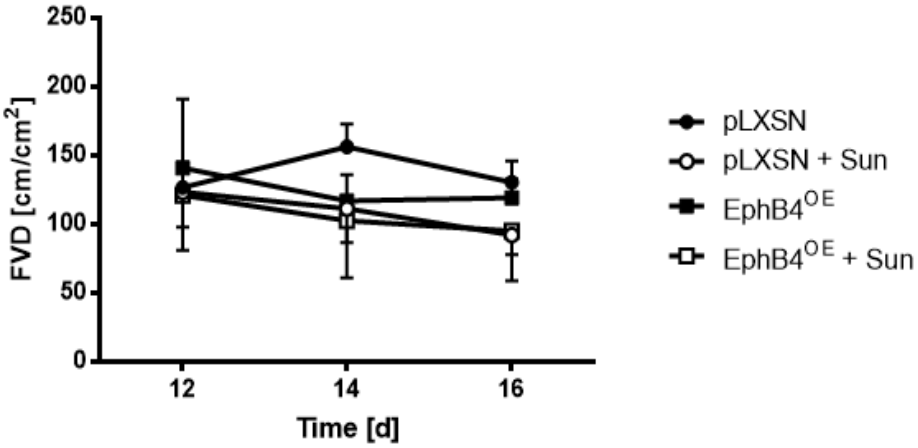

Figure 36: Functional vascular density in cm/cm^2 over time in days. All groups. Mean±SD.

FVD of untreated pLXSN-tumors presented a peak on day 14 p.o., while the FVD of the treated pLXSN-tumors declined constantly (Fig. 37).
(pLXSN: 126.8 cm/cm^2 on day 12, 156.3 cm/cm^2 on day 14, 130.5 cm/cm^2 on day 16; pLXSN+Sun: 123.4 cm/cm^2 on day 12, 109.5, cm/cm^2 on day 14, 92.18 cm/cm^2 on day 16; $p<0.01$ on day 14 p.o., $p<0.05$ on day 16 p.o.)

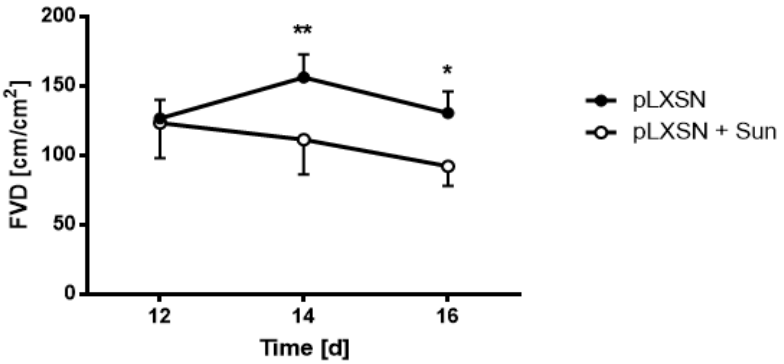

Figure 37: Functional vascular density in cm/cm^2 over time in days. pLXSN vs. pLXSN+Sun. Mean±SD. Two-way Anova with Sidak correction. **p<0.01, *p<0.05

Untreated pLXSN-tumors demonstrated an increase of FVD compared to untreated EphB4^{OE}-tumors, yet the results were not statistically significant (Fig. 38).
(pLXSN: 126.8 cm/cm^2 on day 12, 156.3 cm/cm^2 on day 14, 130.5 cm/cm^2 on day 16; EphB4^{OE}: 140.9 cm/cm^2 on day 12, 117 cm/cm^2 on day 14, 119.3 cm/cm^2 on day 16).

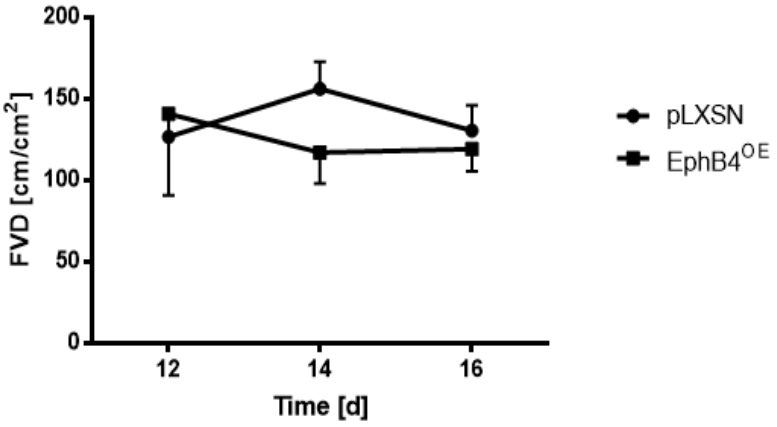

Figure 38: Functional vascular density in cm/cm^2 over time in days. pLXSN vs. EphB4^{OE}. Mean±SD.

In contrast to the control, no differences in FVD were observed while comparing the EphB4^{OE}-tumors (Fig. 39).
(EphB4^{OE}: 140.9 cm/cm^2 on day 12, 117 cm/cm^2 on day 14, 119.3 cm/cm^2 on day 16; EphB4^{OE} + Sun: 121.2 cm/cm^2 on day 12, 102.2 cm/cm^2 on day 14, 95.17 cm/cm^2 on day 16).

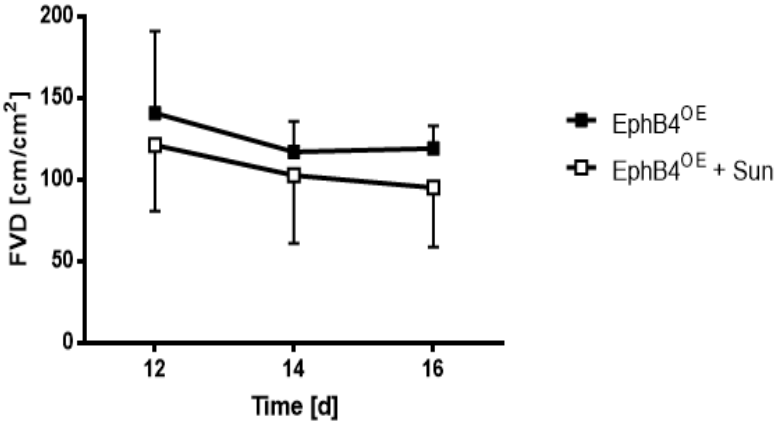

Figure 39: Functional vascular density in cm/cm^2 over time in days. EphB4^{OE} vs. EphB4^{OE}+Sun. Mean±SD.

3.3.3 Perfusion Index

PI calculation revealed a significantly ($p<0.05$) higher perfusion in untreated EphB4^{OE}-tumors on day 12 p.o. compared to the untreated pLXSN-tumors (Fig. 40), while no differences were detected between the other groups (overview Fig. 41).
(pLXSN: 87.8 on day 12, 90.4 on day 14, 91.8 on day 16; pLXSN+Sun: 92.6 on day 12, 95.4 on day 14, 95.0 on day 16; EphB4^{OE}: 95.0 on day 12, 90.8 on day 14, 92.6 on day 16; EphB4^{OE}+Sun: 92.3 on day 12, 93.5 on day 14, 93.2 on day 16).

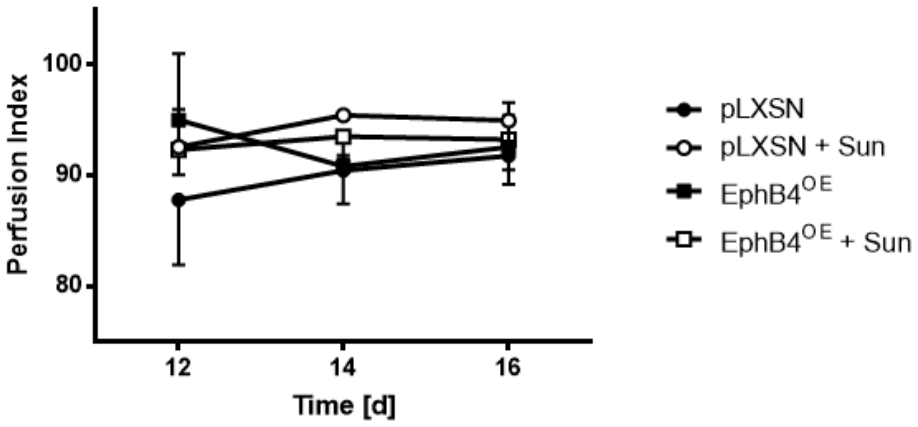

Figure 40: Perfusion Index over time in days. All groups. Mean±SD.

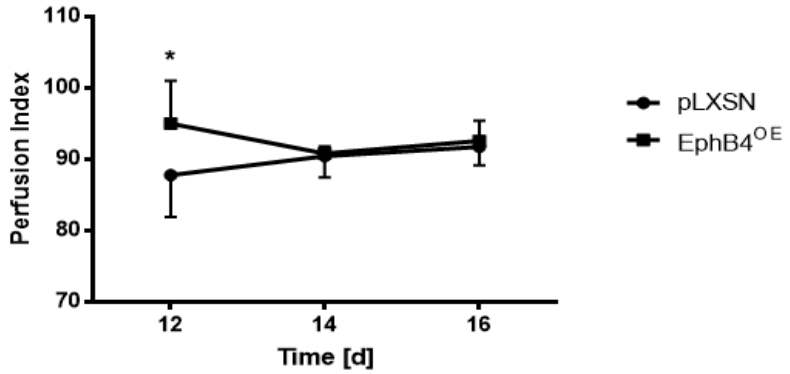

Figure 41: Perfusion Index over time in days. pLXSN vs. EphB4^{OE}. Mean±SD.
Two-way Anova with Sidak correction. *p<0.05

3.3.4 Vessel Diameter

Vessel diameters were found to be highest in the EphB4-overexpression group reaching their maxima on days 14 and 16 p.o. Vessel diameters of treated EphB4^{OE}-tumors decreased over time, while treated pLXSN-tumors displayed only slightly increased vessel diameters (Fig. 42).

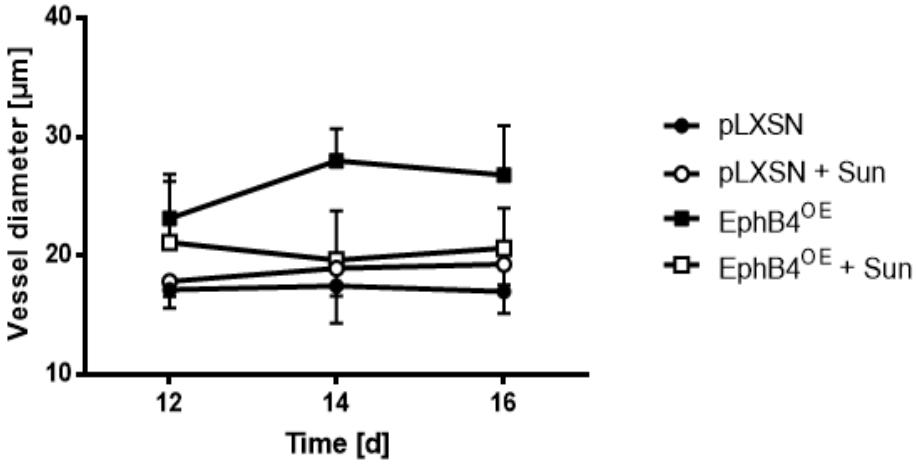

Figure 42: Vessel diameter in µm over time in days. All groups. Mean±SD.

Fig. 43 shows the effect of EphB4-overexpression on tumor vessel diameters. Compared to the untreated pLXSN-tumors, diameters were significantly higher at all three time points of measurement.
(pLXSN: 17.2 µm on day 12, 17.5 µm on day 14, 17.0 µm on day 16; EphB4^{OE}: 23.1 µm on day 12, 28.0 µm on day 14, 26.8 µm on day 16; $p<0.05$ on day 12 p.o., $p<0.0001$ on days 14 and 16 p.o.).

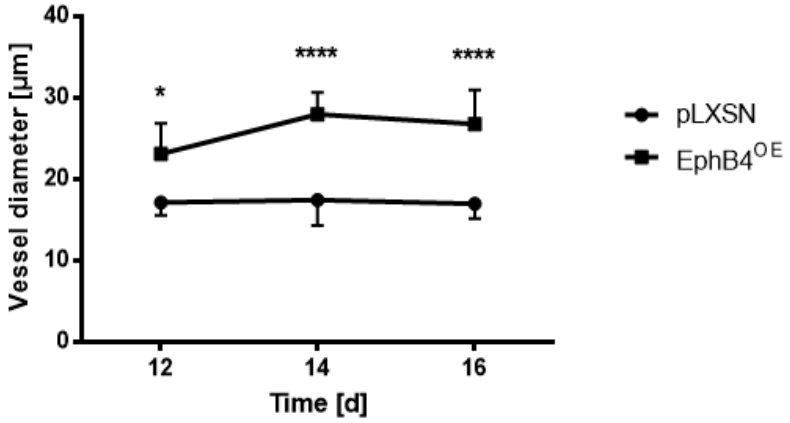

Figure 43: Vessel diameter in µm over time in days. pLXSN vs. EphB4^{OE}. Mean±SD. Two-way Anova with Sidak correction. *p<0.01, **** p<0.0001

Treated pLXSN-tumors experienced a modest increase in vessel diameter during treatment, while the untreated ones demonstrated slightly smaller vessels, which remained constant over the course of the experiment (Fig. 44).
(pLXSN: 17.15 µm on day 12, 17.45 µm on day 14, 16.98 µm on day 16; pLXSN+Sun: 17.84 µm on day 12, 18.94 µm on day 14, 19.29 µm on day 16)

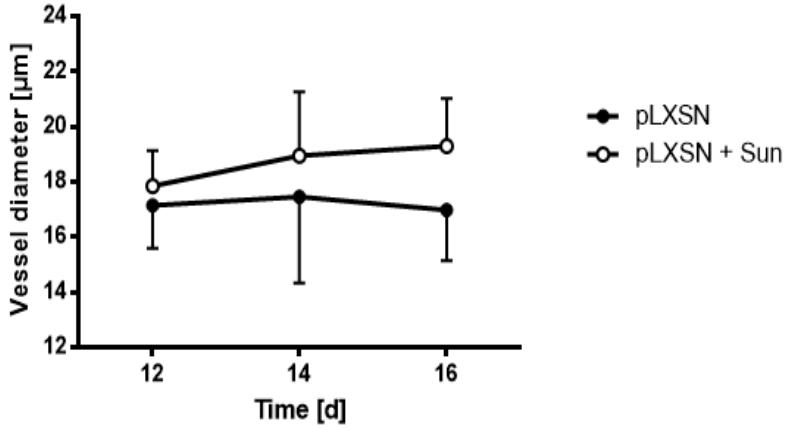

Figure 44: Vessel diameter in µm over time in days. pLXSN vs. pLXSN+ Sun. Mean±SD.

After Sunitinib treatment, vessel diameters were reduced in the treated EphB4^{OE} group, this reduction being significant ($p<0.01$) compared to the untreated group on day 14 p.o. (Fig. 45).

(EphB4^{OE}: 23.13 µm on day 12, 27.99 µm on day 14, 26.79 µm on day 16; EphB4^{OE}+Sun: 21.11 µm on day 12, 19.65 µm on day 14, 20.65 µm on day 16)

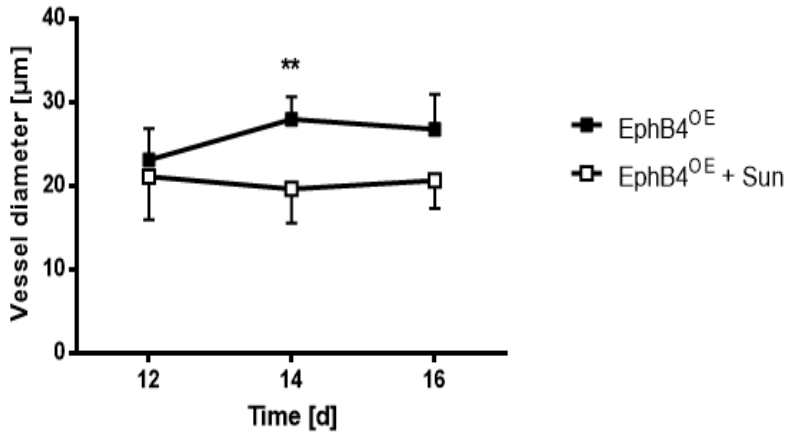

Figure 45: Vessel diameter in µm over time in days. EphB4^{OE} vs. EphB4^{OE}+ Sun. Mean±SD. Two-way Anova with Sidak correction. **p<0.01

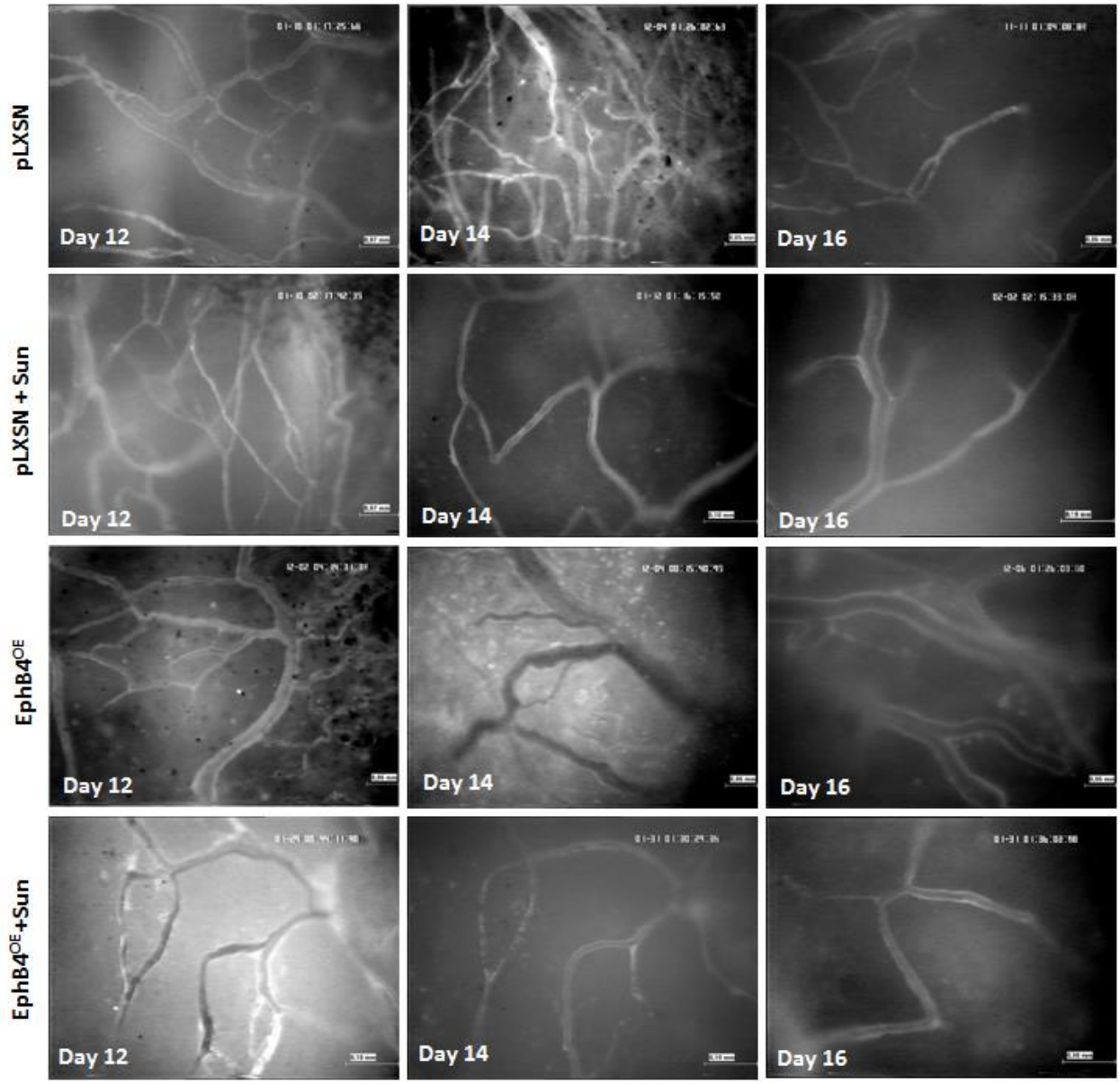

Figure 46: IVM-Images after retro-orbital injection of 100µl 2% FITC-Dextran 150 kD, demonstrating the proliferative effect of EphB4-overexpression on tumor vessels. Untreated pLXSN tumors displaying small vessels and a high vascular density. Treated pLXSN-tumors experienced a moderate increase in vessel diameter during therapy with Sunitinib. Untreated EphB4^{OE}-tumors exhibited enlarged vessel diameters, however this effect was reversed in the treated EphB4^{OE}-tumors.

3.3.5 Volumetrical Blood Flow (Q_v)

Volumetrical blood flow was high in untreated EphB4^{OE}-tumors, while blood flow in treated EphB4^{OE}-tumors was decreased on day 14 p.o. Treated pLXSN-tumors experienced an increase in blood flow, while the blood flow in the untreated pLXSN-tumors remained constant (Fig. 47).

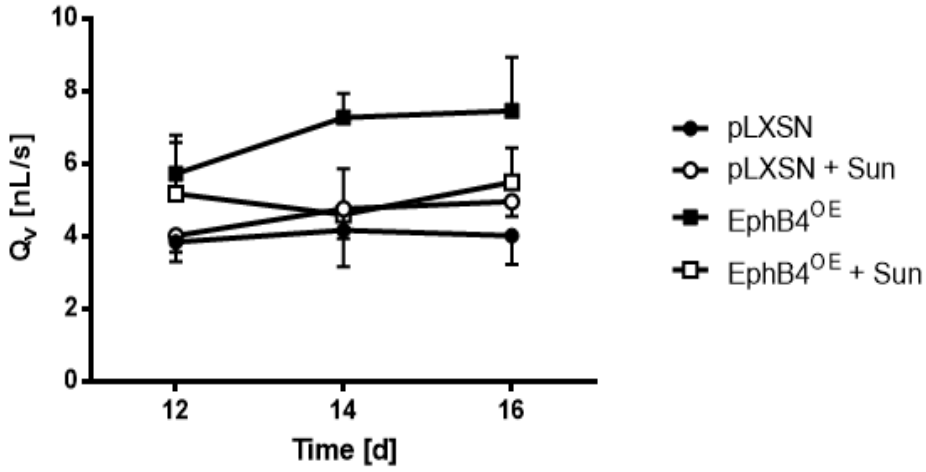

Figure 47: Blood flow in nL/s over time in days. All groups. Mean±SD.

EphB4-overexpression resulted in a significantly increased blood flow on days 12 ($p<0.05$), 14 ($p<0.0001$) and 16 ($p<0.0001$) p.o., while untreated pLXSN-tumors displayed constant blood flow at all time points (Fig. 48).
(pLXSN: 3.8 nL/s on day 12, 4.2 nL/s on day 14, 4.0 nL/s on day 16; EphB4^{OE}: 5.7 nL/s on day 12, 7.3 nL/s on day 14, 7.5 nL/s on day 16).

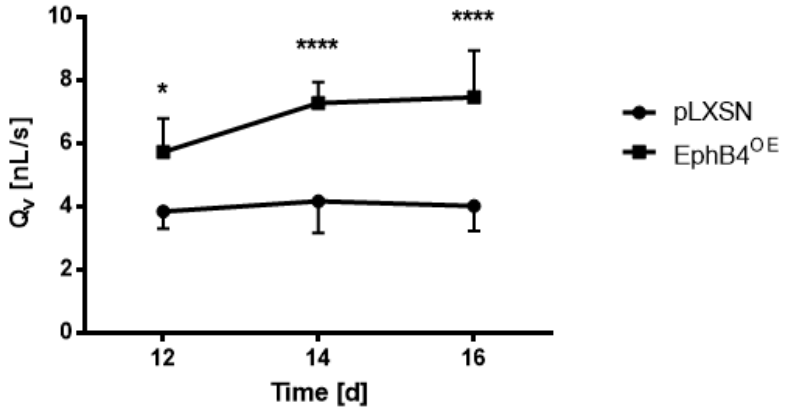

Figure 48: Blood flow in nL/s over time in days. pLXSN vs. EphB4^{OE}. Mean±SD.
Two-way Anova with Sidak correction. *p<0.05, **** p<0.0001

No significant difference was detected between the pLXSN-groups, yet the treated pLXSN-tumors presented a gradually increased blood flow, corresponding to their notable augmentation in vessel diameter (Fig. 49).

(pLXSN: 3.84 nL/s on day 12, 4.17 nL/s on day 14, 4.02 nL/s on day 16; pLXSN+Sun: 4.02 nL/s on day 12, 4.76 nL/s on day 14, 4.97 nL/s on day 16).

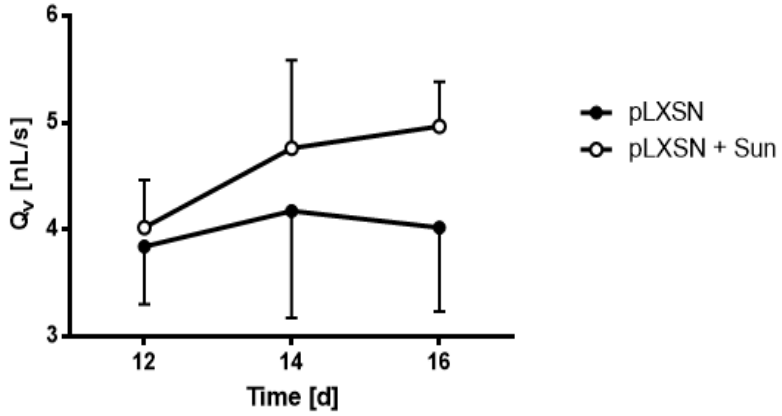

Figure 49: Blood flow in n/s over time in days. Comparing pLXSN and pLXSN+Sun. Mean ± SD.

Comparison between EphB4^{OE} groups revealed significant differences, reflecting the effect of the treatment on day 14 ($p<0.01$) and day 16 ($p<0.05$) p.o. (Fig. 50).
(EphB4^{OE}: 5.73 nL/s on day 12, 7.28 nL/s on day 14, 7.46 nL/s on day 16; EphB4^{OE}+Sun: 5.18 nL/s on day 12, 4.6 nL/s on day 14, 5.5 nL/s on day 16)

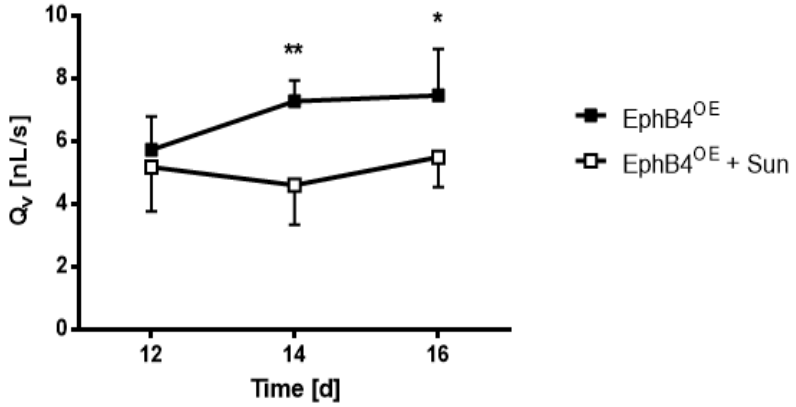

Figure 50: Blood flow in nL/s over time in days. EphB4^{OE} vs. EphB4^{OE}+Sun. Mean±SD. Two-way Anova with Sidak correction. **p<0.01, * p<0.05

3.3.6 Permeability Index

High extravasation of the fluorescence marker was found in all four groups resulting in no statistical differences between the groups. Neither EphB4-overexpression nor Sunitinib treatment seemed to have an effect on vascular sealing (Fig. 51).
(pLXSN 1.07 on day 12, 1.07 on day 14, 1.07 on day 16; pLXSN + Sun: 1.09 on day 12, 1.08 on day 14, 1.09 on day 16; EphB4^{OE}: 1.08 on day 12, 1.09 on day 14, 1.08 on day 16; EphB4^{OE}+Sun: 1.08 on day 12, 1.08 on day 14, 1.06 on day 16).

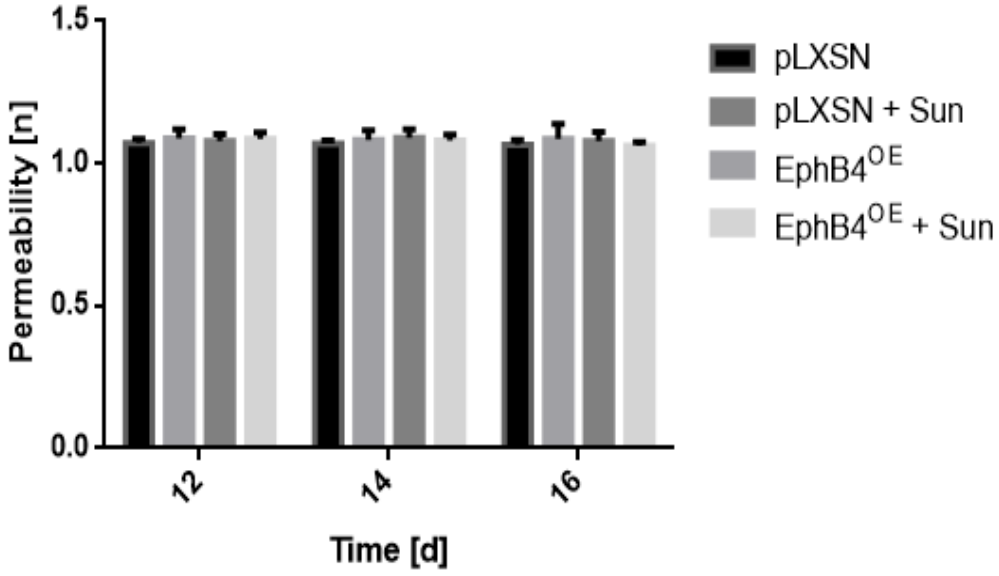

Figure 51: Permeability index over time in days. All groups. Mean ± SD.

4 Discussion

4.1 Methods

4.1.1 Ecotropic System

The ecotropic system is a method of using highly transfectable HEK 293 T-cells, which produce large quantities of viral vectors that can transport a gene of interest into a target cell. Phoenix-ECO cells, created in 1993 and improved by introduction of EBV-episomes in 1996, are an easy and secure way to induce an overexpression of genes of interest by generating a stable retrovirus as soon as 48 hours, and for at least 30 days [71, 72].

Since studies have shown that the EphB4-receptor in glioma is mainly expressed on vascular ECs, it was necessary to establish an EphB4-overexpression only on ECs of the tumor vessels, not the tumor tissue itself [39, 82]. Therefore we used a viral vector that was aimed at murine cells only, and coimplanted human glioma cells together with the Phoenix-ECO cells into nude mice. The objective of this approach was that the human glioma cells would not be infected by the viral vectors of the Phoenix-ECO cells, but rather the ECs of the mice, which were acquired by the tumor for angiogenesis.

We used Phoenix-ECO cells, which had been established in our laboratory and whose successful functioning for inducing an EphB4-overexpression had been proven by Erber *et al.* via transfection of murine NIH 3T3 fibroblast cells, followed by immunohistochemical staining for EphB4, demonstrating its correct presence on the cell surface [39]. The counter experiment had been performed by adding SF126 glioma-cells to the Phoenix-ECO cells, and following that selection for Neomycin resistance, which resulted in decay of all SF126 cells [39]. Further analysis by means of Western Blot and polymerase chain reaction (PCR) had substantiated the infection of murine but not glioma cells [39]. The functioning of the RTK itself had been shown by immunoprecipitation of EphB4 to assess phosphorylation of the receptor**,** as well as immunoblotting with an antiphosphotyrosine-specific antibody in infected NIH 3T3 cells, displaying increased results compared to control vectors [39]. Immunohistochemistry of SF126-xenografts, coimplanted subcutaneously with Phoenix-ECO cells, had confirmed infection of ECs and exclusive expression of EphB4 on tumor vessels [39]. Again real-time PCR and immunoblot had verified the presence and overexpression of EphB4 within the tumors [39].

We also tested for complete equipment of the retrovirus by the packaging cell, by selecting a triple-therapy consisting of hygromycin (selecting for gag-pol protein), diphtheria toxin (selecting the env protein) and G418 (testing for the Neomycin resistance gene), which are necessary for the virus' infectiousness.
In addition, an authentication report was ordered, confirming the 100% pure quality of the Phoenix-ECO cells' DNA and their accordance to cell bank data, before the start of the experiments.

4.1.2 Orthotopic Implantation

The orthotopic implantation is a minimally invasive operation, importing the cells using the smallest possible access way, by means of a 1µl Hamilton-needle. Thus, potential bleedings as well as inflammatory processes subsequent to the operation should be excluded, which could alter the tumor environment and in this way distort the experimental results.
The advantages of the orthotopic model compared to a heterotopic one, e.g. in subcutaneous implantation of glioma cells, are lower implanted cell numbers, allowing a more precise differentiation of tumor growth, as well as the specific microenvironment of the brain, which significantly differs from the one in the subcutis. The disadvantages of the orthotopic model are the more complex technique of implantation, as well as time and costs in measuring the tumors by means of small-animal MRIs, whereas subcutaneously implanted tumors are simply injected under the skin and measured by manometric devices.

Factors that can modify the operation and cause variances between the groups are the use of different cell passages, wrong cell concentrations and the injury of brain tissue while preparing the access in the skull with the 23-gauge needle. To minimize these complications, we always used the same cell passage for each implantation and tried to reduce the error of wrong cell concentrations by optimizing the protocols for preparation in the cell culture. Appropriate practice by injection of Evans blue into training animals before initiation of the experimental studies was intended to resolve the last-mentioned complication.

Regarding the question, whether implantation of human SF126- glioma cells within an orthotopic, but non-human tissue, may have affected the experimental results, e.g. by developing mutations, a study by Jones *et al.* showed that CRC-cells, maintained as cell lines *in vitro* and as xenografts in nude mice, displayed the same gene mutations as the original tissue [83]. A large-scale analysis by Winter *et al.*, concerning gene expression investigated by highly cited study groups, resumed that gene mutations tend to be found more often in cell lines and xenografts than in primary tissues, without, however, showing significant differences [84]. Other studies supported the orthotopic model, proving that tumors grown in immunodeficient mice featured the same genetic profile and phenotype as the original tissue [85, 86].

4.1.3 Antiangiogenic Therapy

The big difference in tumor growth between EphB4^{OE} and pLXSN-tumors raised the question of whether to treat the tumors simultaneously, or to determine a certain tumor volume as a starting point for treatment. Since we considered the latter method as adding complexity to the statistical evaluation and interpretation, and also the fact that we would have to extend the protocol for EphB4^{OE}-tumors for more than 30 days, uncertain if the Phoenix-ECO cells would still produce retroviral vectors, we decided to go with the first experimental setup. It was also uncertain up to that point if the small EphB4^{OE}-tumors would survive the high-dose antiangiogenic treatment, and if there would still be enough material to be evaluated in the immunohistochemistry.

The antiangiogenic therapy posed difficulties in itself, especially regarding the control animals, which carried a heavier tumor load, frequently causing a reduced status in the animals. These adverse side effects were most likely due to the high dose of 80mg/kg/BW Sunitinib (recommended Sunitinib dose in human patients: 50 mg/kg/BW) [78]. The high dose administration was chosen on the basis of previous experiments in our study group, which had shown no effect of low-dose treatment on implanted tumors within the brain.

4.1.4 Magnetic Resonance Imaging

Initially we performed MRI-scans in T1- and T2- weighting to determine tumor edema, by subtracting the results of the contrast-enhancing T1-weighting from the liquid-revealing T2-weighting. However T1-scans presented stronger signals than the respective T2-scans, therefore calculation of edema was not feasible. Thus, only tumor volume was determined by evaluation of the scans in the T1-weighting.
Anesthesia of treated mice in the MRI proposed difficulties, since low concentrations of anesthesia resulted in blurry pictures caused by the moving mice, while higher doses would cause bradypnoe and subsequent imminent exitus of animals. Thus, a close monitoring of the respiration of the mice as well as a correspondingly continuous adjustment of the anesthesia was indispensable.

4.1.5 Immunohistochemistry

The reasons for the differences observed in tumor growth were set to be revealed by immunohistochemical staining of the tumors. In this area, falsification of data could happen by varying perfusion quality or cutting quality of the tumor slices. The researcher's subjectivity was a factor while assessing vessel density and pericyte coverage. To avoid biased acquisition of data, all images were evaluated blindfolded.

4.1.6 3D-Spheroid Essay

Instead of just spraying the tumor and Phoenix-ECO cells onto the prepared surface of the brain in the chronic cranial window experiments, we decided to perform a 3D-Spheroid Assay. The 3D-Spheroid imitates glioma development and angiogenesis realistically by facilitating vessel network formation by providing multiple starting points for sprouting ECs [80]. The spheroid further allows more subtle detection of newly formed vessels during initial steps of angiogenesis, while the tumors, which are sprayed on the cerebral surface in the chronic cranial window, are too large to enable delicate observation of these early processes [87]. Thus, vessels can only be examined in completed tumor vasculogenesis in this model [87].

4.1.7 Chronic cranial window

The chronic cranial window was set up to retrieve live pictures of the tumor vessels, confirming the effect of EphB4-overexpression on vascular morphology shown by Erber *et al.* as well as to verify EphB4-mediated resistance towards antiangiogenic treatment, which had been observed in the dorsal skinfold chamber in previous experiments in our study group [39].

The method of the operation has long been established and continuously improved in the laboratory, its main difficulties are based on the complexity of the operation. Being an open skull surgery, it carried risk factors such as rupture of the sagittal sinus while removing the bone flap, injury to the brain surface while removing the dura mater or intrusion of dental cement into the operative window. Ruptures of the sagittal sinus were compressed with small swabs that were soaked with saline solution until the bleeding ceased. Injuries of the brain surface were treated by rinsing with saline solution and compression with small swabs that were soaked with saline solution. Following intrusion of dental cement into the operative window, a new site for implantation of the spheroid was required, when the first one had been damaged. These complications did not cause exitus of the animals; however, they diminished the quality of the experiments due to subsequent inflammatory processes in the site of implantation. The challenges were met by appropriate training before initiation of the experiments.

4.1.8 Intravital Microscopy

IVM was performed to examine angiogenesis and tumor behavior *in vivo*, thereby delivering dynamic impressions and details about the vascular system. The advantages over 2D-images in immunohistochemistry are: the possibility of observing the tumor in a 3-D access; live determination of vessel functionality, the tendency of sprouting and blood flow as well as evaluation of vascular sealing by extravasation of FITC-Dextran; and in general displaying processes more realistically than *in vitro*.

A detrimental factor was the relatively late date of the examination days, starting on day 12 p.o., which was based on the observations by Erber *et al.*, who had documented the most remarkable effects of EphB4-overexpression on day 14 p.o. [39]. However these data had been acquired in a dorsal skinfold chamber, which provides a higher durability

compared to the chronic cranial window of the head, whose quality decreased after day 14 p.o. On day 16 p.o. besides a reduced quality of the window, furthermore, edema, as a consequence of progressive tumor development, posed noteworthy challenges.

In addition, it has to be taken into account that placement of the spheroid on the cerebral surface does not represent the natural location of glioma, which typically develop intracerebrally. Regarding this limitation, Coomber *et al.* had conducted experiments demonstrating similar vessel morphology and network formation of glioma cells implanted into muscular tissue and into brain tissue, which clearly differed from the vessels of the host tissue [88]. Referring to this study it is possible to assume that these findings can also be transferred to vessel networks of glioma located on the cortex and in the cerebrum.

4.2 Results

4.2.1 Orthotopic Xenografts

Analysis of the orthotopic xenografts revealed significantly slower tumor growth by EphB4^{OE}-tumors compared to pLXSN tumors. These results conflict with previous data in our study group as well as with data by Erber *et al.* in s.c. implantations, where EphB4^{OE}- and pLXSN-tumors displayed the same growth velocity [39, 69].

Explanatory approaches comprise the different locations of implantation as well as varying cell concentrations in the experimental setups. In earlier experiments of our study group $4x10^6$ cells had been implanted into the subcutis; Erber *et al.* had injected $1x10^6$ cells, while in our case $2x10^4$ cells were implanted into the cerebrum [39, 69].
In addition the brain presents a different microenvironment than the subcutis, featuring the blood-brain barrier, micro-glia and astrocytes, possibly influencing tumor growth and development.
Supporting the argument of different environments affecting tumor tissue, a study by Fukumura *et al.* revealed that subcutaneously implanted colon carcinoma tumors displayed higher amounts of vessels than their orthotopic counterparts metastasizing into the liver [89].

Contradicting this argument are the experiments by Coomber *et al.*, who observed similar vessel characteristics within astrocytoma tumors, implanted into muscles and the brain, clearly differing from their respective environment [88].

In order to guarantee sufficient experimental quality standards, new SF126-glioma cells were purchased and used in our experiments in order to avoid cellular changes due to genetic and molecular alterations that may occur in high passage cells. Trial orthotopic experiments with high passage SF126-glioma cells revealed aggressive and fast tumor growth, which was not tolerated by experimental animals, especially in combination with Sunitinib treatment.

In addition to the experiments by our study group and Erber *et al.*, a study by Chen *et al.* investigated effects of an EphB4-overexpression in glioma [90]. By means of plasmid transfection in U87 and U257 glioma cells, a significantly increased tumor growth in subcutaneously implanted xenografts was observed [90]. However the experimental design of this study group was based on the assumption that EphB4 is generally overexpressed by all cells in glioma tissue and neglects the observations by Erber *et al.*, who had shown that EphB4 is predominantly expressed on the ECs of the tumor vessels [39, 90]. Furthermore, their study differed with regard to the cell lines used, the lower injected cell concentration ($1x10^6$) and the method of inducing the overexpression [90].
Conclusively, the approach of transfection, the method of overexpression as well as microenvironment of the implantation site seem to play a relevant role, exerting very different effects concerning the growth behavior of the tumors. Thus, only a comparison between the different experimental groups is possible; however, no general declarations regarding the influence of EphB4 on the growth behavior of glioma can be deduced.

Concerning the main focus of the current study, EphB4-mediated resistance towards antiangiogenic treatment, EphB4-overexpressing tumors were revealed to be clearly less affected by the treatment than the treated pLXSN-tumors. These findings support previous data of our study group, which demonstrated a resistance of $EphB4^{OE}$-tumors towards Sunitinib in the s.c. xenograft model [69]. Yet our immunohistochemical stainings did not confirm the findings of sustained pericyte-endothelial cell interaction, which was depicted as the pivotal factor for antiangiogenic resistance in these

experiments [69]. This difference is probably due to the varying concentrations of Sunitinib, as in the experiments performed in the s.c. model 40 mg/kg BW Sunitinib were applied, whereas in this study 80 mg/kg BW were administered [69].

Treated EphB4^{OE}-tumors further displayed the same radical reduction in pericyte-endothelial cell interaction as treated pLXSN-tumors, and a considerable destruction of vessels, which even though it did not test statistically significant in vessel density, was nevertheless clearly observed in the stainings.

Despite the considerable effect of Sunitinib on the vascular system, no significant difference in growth behavior between treated and untreated EphB4^{OE}-tumors was observed. Neither proliferation was remarkably impaired, nor was the number of apoptotic cells increased in contrast to the pLXSN-tumors, where huge apoptotic areas characterized the tumor tissue and proliferation was diminished considerably in response to Sunitinib treatment.

4.2.2 Intravital Microscopy

Analysis of IVM recordings confirmed the EphB4-overexpressing effect on vessel morphology as shown by Erber *et al.* and by previous experiments of our study group in the dorsal skinfold chamber [39, 69]. Yet, in contrast to the findings in our study group the vascular effect of the EphB4-overexpression by enlarging vessel diameter was inhibited following antiangiogenic treatment [69]. Differing concentrations of the administered treatments in the respective experimental setups (high dose vs. low dose Sunitinib application) are a possible explanation for these discrepancies.

PLXSN-tumors experienced a slight increase in vessel diameter following treatment, supporting data by Czabanka *et al.*, who had shown a considerable increase in vessel diameter in implanted SF126-glioma cells during treatment [63]. Correlating with the results concerning vessel diameter are the results regarding blood flow. EphB4-overexpressing tumors displayed an increased blood flow compared to the untreated pLXSN-tumors, yet the blood flow was reduced in the EphB4^{OE}-tumors following treatment. Between the pLXSN-groups an increase in blood flow in treated tumors was observed, however testing insignificant, most likely due to a high standard deviation.

Interestingly, in the previous experiments in the dorsal skinfold chamber the highest blood flow was found within treated EphB4^{OE} groups, followed by the untreated

EphB4^{OE}- group and treated pLXSN-tumors [69]. These differences are most likely due to the high dose treatment with Sunitinib, whose antiangiogenic effects at these concentrations are presumably so toxic that vessels are destroyed in large amounts.

High dose treatment significantly reduced TVD and FVD in the pLXSN-tumors, while no difference was observed between the EphB4^{OE}-tumors. These results support previous findings of our study group, in the dorsal skinfold chamber, with the same experimental groups as well as data by Czabanka *et al.*, who described a significant decrease of TVD and FVD in antiangiogenically treated SF126 glioma cells [63, 69].

Regarding vessel permeability (PI), no significant differences were detected between the four groups.

Vascular permeability was high at all time points, showing no visible or statistical difference between any groups. Erber *et al.* had demonstrated a decreased permeability of EphB4-overexpressing tumors, however on day 21 p.o. [39]. The previous experiments of our study group in the dorsal skinfold chamber had revealed the lowest permeability within treated EphB4^{OE}-tumors on day 18 p.o., but since the chronic cranial window only provided images of high-quality until day 16 p.o. we were not able to confirm these findings [69].

4.3 Role of EphB4-ephrinB2 signaling in different tumor entities

4.3.1 Forward, Reverse and Ligand-Independent Signaling

Next to divergent experimental setups, which likely effected diverse outcomes between studies targeting the role of EphB4 in glioma, bidirectional signaling of the EphB4-ephrinB2 pathway has to be taken into account. Due to the several components of this pathway, it is difficult to define which one is responsible for the respective findings in the different studies. In the case of EphB4-overexpression, it is supposed that on the one hand forward signaling in the EphB4-expressing cell is increasingly being activated, on the other it also has to be reckoned that reverse signaling in the ephrinB2-expressing cell might be progressively turned on.

The individual parts of the EphB4-ephrinB2 system have been attributed with differing impacts on tumor progression and suppression, depending on whether forward signaling, reverse-signaling or ligand-independent signaling are activated primarily. Ligand-independent signaling confers to mechanisms such as Eph-receptor clustering, which without binding of a ligand, results in phosphorylation and activation of the tyrosine kinase as well heterooligomerization of EphAs and EphBs and thereby subsequent triggering of signaling [91, 92]. Even mere overexpression of Eph-receptors can exert ligand-independent signaling [93].

4.3.2 EphB4 in Breast Cancer and Prostate Cancer

In breast cancer, ligand-independent signaling is currently attributed with a highly tumorigenic effect, since EphB4 has been found to be elevated and less phosphorylated than normal in a majority of these tumors, while ephrinB2 is reduced simultaneously [94-97]. Overexpression of EphB4 in non-transformed mammary epithelial cells resulted in conversion to a malignant phenotype and further intensified proliferation, migration and invasion of breast cancer and prostate cancer cells *in vitro* [94]. An inhibition of tumor growth and even reversal of the effects of EphB4-overexpression *in vitro* and *in vivo* was achieved in several studies by induction of forward signaling via ephrinB2-Fc [94, 95, 98]. Diminished cell motility and invasion by inhibition of matrix metalloproteinase 2 (MMP-2), as well as reduced cell viability by activation of the Abl-Crk signaling pathway have been detected to be responsible for this effect [95]. Experiments, targeted on blocking the effects of EphB4 or knocking-down the receptor *in vivo*, revealed a reduced tumor growth and microvasculature as well as increased apoptosis within the xenografts, further underling the tumor promoting effect of EphB4 [96, 99].

Fortified stimulation of reverse signaling in breast cancer *in vivo* by means of EphB4-Fc, lacking the cytoplasmatic domain, revealed to be cancer promoting by producing larger tumors as well as increased vessel diameters [100].

Since the normal mammary gland expresses both EphB4 and ephrinB2, their homeoostasis seems to be pivotal for prevention of tissue degeneration [100].

4.3.3 EphB4 in Squamous Cell Carcinomas of the Head and Neck and Renal Cell Carcinoma

Supporting the importance of EphB4-overexpression as well as ligand-independent signaling on tumor progression in breast cancer are findings in the squamous cell carcinomas of the head and neck (HNSCC). Ferguson *et al.* proved via immunohistochemical stainings a significant increase of EphB4 during cancer progression, from a very low expression in normal tissue, to dysplasia and finally cancer in HNSCC [101]. Interestingly the same study group also attributed EphB4 tumor suppressive effects, as they examined RCC, and detected decreased EphB4-expressions contrariwise to tumor progression [101].

Similar to experiments in breast cancer cells increased activation of forward signaling in HNSCC resulted in an inhibited growth *in vivo* just like knock-down of EphB4 or blockade of EphB4-ephrinB2 interaction would do [99, 102, 103].
Immunohistochemical stainings of tumors, which underwent an increased forward signaling, thereby revealed findings similar to the ones made in our study, such as a significant reduction of Ki67-positive cells, yet without affection of apoptosis or vessel density [102]. Vessel diameter however was decreased [102]. Furthermore, an increased α-smooth muscle actin (α-SMA, detects pericytes) endothelial cell interaction was detected, which is related to a higher vessel maturation [102]. Thus ephrinB2-Fc induced signaling was held responsible for improved equipment of vessels with pericytes, without influencing the vascular network formation [102]. For the inhibited tumor growth, reduced activation of two important promotors of angiogenesis in the form of MMP-2 as well as VEGF-A was accounted [102].

4.3.4 EphB4 in Melanoma

Studies, which focused on the role of EphB4 in melanoma cells, produced differing, in parts contradictive results. Yang *et al.* found elevated levels of EphB4 in highly aggressive, metastasizing murine melanoma cells *in vitro* [104]. In contrast to the observed suppressive effects of ephrinB2-induced forward signaling in breast cancer and HNSCC, this signaling pathway was accredited a tumor promoting impact by

facilitating cell migration and invasiveness via the RhoA-pathway (modulates the cytoskeleton), while its inhibition depleted these effects [104]. Ligand-independent signaling also does not seem to play a pivotal part in this tumor entity, as they demonstrated equal coexpression of both ligand and receptor [104].
The same study group confirmed their findings four years later in an *in vivo* study with the same cell types, observing an accelerated tumor growth, reduced apoptosis and enlarged vessel diameters in melanoma cells, coexpressing elevated numbers of EphB4 and ephrinB2 [105].

Yet a study by Huang *et al.*, examining human B16 melanoma cells that were subjected to an induced EphB4-overexpression, revealed a clear deceleration of growth velocity in s.c. xenografts, whereas knock-down of EphB4 enhanced tumor growth [106]. The study group accounted a disturbed arterial-venous-vessel pattern for the findings in the EphB4-overexpressing tumors, since immunohistochemical stainings displayed on the one hand significantly reduced vessel densities, on the other almost complete eradication of ephrinB2 on ECs [106]. As a cause, they determined an EphB4-directed induction of apoptosis in ephrinB2-presenting cells [106].

Martiny-Baron *et al.* conducted experiments concerning EphB4-signaling in melanoma cells, type A-375, by creating tumor cells, which expressed soluble EphB4-receptors, lacking the intracellular domain [62]. Thus, interfering with signal activation in both ways effectuated complete inhibition of growth *in vivo* as well as inhibited capillary sprout formation in 3-D angiogenesis essays and cell-to-cell adhesion *in vitro* [62].

4.3.5 EphB4 in Colorectal Carcinoma

In CRC, EphB4 and ephrinB2 also play a decisive and ambiguous role. While Batlle *et al.* revealed that EphB4 is less expressed the more a tumor is progressing, later studies by Kumar *et al.* and Lv *et al.* depicted EphB4 as a key factor in cell degeneration, as they presented increased levels of the receptor in higher grades of CRC, whereas normal colon tissue did not express the receptor [55, 61, 107]. Knock-down of EphB4 by Kumar *et al.* resulted in significantly reduced CRC cell numbers *in vitro*, while knock-

down of ephrinB2 proved to have no effect, for which reason ligand-independent signaling was accredited a pivotal role for tumor progression [55].

Liu *et al.*, induced an ephrinB2-overexpression in CRC-cells, expecting enhanced tumor growth and progression via improved angiogenesis, however obtaining results contrariwise, in particular by prevention of growth in subcutaneously implanted tumors [108]. Immunohistological stainings revealed an increased vessel density as well as reduced cell proliferation, for which reason it was concluded that ephrinB2-overexpression inhibited tumor growth by causing an insufficient vascular system [108].

4.3.6 EphB4 in Glioma

Both EphB4 and ephrinB2 are barely to be found in the normal brain, whereas EphB4 has been proven to be significantly increased in glioma, while concerning ephrinB2 unmodified and augmented levels have been detected [39, 82]. Erber *et al.*, who found both to be significantly elevated and coexpressed in glioma, focused on examining EphB4-overexpression in general and on enhanced reverse signaling in ECs, which both produced similar results [39]. EphB4-overexpression did not affect initial tumor angiogenesis; however, subsequent vessel morphology and stability by means of enlarged vessel diameters and reduced permeability via intensified pericyte-endothelial interaction and stronger activation of the angiopoietin system [39]. According to these findings, ephrinB2-reverse signaling as well as generally enhanced pathway activation exert a tumor promoting effect in glioma.

Chen *et al.* also showed a tumor promoting effect by means of solely EphB4-overexpression *in vivo*, resulting in significantly increased tumors and improved tumorigenicity *in vitro*, while knockdown of the receptor reverted those results [90]. Induction of forward-signaling via ephrinB2-Fc did not affect tumor growth, neither in EphB4-overexpressing, nor in control tumors [90].

A study by Li *et al*. established a connection between EphB4 and the Notch signaling pathway and one of its ligands DLL4, both having been found to exert crucial roles on physiological angiogenesis during embryonal development and tumor vasculature as

well [109]. Furthermore ephrinB2 represents one of the possible downstream targets following activation of the Notch signaling pathway [109]. Since DLL4 has been found to be upregulated in tumor vasculature in adults, Li *et al.* created DLL4-overexpressing U87-glioblastoma cells, by means of retroviral vectors which were implanted subcutaneously into immunodeficient mice [109]. DLL4-overexpressing tumors proved to promote tumor growth as well as to reduce survival of the mice [109]. When treated with bevacizumab the DLL4-overexpressing tumors were revealed to be resistant towards treatment, while tumor growth was reduced and survival of the mice significantly increased following treatment in the control groups [109]. Subsequent histological examination of the tumors revealed that untreated DLL4-overexpressing tumors displayed reduced amounts of vessels, however, remarkably increased vessel diameters, which apparently were similar to the altered vessels of EphB4-overexpressing tumors in this study [109]. These morphologically alternated vessels featured a reduced pericyte coverage, yet they still persisted during treatment, which is why Li *et al.* suspected them to play a major role in mediating resistance towards bevacizumab [109]. Thus, similar to findings in this study, the resistance towards antiangiogenic treatment was delivered independently of the status of pericyte coverage.

Because in additional histological stainings of DLL4-signaling less necrosis and less hypoxia was detected, the role of those enlarged vessels was assumed to preserve the blood and oxygen supply in the otherwise hypoxic tumor areas during bevacizumab treatment [109].

Interestingly, DLL4-overexpressing tumors displayed increased upregulation of EphB4, while ephrinB2-levels were not altered significantly [109]. Inhibition of ephrinB2 mediated signaling using sEphB4 or anti-ephrinB2 alone did not affect tumor growth of the DLL4-overexpressing tumors, however both combined with bevacizumab resulted in significantly diminished tumor growth and prolonged survival [109]. Thus the study group assumed that enhanced ephrinB2 reverse signaling was contributing to mediating antiangiogenic resistance [109]. CD31-stainings of DLL4-overexpressing tumors treated with sEphB4 and anti-ephrinB2 showed reduced vessel numbers and less oversized vessels; the tumors which were additionally treated with bevacizumab revealed almost complete eradication of all oversized vessels [109]. Therefore, the study group concluded that the blockade of the EphB4-ephrinB2 pathway resensitized the tumors for treatment with bevacizumab [109]. The findings by Li *et al.* support our results by

attributing EphB4-overexpression with a major part in mediating resistance towards antiangiogenic treatment as well as by showing that blockade of the pathway results in resensitization of bevacizumab versus primarily resistant tumors.

Adding to the differing effects of EphB4 and ephrinB2, depending on pathway activation and the receptor expression equilibrium, as well as the impact of associated signaling pathways such as Notch signaling pathway, which presumably account for the varying findings in the aforementioned studies, is the heterogeneity in glioma tissue itself. This is represented by current changes in neuropathological classification of brain tumors [110]. The new classification comprises, next to the conventional WHO classification system, of molecular fingerprints such as methylation status, which intend to explain the varying pathological and clinical courses observed in clinical treatment of glioma, and which might also be an explanatory approach for the distinct findings concerning the role of the EphB4-ephrinB2 system in basic research [110].

4.3.7 Résumé

EphB4 and ephrinB2 have been shown to exert differing effects in various tumor entities, in which especially EphB4-overexpression and simultaneous ligand-independent signaling have been found to act as tumor promoting. Contrarily, ephrinB2-induced forward signaling frequently causes tumor suppression. Our study is the first one to observe a tumor suppressive effect in glioma following EphB4-overexpression on ECs, however as the effect seems to be dependent on the method of transfection, cell type and implantation site, no general conclusions can be drawn.

4.4 Resistance Mechanisms towards Sunitinib

Despite showing significant losses in pericyte-endothelial interactions as well as shedding of the vessel enlarging effect of EphB4, EphB4^{OE}-tumors resisted high dose Sunitinib treatment in part, by maintaining a stable equilibrium of apoptotic and proliferating cell numbers. Furthermore a functioning vessel network was preserved, as demonstrated in the IVM.

Resistance mechanisms towards Sunitinib treatment have been described in previous studies, such as by Zhou *et al.*, who performed experiments in Sunitinib-resistant glioma *in vivo* [111]. They detected several genes that had been upregulated in tumors insensitive towards treatment, such as phospholipase-gamma 1 (PLC-γ1) as well as phosphorylated and total c-Jun, and the efflux-transporter ATP-binding cassette G2 (ABCG2) [111]. They further demonstrated via immunohistochemical stainings no significant differences between treatment-sensitive and insensitive tumors concerning vessel density and pericyte coverage, since both parameters proved to be reduced [111]. By means of costaining with α-SMA and CD31 they detected that the effect of Sunitinib mainly affects new vessel formations, rather than mature vessels [111].

PLC-γ1, an intracellular signaling molecule, which is activated by signaling factors such as PDGF and epidermal growth factor (EGF), has been shown to promote cancer development and metastasis in multiple tumor sides [112-116]. Also, in glioma the role of EGF-signaling and subsequent activation of PLC-γ1 have been shown to enhance tumor invasiveness and tumor cell motility [117-119]. Interestingly Chen *et al.*, who examined correlation of EphB4, EGF-receptor (EGFR) and glioma growth, detected next to a tumor promoting effect of an EphB4-overexpression, also a simultaneously increased activation of EGFR [90].

C-Jun NH(2)-terminal kinases (JNKs), a subgroup of mitogen-activated protein (MAP) kinases, are activated by cellular stress, inflammatory cytokines and DNA damage and have been described to interact with the immune system by engaging with the T-cell receptor and inducing cell proliferation as well as apoptosis [120-124]. C-Jun has been shown to mediate resistance towards Cisplatin in ovarian carcinomas as well as towards vinblastin in fibroblast cells and in breast cancer cells, in the latter case by reduction of apoptosis [125-127]. Inhibition of the pathway has been proven to reduce tumor growth and to increase apoptosis significantly, while overexpression improved cell viability [128-130].
Next to cellular stress, JNKS are activated by EGF as well as RhoA, whose pathway has been shown to be activated following EphB4-signaling [104, 123, 131-133].

ATP- depending efflux pump ABCG2 (syn.: breast cancer resistance protein), a member of the APC-transporter family, represented the last-mentioned upregulated protein of the study by Zhou *et al.* [111]. ABCG2 has been demonstrated to take a major part in mediating multi drug resistance by removing cell-toxic substances out of intracellular locations across the cell membrane [134-137].
Several studies have presented diverse, in part contradictive, findings concerning ABCG2 and Sunitinib interaction. On the one hand restricted effectiveness of Sunitinib was demonstrated, by acting as a substrate to ABCG2, on the other it was shown that Sunitinib is capable of blocking ABCG2 and to reverse its mediated chemotherapeutical resistance [138-141]. According to current the current status of studies, ABCG2-activity is primarily regulated via Hypoxia-inducible factor 1-alpha, estrogen receptor and peroxisome proliferator activated receptor [137].

Further studies examining causes for Sunitinib resistance in tumor tissues other than brain tumors, covered spectra ranging from mediated resistance via Interleukin-8 in RCC, Interleukin-6 mediated resistance in castration-resistant prostate cancer and in CRC, upregulation of genes of RTK such as PRKX, TTBK2 and RSK4 in kidney carcinoma and melanoma cells as well as silencing of the PTEN-gene in gastrointestinal stromal tumor cells [86, 142-144]. The latter, a tumor suppressor gene, has been shown to be frequently mutated and lost in glioma [9, 145, 146]. A study by Joshi *et al.* proved the ineffectiveness of Sunitinib targeting GBM cells *in vivo,* boasting an inactivating mutation of the PTEN-gene, by failing to prolong OS [147]. However the dosage was administered at the FDA-approved amount of 15mg/kg BW, thus the treatment probably failed due to not reaching a sufficient concentration within the brain [147].

4.5 Conclusion

As this study is the first one to attribute EphB4-overexpression with a growth inhibiting effect in glioma, however, still delivering a resistance mediating effect, future studies ought to examine the exact pathway (reverse, forward or ligand-independent signaling) which is responsible for the findings.

The essential observation of this study is that EphB4-overexpression on ECs induces enlarged vessels in glioma as well as a resistance towards antiangiogenic treatment by means of stabilizing proliferation and apoptosis within the tumors.

5 Summary

Despite all medical efforts GBM has been proven to be a challenging tumor entity, featuring low OS and a high recurrence rate. Antiangiogenic therapies, which had been demonstrated to be effective in other tumor entities, were not capable of prolonging OS significantly.

Angiogenic systems such as the EphB4-ephrinB2 signaling pathway have been suspected of taking part in mediating therapeutical resistance. To examine the role of EphB4 in mediating resistance, we coimplanted SF126 glioma cells together with EphB4-overexpressing reporter cells orthotopically, followed by sequential MRI and immunohistochemistry, determining tumor volume as well as vascular parameters, tumor cell apoptosis and proliferation. Antiangiogenic treatment was administered by means of Sunitinib, a VEGF-receptor 2 blocker.
We further created 3D-spheroids of the SF126 glioma cells and the reporter cells, which we implanted in chronic cranial window operations, followed by IVM, to examine the effect of EphB4-overexpression on vessel network formation, as well as possible protective mechanisms during treatment.

The experiments revealed a significantly reduced tumor growth in EphB4-overexpressing xenografts. Nevertheless the tumors proved to be resistant towards antiangiogenic treatment, by maintaining a stable equilibrium of proliferating and apoptotic cell numbers as well as a stable vessel density. EphB4-ovexpressing tumors displayed enlarged vessel diameters. Moreover EphB4-overexpressing tumors were capable of preserving a functional vessel network during treatment.

Since the tumor promoting and suppressing effects of EphB4 seem to be very dependent on the experimental setup, the main conclusion of this study is that EphB4-overexpression on ECs produces tumors with increased vessel diameters and poses a possible resistance mechanism towards antiangiogenic treatment by means of a stabilized tumor microenvironment.

6 References

1. Ostrom, Q.T., Gittleman, H., Fulop, J., Liu, M., Blanda, R., Kromer, C., Wolinsky, Y., Kruchko, C. and Barnholtz-Sloan, J.S., *CBTRUS Statistical Report: Primary Brain and Central Nervous System Tumors Diagnosed in the United States in 2008-2012.* Neuro Oncol, 2015. **17 Suppl 4**: p. iv1-iv62.
2. Louis, D.N., Ohgaki, H., Wiestler, O.D., Cavenee, W.K., Burger, P.C., Jouvet, A., Scheithauer, B.W. and Kleihues, P., *The 2007 WHO classification of tumours of the central nervous system.* Acta Neuropathol, 2007. **114**(2): p. 97-109.
3. Louis, D.N., Perry, A., Reifenberger, G., von Deimling, A., Figarella-Branger, D., Cavenee, W.K., Ohgaki, H., Wiestler, O.D., Kleihues, P. and Ellison, D.W., *The 2016 World Health Organization Classification of Tumors of the Central Nervous System: a summary.* Acta Neuropathol, 2016. **131**(6): p. 803-20.
4. Holland, E.C., *Glioblastoma multiforme: the terminator.* Proc Natl Acad Sci U S A, 2000. **97**(12): p. 6242-4.
5. DeAngelis, L.M. and Mellinghoff, I.K., *Virchow 2011 or how to ID(H) human glioblastoma.* J Clin Oncol, 2011. **29**(34): p. 4473-4.
6. Scherer, H.J., *Cerebral astrocytomas and their derivates.* Am J Cancer, 1940. **XL**.
7. Sahm, F., Capper, D., Jeibmann, A., Habel, A., Paulus, W., Troost, D. and von Deimling, A., *Addressing diffuse glioma as a systemic brain disease with single-cell analysis.* Arch Neurol, 2012. **69**(4): p. 523-6.
8. Ohgaki, H. and Kleihues, P., *The definition of primary and secondary glioblastoma.* Clin Cancer Res, 2013. **19**(4): p. 764-72.
9. Parsons, D.W., Jones, S., Zhang, X., Lin, J.C., Leary, R.J., Angenendt, P., Mankoo, P., Carter, H., Siu, I.M., Gallia, G.L., Olivi, A., McLendon, R., Rasheed, B.A., Keir, S., Nikolskaya, T., Nikolsky, Y., Busam, D.A., Tekleab, H., Diaz, L.A., Jr., Hartigan, J., Smith, D.R., Strausberg, R.L., Marie, S.K., Shinjo, S.M., Yan, H., Riggins, G.J., Bigner, D.D., Karchin, R., Papadopoulos, N., Parmigiani, G., Vogelstein, B., Velculescu, V.E. and Kinzler, K.W., *An integrated genomic analysis of human glioblastoma multiforme.* Science, 2008. **321**(5897): p. 1807-12.
10. Nobusawa, S., Watanabe, T., Kleihues, P. and Ohgaki, H., *IDH1 mutations as molecular signature and predictive factor of secondary glioblastomas.* Clin Cancer Res, 2009. **15**(19): p. 6002-7.
11. Ohgaki, H., Dessen, P., Jourde, B., Horstmann, S., Nishikawa, T., Di Patre, P.L., Burkhard, C., Schuler, D., Probst-Hensch, N.M., Maiorka, P.C., Baeza, N., Pisani, P., Yonekawa, Y., Yasargil, M.G., Lutolf, U.M. and Kleihues, P., *Genetic pathways to glioblastoma: a population-based study.* Cancer Res, 2004. **64**(19): p. 6892-9.
12. Balss, J., Meyer, J., Mueller, W., Korshunov, A., Hartmann, C. and von Deimling, A., *Analysis of the IDH1 codon 132 mutation in brain tumors.* Acta Neuropathol, 2008. **116**(6): p. 597-602.
13. Watanabe, T., Nobusawa, S., Kleihues, P. and Ohgaki, H., *IDH1 mutations are early events in the development of astrocytomas and oligodendrogliomas.* Am J Pathol, 2009. **174**(4): p. 1149-53.
14. Rassow, J., Hauser, H., Netzker, H. and Deutzmann, R., *Duale Reihe - Biochemie*. 2008, Georg Thieme Verlag KG: Stuttgart. p. 114.
15. Stupp, R., Taillibert, S., Kanner, A.A., Kesari, S., Steinberg, D.M., Toms, S.A., Taylor, L.P., Lieberman, F., Silvani, A., Fink, K.L., Barnett, G.H., Zhu, J.J., Henson, J.W., Engelhard, H.H., Chen, T.C., Tran, D.D., Sroubek, J., Tran, N.D., Hottinger, A.F., Landolfi, J., Desai, R., Caroli, M., Kew, Y., Honnorat, J., Idbaih, A., Kirson, E.D.,

Weinberg, U., Palti, Y., Hegi, M.E. and Ram, Z., *Maintenance Therapy With Tumor-Treating Fields Plus Temozolomide vs Temozolomide Alone for Glioblastoma: A Randomized Clinical Trial.* JAMA, 2015. **314**(23): p. 2535-43.
16. Hegi, M.E., Diserens, A.C., Gorlia, T., Hamou, M.F., de Tribolet, N., Weller, M., Kros, J.M., Hainfellner, J.A., Mason, W., Mariani, L., Bromberg, J.E., Hau, P., Mirimanoff, R.O., Cairncross, J.G., Janzer, R.C. and Stupp, R., *MGMT gene silencing and benefit from temozolomide in glioblastoma.* N Engl J Med, 2005. **352**(10): p. 997-1003.
17. Weller, M., van den Bent, M., Hopkins, K., Tonn, J.C., Stupp, R., Falini, A., Cohen-Jonathan-Moyal, E., Frappaz, D., Henriksson, R., Balana, C., Chinot, O., Ram, Z., Reifenberger, G., Soffietti, R., Wick, W. and European Association for Neuro-Oncology Task Force on Malignant, G., *EANO guideline for the diagnosis and treatment of anaplastic gliomas and glioblastoma.* Lancet Oncol, 2014. **15**(9): p. e395-403.
18. Pegg, A.E., Dolan, M.E. and Moschel, R.C., *Structure, function, and inhibition of O6-alkylguanine-DNA alkyltransferase.* Prog Nucleic Acid Res Mol Biol, 1995. **51**: p. 167-223.
19. Esteller, M., Garcia-Foncillas, J., Andion, E., Goodman, S.N., Hidalgo, O.F., Vanaclocha, V., Baylin, S.B. and Herman, J.G., *Inactivation of the DNA-repair gene MGMT and the clinical response of gliomas to alkylating agents.* N Engl J Med, 2000. **343**(19): p. 1350-4.
20. Herrlinger, U., Tzaridis, T., Mack, F., Steinbach, J., Schlegel, U., Sabel, M., Hau, P., Kortman, R.D., Krex, D., Grauer, O., Goldbrunner, R., Schnell, O., Baehr, O., Uhl, M., Tabatabai, G., Ringel, F., Schmidt-Graf, F., Brehmer, S., Weyerbrock, A., Bullinger, L., Vajkoczy, P., Vatter, H., Schafer, N., Kebir, S., Weller, J., Stummer, W., Simon, M., Keil, V., Nelles, M., Fimmers, R., Pietsch, T., Hattingen, E., Coch, C. and Glas, M., *PHASE III TRIAL OF CCNU/TEMOZOLOMIDE (TMZ) COMBINATION THERAPY VS. STANDARD TMZ THERAPY FOR NEWLY DIAGNOSED MGMT-METHYLATED GLIOBLASTOMA PATIENTS: THE CeTeg/NOA-09 trial.* Neuro-Oncology, 2017. **19**: p. 13-14.
21. Folkman, J., *Tumor angiogenesis: therapeutic implications.* N Engl J Med, 1971. **285**(21): p. 1182-6.
22. Midgley, R. and Kerr, D., *Bevacizumab--current status and future directions.* Ann Oncol, 2005. **16**(7): p. 999-1004.
23. Kerbel, R.S., *Tumor angiogenesis.* N Engl J Med, 2008. **358**(19): p. 2039-49.
24. Hicklin, D.J. and Ellis, L.M., *Role of the vascular endothelial growth factor pathway in tumor growth and angiogenesis.* J Clin Oncol, 2005. **23**(5): p. 1011-27.
25. Oliner, J., Min, H., Leal, J., Yu, D., Rao, S., You, E., Tang, X., Kim, H., Meyer, S., Han, S.J., Hawkins, N., Rosenfeld, R., Davy, E., Graham, K., Jacobsen, F., Stevenson, S., Ho, J., Chen, Q., Hartmann, T., Michaels, M., Kelley, M., Li, L., Sitney, K., Martin, F., Sun, J.R., Zhang, N., Lu, J., Estrada, J., Kumar, R., Coxon, A., Kaufman, S., Pretorius, J., Scully, S., Cattley, R., Payton, M., Coats, S., Nguyen, L., Desilva, B., Ndifor, A., Hayward, I., Radinsky, R., Boone, T. and Kendall, R., *Suppression of angiogenesis and tumor growth by selective inhibition of angiopoietin-2.* Cancer Cell, 2004. **6**(5): p. 507-16.
26. Sainson, R.C. and Harris, A.L., *Anti-Dll4 therapy: can we block tumour growth by increasing angiogenesis?* Trends Mol Med, 2007. **13**(9): p. 389-95.
27. Semenza, G.L., *Targeting HIF-1 for cancer therapy.* Nat Rev Cancer, 2003. **3**(10): p. 721-32.
28. *ANGIOGENESIS INHIBITORS FOR CANCER*. 2015; Available from: https://www.angio.org/learn/treatments/?searchid=591#591.

29. Eskens, F.A. and Verweij, J., *The clinical toxicity profile of vascular endothelial growth factor (VEGF) and vascular endothelial growth factor receptor (VEGFR) targeting angiogenesis inhibitors; a review.* Eur J Cancer, 2006. **42**(18): p. 3127-39.
30. Berenson, A., *A cancer drug shows promise, at a price that many can't pay*, in *New York Times*. 2006.
31. Chinot, O.L., Wick, W., Mason, W., Henriksson, R., Saran, F., Nishikawa, R., Carpentier, A.F., Hoang-Xuan, K., Kavan, P., Cernea, D., Brandes, A.A., Hilton, M., Abrey, L. and Cloughesy, T., *Bevacizumab plus radiotherapy-temozolomide for newly diagnosed glioblastoma.* N Engl J Med, 2014. **370**(8): p. 709-22.
32. Chinot, O.L., Nishikawa, R., Mason, W., Henriksson, R., Saran, F., Cloughesy, T., Garcia, J., Revil, C., Abrey, L. and Wick, W., *Upfront bevacizumab may extend survival for glioblastoma patients who do not receive second-line therapy: an exploratory analysis of AVAglio.* Neuro Oncol, 2016. **18**(9): p. 1313-8.
33. Seystahl, K., Gramatzki, D., Roth, P. and Weller, M., *Pharmacotherapies for the treatment of glioblastoma - current evidence and perspectives.* Expert Opin Pharmacother, 2016. **17**(9): p. 1259-70.
34. Wick, W., Puduvalli, V.K., Chamberlain, M.C., van den Bent, M.J., Carpentier, A.F., Cher, L.M., Mason, W., Weller, M., Hong, S., Musib, L., Liepa, A.M., Thornton, D.E. and Fine, H.A., *Phase III study of enzastaurin compared with lomustine in the treatment of recurrent intracranial glioblastoma.* J Clin Oncol, 2010. **28**(7): p. 1168-74.
35. Stupp, R., Hegi, M.E., Gorlia, T., Erridge, S.C., Perry, J., Hong, Y.K., Aldape, K.D., Lhermitte, B., Pietsch, T., Grujicic, D., Steinbach, J.P., Wick, W., Tarnawski, R., Nam, D.H., Hau, P., Weyerbrock, A., Taphoorn, M.J., Shen, C.C., Rao, N., Thurzo, L., Herrlinger, U., Gupta, T., Kortmann, R.D., Adamska, K., McBain, C., Brandes, A.A., Tonn, J.C., Schnell, O., Wiegel, T., Kim, C.Y., Nabors, L.B., Reardon, D.A., van den Bent, M.J., Hicking, C., Markivskyy, A., Picard, M., Weller, M., European Organisation for, R., Treatment of, C., Canadian Brain Tumor, C. and team, C.s., *Cilengitide combined with standard treatment for patients with newly diagnosed glioblastoma with methylated MGMT promoter (CENTRIC EORTC 26071-22072 study): a multicentre, randomised, open-label, phase 3 trial.* Lancet Oncol, 2014. **15**(10): p. 1100-8.
36. Batchelor, T.T., Mulholland, P., Neyns, B., Nabors, L.B., Campone, M., Wick, A., Mason, W., Mikkelsen, T., Phuphanich, S., Ashby, L.S., Degroot, J., Gattamaneni, R., Cher, L., Rosenthal, M., Payer, F., Jurgensmeier, J.M., Jain, R.K., Sorensen, A.G., Xu, J., Liu, Q. and van den Bent, M., *Phase III randomized trial comparing the efficacy of cediranib as monotherapy, and in combination with lomustine, versus lomustine alone in patients with recurrent glioblastoma.* J Clin Oncol, 2013. **31**(26): p. 3212-8.
37. Maj, E., Papiernik, D. and Wietrzyk, J., *Antiangiogenic cancer treatment: The great discovery and greater complexity (Review).* Int J Oncol, 2016. **49**(5): p. 1773-1784.
38. van Beijnum, J.R., Nowak-Sliwinska, P., Huijbers, E.J., Thijssen, V.L. and Griffioen, A.W., *The great escape; the hallmarks of resistance to antiangiogenic therapy.* Pharmacol Rev, 2015. **67**(2): p. 441-61.
39. Erber, R., Eichelsbacher, U., Powajbo, V., Korn, T., Djonov, V., Lin, J., Hammes, H.P., Grobholz, R., Ullrich, A. and Vajkoczy, P., *EphB4 controls blood vascular morphogenesis during postnatal angiogenesis.* EMBO J, 2006. **25**(3): p. 628-41.
40. Pasquale, E.B., *Eph receptors and ephrins in cancer: bidirectional signalling and beyond.* Nat Rev Cancer, 2010. **10**(3): p. 165-80.
41. Riedl, S.J. and Pasquale, E.B., *Targeting the Eph System with Peptides and Peptide Conjugates.* Curr Drug Targets, 2015. **16**(10): p. 1031-47.
42. Lisabeth, E.M., Falivelli, G. and Pasquale, E.B., *Eph receptor signaling and ephrins.* Cold Spring Harb Perspect Biol, 2013. **5**(9).

43. Pasquale, E.B., *Eph-ephrin bidirectional signaling in physiology and disease.* Cell, 2008. **133**(1): p. 38-52.
44. Noren, N.K. and Pasquale, E.B., *Paradoxes of the EphB4 receptor in cancer.* Cancer Res, 2007. **67**(9): p. 3994-7.
45. Holder, N. and Klein, R., *Eph receptors and ephrins: effectors of morphogenesis.* Development, 1999. **126**(10): p. 2033-44.
46. Adams, R.H., Diella, F., Hennig, S., Helmbacher, F., Deutsch, U. and Klein, R., *The cytoplasmic domain of the ligand ephrinB2 is required for vascular morphogenesis but not cranial neural crest migration.* Cell, 2001. **104**(1): p. 57-69.
47. Fuller, T., Korff, T., Kilian, A., Dandekar, G. and Augustin, H.G., *Forward EphB4 signaling in endothelial cells controls cellular repulsion and segregation from ephrinB2 positive cells.* J Cell Sci, 2003. **116**(Pt 12): p. 2461-70.
48. Adams, R.H., Wilkinson, G.A., Weiss, C., Diella, F., Gale, N.W., Deutsch, U., Risau, W. and Klein, R., *Roles of ephrinB ligands and EphB receptors in cardiovascular development: demarcation of arterial/venous domains, vascular morphogenesis, and sprouting angiogenesis.* Genes Dev, 1999. **13**(3): p. 295-306.
49. Sawamiphak, S., Seidel, S., Essmann, C.L., Wilkinson, G.A., Pitulescu, M.E., Acker, T. and Acker-Palmer, A., *Ephrin-B2 regulates VEGFR2 function in developmental and tumour angiogenesis.* Nature, 2010. **465**(7297): p. 487-91.
50. Ireton, R.C. and Chen, J., *EphA2 receptor tyrosine kinase as a promising target for cancer therapeutics.* Curr Cancer Drug Targets, 2005. **5**(3): p. 149-57.
51. Fox, B.P. and Kandpal, R.P., *Invasiveness of breast carcinoma cells and transcript profile: Eph receptors and ephrin ligands as molecular markers of potential diagnostic and prognostic application.* Biochem Biophys Res Commun, 2004. **318**(4): p. 882-92.
52. Xia, G., Kumar, S.R., Masood, R., Koss, M., Templeman, C., Quinn, D., Zhu, S., Reddy, R., Krasnoperov, V. and Gill, P.S., *Up-regulation of EphB4 in mesothelioma and its biological significance.* Clin Cancer Res, 2005. **11**(12): p. 4305-15.
53. Xia, G., Kumar, S.R., Stein, J.P., Singh, J., Krasnoperov, V., Zhu, S., Hassanieh, L., Smith, D.L., Buscarini, M., Broek, D., Quinn, D.I., Weaver, F.A. and Gill, P.S., *EphB4 receptor tyrosine kinase is expressed in bladder cancer and provides signals for cell survival.* Oncogene, 2006. **25**(5): p. 769-80.
54. Xia, G., Kumar, S.R., Masood, R., Zhu, S., Reddy, R., Krasnoperov, V., Quinn, D.I., Henshall, S.M., Sutherland, R.L., Pinski, J.K., Daneshmand, S., Buscarini, M., Stein, J.P., Zhong, C., Broek, D., Roy-Burman, P. and Gill, P.S., *EphB4 expression and biological significance in prostate cancer.* Cancer Res, 2005. **65**(11): p. 4623-32.
55. Kumar, S.R., Scehnet, J.S., Ley, E.J., Singh, J., Krasnoperov, V., Liu, R., Manchanda, P.K., Ladner, R.D., Hawes, D., Weaver, F.A., Beart, R.W., Singh, G., Nguyen, C., Kahn, M. and Gill, P.S., *Preferential induction of EphB4 over EphB2 and its implication in colorectal cancer progression.* Cancer Res, 2009. **69**(9): p. 3736-45.
56. Fox, B.P., Tabone, C.J. and Kandpal, R.P., *Potential clinical relevance of Eph receptors and ephrin ligands expressed in prostate carcinoma cell lines.* Biochem Biophys Res Commun, 2006. **342**(4): p. 1263-72.
57. Hafner, C., Becker, B., Landthaler, M. and Vogt, T., *Expression profile of Eph receptors and ephrin ligands in human skin and downregulation of EphA1 in nonmelanoma skin cancer.* Mod Pathol, 2006. **19**(10): p. 1369-77.
58. Holmberg, J., Clarke, D.L. and Frisen, J., *Regulation of repulsion versus adhesion by different splice forms of an Eph receptor.* Nature, 2000. **408**(6809): p. 203-6.
59. Wang, H.U., Chen, Z.F. and Anderson, D.J., *Molecular distinction and angiogenic interaction between embryonic arteries and veins revealed by ephrin-B2 and its receptor Eph-B4.* Cell, 1998. **93**(5): p. 741-53.

60. Gerety, S.S., Wang, H.U., Chen, Z.F. and Anderson, D.J., *Symmetrical mutant phenotypes of the receptor EphB4 and its specific transmembrane ligand ephrin-B2 in cardiovascular development.* Mol Cell, 1999. **4**(3): p. 403-14.
61. Lv, J., Xia, Q., Wang, J., Shen, Q., Zhang, J. and Zhou, X., *EphB4 promotes the proliferation, invasion, and angiogenesis of human colorectal cancer.* Exp Mol Pathol, 2016. **100**(3): p. 402-8.
62. Martiny-Baron, G., Korff, T., Schaffner, F., Esser, N., Eggstein, S., Marme, D. and Augustin, H.G., *Inhibition of tumor growth and angiogenesis by soluble EphB4.* Neoplasia, 2004. **6**(3): p. 248-57.
63. Czabanka, M., Vinci, M., Heppner, F., Ullrich, A. and Vajkoczy, P., *Effects of sunitinib on tumor hemodynamics and delivery of chemotherapy.* Int J Cancer, 2009. **124**(6): p. 1293-300.
64. Tu, Y., He, S., Fu, J., Li, G., Xu, R., Lu, H. and Deng, J., *Expression of EphrinB2 and EphB4 in glioma tissues correlated to the progression of glioma and the prognosis of glioblastoma patients.* Clin Transl Oncol, 2012. **14**(3): p. 214-20.
65. Vajkoczy, P., Schilling, L., Ullrich, A., Schmiedek, P. and Menger, M.D., *Characterization of angiogenesis and microcirculation of high-grade glioma: an intravital multifluorescence microscopic approach in the athymic nude mouse.* J Cereb Blood Flow Metab, 1998. **18**(5): p. 510-20.
66. Endrich, B., Intaglietta, M., Reinhold, H.S. and Gross, J.F., *Hemodynamic characteristics in microcirculatory blood channels during early tumor growth.* Cancer Res, 1979. **39**(1): p. 17-23.
67. Asaishi, K., Endrich, B., Gotz, A. and Messmer, K., *Quantitative analysis of microvascular structure and function in the amelanotic melanoma A-Mel-3.* Cancer Res, 1981. **41**(5): p. 1898-904.
68. Vajkoczy, P., Menger, M.D., Vollmar, B., Schilling, L., Schmiedek, P., Hirth, K.P., Ullrich, A. and Fong, T.A., *Inhibition of tumor growth, angiogenesis, and microcirculation by the novel Flk-1 inhibitor SU5416 as assessed by intravital multi-fluorescence videomicroscopy.* Neoplasia, 1999. **1**(1): p. 31-41.
69. Markel, M., *Der Einfluss von EphB4 auf die Vermittlung vaskulärer Resistenz im Rahmen einer antiangiogenen Therapie*, in *Neurosurgery*. 2016, Charité-Universitätsmedizin Berlin.
70. *Nolan Lab*. Available from: https://web.stanford.edu/group/nolan/_OldWebsite/retroviral_systems/phx.html.
71. Pear, W.S., Nolan, G.P., Scott, M.L. and Baltimore, D., *Production of high-titer helper-free retroviruses by transient transfection.* Proc Natl Acad Sci U S A, 1993. **90**(18): p. 8392-6.
72. Kinsella, T.M. and Nolan, G.P., *Episomal vectors rapidly and stably produce high-titer recombinant retrovirus.* Hum Gene Ther, 1996. **7**(12): p. 1405-13.
73. *Phoenix™ Retrovirus Expression System*. Available from: http://www.gentaurpdf.com/pdf/Phoenix%E2%84%A2%20Retrovirus%20Expression%20System.pdf.
74. Goodman, V.L., Rock, E.P., Dagher, R., Ramchandani, R.P., Abraham, S., Gobburu, J.V., Booth, B.P., Verbois, S.L., Morse, D.E., Liang, C.Y., Chidambaram, N., Jiang, J.X., Tang, S., Mahjoob, K., Justice, R. and Pazdur, R., *Approval summary: sunitinib for the treatment of imatinib refractory or intolerant gastrointestinal stromal tumors and advanced renal cell carcinoma.* Clin Cancer Res, 2007. **13**(5): p. 1367-73.
75. Blumenthal, G.M., Cortazar, P., Zhang, J.J., Tang, S., Sridhara, R., Murgo, A., Justice, R. and Pazdur, R., *FDA approval summary: sunitinib for the treatment of progressive well-*

differentiated locally advanced or metastatic pancreatic neuroendocrine tumors. Oncologist, 2012. **17**(8): p. 1108-13.
76. Hao, Z. and Sadek, I., *Sunitinib: the antiangiogenic effects and beyond.* Onco Targets Ther, 2016. **9**: p. 5495-505.
77. Sun, L., Liang, C., Shirazian, S., Zhou, Y., Miller, T., Cui, J., Fukuda, J.Y., Chu, J.Y., Nematalla, A., Wang, X., Chen, H., Sistla, A., Luu, T.C., Tang, F., Wei, J. and Tang, C., *Discovery of 5-[5-fluoro-2-oxo-1,2- dihydroindol-(3Z)-ylidenemethyl]-2,4- dimethyl-1H-pyrrole-3-carboxylic acid (2-diethylaminoethyl)amide, a novel tyrosine kinase inhibitor targeting vascular endothelial and platelet-derived growth factor receptor tyrosine kinase.* J Med Chem, 2003. **46**(7): p. 1116-9.
78. Rini, B.I., *Sunitinib.* Expert Opin Pharmacother, 2007. **8**(14): p. 2359-69.
79. O'Farrell, A.M., Abrams, T.J., Yuen, H.A., Ngai, T.J., Louie, S.G., Yee, K.W., Wong, L.M., Hong, W., Lee, L.B., Town, A., Smolich, B.D., Manning, W.C., Murray, L.J., Heinrich, M.C. and Cherrington, J.M., *SU11248 is a novel FLT3 tyrosine kinase inhibitor with potent activity in vitro and in vivo.* Blood, 2003. **101**(9): p. 3597-605.
80. Laib, A.M., Bartol, A., Alajati, A., Korff, T., Weber, H. and Augustin, H.G., *Spheroid-based human endothelial cell microvessel formation in vivo.* Nat Protoc, 2009. **4**(8): p. 1202-15.
81. Baker M., W.H., *On-line volume flow rate and velocity profile measurement for blood in microvessels.* . Microvasc Res, 1974. **7**: p. 131–43.
82. Hafner, C., Schmitz, G., Meyer, S., Bataille, F., Hau, P., Langmann, T., Dietmaier, W., Landthaler, M. and Vogt, T., *Differential gene expression of Eph receptors and ephrins in benign human tissues and cancers.* Clin Chem, 2004. **50**(3): p. 490-9.
83. Jones, S., Chen, W.D., Parmigiani, G., Diehl, F., Beerenwinkel, N., Antal, T., Traulsen, A., Nowak, M.A., Siegel, C., Velculescu, V.E., Kinzler, K.W., Vogelstein, B., Willis, J. and Markowitz, S.D., *Comparative lesion sequencing provides insights into tumor evolution.* Proc Natl Acad Sci U S A, 2008. **105**(11): p. 4283-8.
84. Winter, J.M., Brody, J.R. and Kern, S.E., *Multiple-criterion evaluation of reported mutations: a proposed scoring system for the intragenic somatic mutation literature.* Cancer Biol Ther, 2006. **5**(4): p. 360-70.
85. Casanovas, O., Hicklin, D.J., Bergers, G. and Hanahan, D., *Drug resistance by evasion of antiangiogenic targeting of VEGF signaling in late-stage pancreatic islet tumors.* Cancer Cell, 2005. **8**(4): p. 299-309.
86. Huang, D., Ding, Y., Zhou, M., Rini, B.I., Petillo, D., Qian, C.N., Kahnoski, R., Futreal, P.A., Furge, K.A. and Teh, B.T., *Interleukin-8 mediates resistance to antiangiogenic agent sunitinib in renal cell carcinoma.* Cancer Res, 2010. **70**(3): p. 1063-71.
87. Vajkoczy, P., Ullrich, A. and Menger, M.D., *Intravital fluorescence videomicroscopy to study tumor angiogenesis and microcirculation.* Neoplasia, 2000. **2**(1-2): p. 53-61.
88. Coomber, B.L., Stewart, P.A., Hayakawa, E.M., Farrell, C.L. and Del Maestro, R.F., *A quantitative assessment of microvessel ultrastructure in C6 astrocytoma spheroids transplanted to brain and to muscle.* J Neuropathol Exp Neurol, 1988. **47**(1): p. 29-40.
89. Fukumura, D., Yuan, F., Monsky, W.L., Chen, Y. and Jain, R.K., *Effect of host microenvironment on the microcirculation of human colon adenocarcinoma.* Am J Pathol, 1997. **151**(3): p. 679-88.
90. Chen, T., Liu, X., Yi, S., Zhang, J., Ge, J. and Liu, Z., *EphB4 is overexpressed in gliomas and promotes the growth of glioma cells.* Tumour Biol, 2013. **34**(1): p. 379-85.
91. Wimmer-Kleikamp, S.H., Janes, P.W., Squire, A., Bastiaens, P.I. and Lackmann, M., *Recruitment of Eph receptors into signaling clusters does not require ephrin contact.* J Cell Biol, 2004. **164**(5): p. 661-6.

92. Janes, P.W., Griesshaber, B., Atapattu, L., Nievergall, E., Hii, L.L., Mensinga, A., Chheang, C., Day, B.W., Boyd, A.W., Bastiaens, P.I., Jorgensen, C., Pawson, T. and Lackmann, M., *Eph receptor function is modulated by heterooligomerization of A and B type Eph receptors.* J Cell Biol, 2011. **195**(6): p. 1033-45.
93. Taddei, M.L., Parri, M., Angelucci, A., Onnis, B., Bianchini, F., Giannoni, E., Raugei, G., Calorini, L., Rucci, N., Teti, A., Bologna, M. and Chiarugi, P., *Kinase-dependent and -independent roles of EphA2 in the regulation of prostate cancer invasion and metastasis.* Am J Pathol, 2009. **174**(4): p. 1492-503.
94. Rutkowski, R., Mertens-Walker, I., Lisle, J.E., Herington, A.C. and Stephenson, S.A., *Evidence for a dual function of EphB4 as tumor promoter and suppressor regulated by the absence or presence of the ephrin-B2 ligand.* Int J Cancer, 2012. **131**(5): p. E614-24.
95. Noren, N.K., Foos, G., Hauser, C.A. and Pasquale, E.B., *The EphB4 receptor suppresses breast cancer cell tumorigenicity through an Abl-Crk pathway.* Nat Cell Biol, 2006. **8**(8): p. 815-25.
96. Kumar, S.R., Singh, J., Xia, G., Krasnoperov, V., Hassanieh, L., Ley, E.J., Scehnet, J., Kumar, N.G., Hawes, D., Press, M.F., Weaver, F.A. and Gill, P.S., *Receptor tyrosine kinase EphB4 is a survival factor in breast cancer.* Am J Pathol, 2006. **169**(1): p. 279-93.
97. Wu, Q., Suo, Z., Risberg, B., Karlsson, M.G., Villman, K. and Nesland, J.M., *Expression of Ephb2 and Ephb4 in breast carcinoma.* Pathol Oncol Res, 2004. **10**(1): p. 26-33.
98. Barneh, F., Moshayedi, M., Mirmohammadsadeghi, H., Haghjooy-Javanmard, S., Sabzghabaee, A.M. and Badri, S., *EphB4 tyrosine kinase stimulation inhibits growth of MDA-MB-231 breast cancer cells in a dose and time dependent manner.* Dis Markers, 2013. **35**(6): p. 933-8.
99. Kertesz, N., Krasnoperov, V., Reddy, R., Leshanski, L., Kumar, S.R., Zozulya, S. and Gill, P.S., *The soluble extracellular domain of EphB4 (sEphB4) antagonizes EphB4-EphrinB2 interaction, modulates angiogenesis, and inhibits tumor growth.* Blood, 2006. **107**(6): p. 2330-8.
100. Noren, N.K., Lu, M., Freeman, A.L., Koolpe, M. and Pasquale, E.B., *Interplay between EphB4 on tumor cells and vascular ephrin-B2 regulates tumor growth.* Proc Natl Acad Sci U S A, 2004. **101**(15): p. 5583-8.
101. Ferguson, B.D., Tretiakova, M.S., Lingen, M.W., Gill, P.S. and Salgia, R., *Expression of the EPHB4 receptor tyrosine kinase in head and neck and renal malignancies--implications for solid tumors and potential for therapeutic inhibition.* Growth Factors, 2014. **32**(6): p. 202-6.
102. Kimura, M., Kato, Y., Sano, D., Fujita, K., Sakakibara, A., Kondo, N., Mikami, Y. and Tsukuda, M., *Soluble form of ephrinB2 inhibits xenograft growth of squamous cell carcinoma of the head and neck.* Int J Oncol, 2009. **34**(2): p. 321-7.
103. Masood, R., Kumar, S.R., Sinha, U.K., Crowe, D.L., Krasnoperov, V., Reddy, R.K., Zozulya, S., Singh, J., Xia, G., Broek, D., Schonthal, A.H. and Gill, P.S., *EphB4 provides survival advantage to squamous cell carcinoma of the head and neck.* Int J Cancer, 2006. **119**(6): p. 1236-48.
104. Yang, N.Y., Pasquale, E.B., Owen, L.B. and Ethell, I.M., *The EphB4 receptor-tyrosine kinase promotes the migration of melanoma cells through Rho-mediated actin cytoskeleton reorganization.* J Biol Chem, 2006. **281**(43): p. 32574-86.
105. Yang, N.Y., Lopez-Bergami, P., Goydos, J.S., Yip, D., Walker, A.M., Pasquale, E.B. and Ethell, I.M., *The EphB4 receptor promotes the growth of melanoma cells expressing the ephrin-B2 ligand.* Pigment Cell Melanoma Res, 2010. **23**(5): p. 684-7.
106. Huang, X., Yamada, Y., Kidoya, H., Naito, H., Nagahama, Y., Kong, L., Katoh, S.Y., Li, W.L., Ueno, M. and Takakura, N., *EphB4 overexpression in B16 melanoma cells affects arterial-venous patterning in tumor angiogenesis.* Cancer Res, 2007. **67**(20): p. 9800-8.

107. Batlle, E., Bacani, J., Begthel, H., Jonkheer, S., Gregorieff, A., van de Born, M., Malats, N., Sancho, E., Boon, E., Pawson, T., Gallinger, S., Pals, S. and Clevers, H., *EphB receptor activity suppresses colorectal cancer progression.* Nature, 2005. **435**(7045): p. 1126-30.
108. Liu, W., Jung, Y.D., Ahmad, S.A., McCarty, M.F., Stoeltzing, O., Reinmuth, N., Fan, F. and Ellis, L.M., *Effects of overexpression of ephrin-B2 on tumour growth in human colorectal cancer.* Br J Cancer, 2004. **90**(8): p. 1620-6.
109. Li, J.L., Sainson, R.C., Oon, C.E., Turley, H., Leek, R., Sheldon, H., Bridges, E., Shi, W., Snell, C., Bowden, E.T., Wu, H., Chowdhury, P.S., Russell, A.J., Montgomery, C.P., Poulsom, R. and Harris, A.L., *DLL4-Notch signaling mediates tumor resistance to anti-VEGF therapy in vivo.* Cancer Res, 2011. **71**(18): p. 6073-83.
110. Capper, D., Jones, D.T.W., Sill, M., Hovestadt, V., Schrimpf, D., Sturm, D., Koelsche, C., Sahm, F., Chavez, L., Reuss, D.E., Kratz, A., Wefers, A.K., Huang, K., Pajtler, K.W., Schweizer, L., Stichel, D., Olar, A., Engel, N.W., Lindenberg, K., Harter, P.N., Braczynski, A.K., Plate, K.H., Dohmen, H., Garvalov, B.K., Coras, R., Holsken, A., Hewer, E., Bewerunge-Hudler, M., Schick, M., Fischer, R., Beschorner, R., Schittenhelm, J., Staszewski, O., Wani, K., Varlet, P., Pages, M., Temming, P., Lohmann, D., Selt, F., Witt, H., Milde, T., Witt, O., Aronica, E., Giangaspero, F., Rushing, E., Scheurlen, W., Geisenberger, C., Rodriguez, F.J., Becker, A., Preusser, M., Haberler, C., Bjerkvig, R., Cryan, J., Farrell, M., Deckert, M., Hench, J., Frank, S., Serrano, J., Kannan, K., Tsirigos, A., Bruck, W., Hofer, S., Brehmer, S., Seiz-Rosenhagen, M., Hanggi, D., Hans, V., Rozsnoki, S., Hansford, J.R., Kohlhof, P., Kristensen, B.W., Lechner, M., Lopes, B., Mawrin, C., Ketter, R., Kulozik, A., Khatib, Z., Heppner, F., Koch, A., Jouvet, A., Keohane, C., Muhleisen, H., Mueller, W., Pohl, U., Prinz, M., Benner, A., Zapatka, M., Gottardo, N.G., Driever, P.H., Kramm, C.M., Muller, H.L., Rutkowski, S., von Hoff, K., Fruhwald, M.C., Gnekow, A., Fleischhack, G., Tippelt, S., Calaminus, G., Monoranu, C.M., Perry, A., Jones, C., Jacques, T.S., Radlwimmer, B., Gessi, M., Pietsch, T., Schramm, J., Schackert, G., Westphal, M., Reifenberger, G., Wesseling, P., Weller, M., Collins, V.P., Blumcke, I., Bendszus, M., Debus, J., Huang, A., Jabado, N., Northcott, P.A., Paulus, W., Gajjar, A., Robinson, G.W., Taylor, M.D., Jaunmuktane, Z., Ryzhova, M., Platten, M., Unterberg, A., Wick, W., Karajannis, M.A., Mittelbronn, M., Acker, T., Hartmann, C., Aldape, K., Schuller, U., Buslei, R., Lichter, P., Kool, M., Herold-Mende, C., Ellison, D.W., Hasselblatt, M., Snuderl, M., Brandner, S., Korshunov, A., von Deimling, A. and Pfister, S.M., *DNA methylation-based classification of central nervous system tumours.* Nature, 2018. **555**(7697): p. 469-474.
111. Zhou, Q., Lv, H., Mazloom, A.R., Xu, H., Ma'ayan, A. and Gallo, J.M., *Activation of alternate prosurvival pathways accounts for acquired sunitinib resistance in U87MG glioma xenografts.* J Pharmacol Exp Ther, 2012. **343**(2): p. 509-19.
112. Poulin, B., Sekiya, F. and Rhee, S.G., *Differential roles of the Src homology 2 domains of phospholipase C-gamma1 (PLC-gamma1) in platelet-derived growth factor-induced activation of PLC-gamma1 in intact cells.* J Biol Chem, 2000. **275**(9): p. 6411-6.
113. Poulin, B., Sekiya, F. and Rhee, S.G., *Intramolecular interaction between phosphorylated tyrosine-783 and the C-terminal Src homology 2 domain activates phospholipase C-gamma1.* Proc Natl Acad Sci U S A, 2005. **102**(12): p. 4276-81.
114. Nozawa, H., Howell, G., Suzuki, S., Zhang, Q., Qi, Y., Klein-Seetharaman, J., Wells, A., Grandis, J.R. and Thomas, S.M., *Combined inhibition of PLC{gamma}-1 and c-Src abrogates epidermal growth factor receptor-mediated head and neck squamous cell carcinoma invasion.* Clin Cancer Res, 2008. **14**(13): p. 4336-44.

115. Piccolo, E., Innominato, P.F., Mariggio, M.A., Maffucci, T., Iacobelli, S. and Falasca, M., *The mechanism involved in the regulation of phospholipase Cgamma1 activity in cell migration.* Oncogene, 2002. **21**(42): p. 6520-9.
116. Price, J.T., Tiganis, T., Agarwal, A., Djakiew, D. and Thompson, E.W., *Epidermal growth factor promotes MDA-MB-231 breast cancer cell migration through a phosphatidylinositol 3'-kinase and phospholipase C-dependent mechanism.* Cancer Res, 1999. **59**(21): p. 5475-8.
117. Khoshyomn, S., Penar, P.L., Rossi, J., Wells, A., Abramson, D.L. and Bhushan, A., *Inhibition of phospholipase C-gamma1 activation blocks glioma cell motility and invasion of fetal rat brain aggregates.* Neurosurgery, 1999. **44**(3): p. 568-77; discussion 577-8.
118. Zheng, Y., Yang, W., Aldape, K., He, J. and Lu, Z., *Epidermal growth factor (EGF)-enhanced vascular cell adhesion molecule-1 (VCAM-1) expression promotes macrophage and glioblastoma cell interaction and tumor cell invasion.* J Biol Chem, 2013. **288**(44): p. 31488-95.
119. Pedersen, P.H., Ness, G.O., Engebraaten, O., Bjerkvig, R., Lillehaug, J.R. and Laerum, O.D., *Heterogeneous response to the growth factors [EGF, PDGF (bb), TGF-alpha, bFGF, IL-2] on glioma spheroid growth, migration and invasion.* Int J Cancer, 1994. **56**(2): p. 255-61.
120. Weston, C.R. and Davis, R.J., *The JNK signal transduction pathway.* Curr Opin Genet Dev, 2002. **12**(1): p. 14-21.
121. Weiss, L., Whitmarsh, A.J., Yang, D.D., Rincon, M., Davis, R.J. and Flavell, R.A., *Regulation of c-Jun NH(2)-terminal kinase (Jnk) gene expression during T cell activation.* J Exp Med, 2000. **191**(1): p. 139-46.
122. Tournier, C., Hess, P., Yang, D.D., Xu, J., Turner, T.K., Nimnual, A., Bar-Sagi, D., Jones, S.N., Flavell, R.A. and Davis, R.J., *Requirement of JNK for stress-induced activation of the cytochrome c-mediated death pathway.* Science, 2000. **288**(5467): p. 870-4.
123. Davis, R.J., *Signal transduction by the JNK group of MAP kinases.* Cell, 2000. **103**(2): p. 239-52.
124. Ip, Y.T. and Davis, R.J., *Signal transduction by the c-Jun N-terminal kinase (JNK)--from inflammation to development.* Curr Opin Cell Biol, 1998. **10**(2): p. 205-19.
125. Pan, B., Yao, K.S., Monia, B.P., Dean, N.M., McKay, R.A., Hamilton, T.C. and O'Dwyer, P.J., *Reversal of cisplatin resistance in human ovarian cancer cell lines by a c-jun antisense oligodeoxynucleotide (ISIS 10582): evidence for the role of transcription factor overexpression in determining resistant phenotype.* Biochem Pharmacol, 2002. **63**(9): p. 1699-707.
126. Obey, T.B., Lyle, C.S. and Chambers, T.C., *Role of c-Jun in cellular sensitivity to the microtubule inhibitor vinblastine.* Biochem Biophys Res Commun, 2005. **335**(4): p. 1179-84.
127. Duan, L., Sterba, K., Kolomeichuk, S., Kim, H., Brown, P.H. and Chambers, T.C., *Inducible overexpression of c-Jun in MCF7 cells causes resistance to vinblastine via inhibition of drug-induced apoptosis and senescence at a step subsequent to mitotic arrest.* Biochem Pharmacol, 2007. **73**(4): p. 481-90.
128. Potapova, O., Gorospe, M., Dougherty, R.H., Dean, N.M., Gaarde, W.A. and Holbrook, N.J., *Inhibition of c-Jun N-terminal kinase 2 expression suppresses growth and induces apoptosis of human tumor cells in a p53-dependent manner.* Mol Cell Biol, 2000. **20**(5): p. 1713-22.
129. Bost, F., McKay, R., Bost, M., Potapova, O., Dean, N.M. and Mercola, D., *The Jun kinase 2 isoform is preferentially required for epidermal growth factor-induced*

transformation of human A549 lung carcinoma cells. Mol Cell Biol, 1999. **19**(3): p. 1938-49.
130. Potapova, O., Gorospe, M., Bost, F., Dean, N.M., Gaarde, W.A., Mercola, D. and Holbrook, N.J., *c-Jun N-terminal kinase is essential for growth of human T98G glioblastoma cells.* J Biol Chem, 2000. **275**(32): p. 24767-75.
131. Logan, S.K., Falasca, M., Hu, P. and Schlessinger, J., *Phosphatidylinositol 3-kinase mediates epidermal growth factor-induced activation of the c-Jun N-terminal kinase signaling pathway.* Mol Cell Biol, 1997. **17**(10): p. 5784-90.
132. Bost, F., McKay, R., Dean, N. and Mercola, D., *The JUN kinase/stress-activated protein kinase pathway is required for epidermal growth factor stimulation of growth of human A549 lung carcinoma cells.* J Biol Chem, 1997. **272**(52): p. 33422-9.
133. Teramoto, H., Crespo, P., Coso, O.A., Igishi, T., Xu, N. and Gutkind, J.S., *The small GTP-binding protein rho activates c-Jun N-terminal kinases/stress-activated protein kinases in human kidney 293T cells. Evidence for a Pak-independent signaling pathway.* J Biol Chem, 1996. **271**(42): p. 25731-4.
134. Zhou, S., Schuetz, J.D., Bunting, K.D., Colapietro, A.M., Sampath, J., Morris, J.J., Lagutina, I., Grosveld, G.C., Osawa, M., Nakauchi, H. and Sorrentino, B.P., *The ABC transporter Bcrp1/ABCG2 is expressed in a wide variety of stem cells and is a molecular determinant of the side-population phenotype.* Nat Med, 2001. **7**(9): p. 1028-34.
135. Spitzwieser, M., Pirker, C., Koblmuller, B., Pfeiler, G., Hacker, S., Berger, W., Heffeter, P. and Cichna-Markl, M., *Promoter methylation patterns of ABCB1, ABCC1 and ABCG2 in human cancer cell lines, multidrug-resistant cell models and tumor, tumor-adjacent and tumor-distant tissues from breast cancer patients.* Oncotarget, 2016.
136. Diestra, J.E., Scheffer, G.L., Catala, I., Maliepaard, M., Schellens, J.H., Scheper, R.J., Germa-Lluch, J.R. and Izquierdo, M.A., *Frequent expression of the multi-drug resistance-associated protein BCRP/MXR/ABCP/ABCG2 in human tumours detected by the BXP-21 monoclonal antibody in paraffin-embedded material.* J Pathol, 2002. **198**(2): p. 213-9.
137. Nakanishi, T. and Ross, D.D., *Breast cancer resistance protein (BCRP/ABCG2): its role in multidrug resistance and regulation of its gene expression.* Chin J Cancer, 2012. **31**(2): p. 73-99.
138. Tang, S.C., Lagas, J.S., Lankheet, N.A., Poller, B., Hillebrand, M.J., Rosing, H., Beijnen, J.H. and Schinkel, A.H., *Brain accumulation of sunitinib is restricted by P-glycoprotein (ABCB1) and breast cancer resistance protein (ABCG2) and can be enhanced by oral elacridar and sunitinib coadministration.* Int J Cancer, 2012. **130**(1): p. 223-33.
139. Dai, C.L., Liang, Y.J., Wang, Y.S., Tiwari, A.K., Yan, Y.Y., Wang, F., Chen, Z.S., Tong, X.Z. and Fu, L.W., *Sensitization of ABCG2-overexpressing cells to conventional chemotherapeutic agent by sunitinib was associated with inhibiting the function of ABCG2.* Cancer Lett, 2009. **279**(1): p. 74-83.
140. Shukla, S., Robey, R.W., Bates, S.E. and Ambudkar, S.V., *Sunitinib (Sutent, SU11248), a small-molecule receptor tyrosine kinase inhibitor, blocks function of the ATP-binding cassette (ABC) transporters P-glycoprotein (ABCB1) and ABCG2.* Drug Metab Dispos, 2009. **37**(2): p. 359-65.
141. Hu, S., Chen, Z., Franke, R., Orwick, S., Zhao, M., Rudek, M.A., Sparreboom, A. and Baker, S.D., *Interaction of the multikinase inhibitors sorafenib and sunitinib with solute carriers and ATP-binding cassette transporters.* Clin Cancer Res, 2009. **15**(19): p. 6062-9.
142. Kutikov, A., Makhov, P., Golovine, K., Canter, D.J., Sirohi, M., Street, R., Simhan, J., Uzzo, R.G. and Kolenko, V.M., *Interleukin-6: a potential biomarker of resistance to*

multitargeted receptor tyrosine kinase inhibitors in castration-resistant prostate cancer. Urology, 2011. **78**(4): p. 968 e7-11.
143. Bender, C. and Ullrich, A., *PRKX, TTBK2 and RSK4 expression causes Sunitinib resistance in kidney carcinoma- and melanoma-cell lines.* Int J Cancer, 2012. **131**(2): p. E45-55.
144. Yang, J., Ikezoe, T., Nishioka, C., Takezaki, Y., Hanazaki, K., Taguchi, T. and Yokoyama, A., *Long-term exposure of gastrointestinal stromal tumor cells to sunitinib induces epigenetic silencing of the PTEN gene.* Int J Cancer, 2012. **130**(4): p. 959-66.
145. Maher, E.A., Brennan, C., Wen, P.Y., Durso, L., Ligon, K.L., Richardson, A., Khatry, D., Feng, B., Sinha, R., Louis, D.N., Quackenbush, J., Black, P.M., Chin, L. and DePinho, R.A., *Marked genomic differences characterize primary and secondary glioblastoma subtypes and identify two distinct molecular and clinical secondary glioblastoma entities.* Cancer Res, 2006. **66**(23): p. 11502-13.
146. Kleihues, P. and Ohgaki, H., *Primary and secondary glioblastomas: from concept to clinical diagnosis.* Neuro Oncol, 1999. **1**(1): p. 44-51.
147. Joshi, A.D., Loilome, W., Siu, I.M., Tyler, B., Gallia, G.L. and Riggins, G.J., *Evaluation of tyrosine kinase inhibitor combinations for glioblastoma therapy.* PLoS One, 2012. **7**(10): p. e44372.

7 Appendix

7.1 List of Figures

7.2. List of Tables

7.3 List of Abbreviations

α-SMA	α-smooth muscle actin
ABCG2	ATP-binding cassette G2
BW	bodyweight
CRC	colorectal carcinoma
DiI	1,1′-dioctadecyl-3,3,3′,3′-tetramethylindocarbocyanine perchlorate
DMEM	Dulbecco's Modified Eagle's Medium
DMSO	dimethylsulfoxide
EBV	Epstein-Barr virus
EC	endothelial cell
EGF	epidermal growth factor
EGFR	epidermal growth factor receptor
EphB4^{OE}	EphB4-overexpressing tumors
EphB4^{OE}+Sun	EphB4-overexpressing tumors + Sunitinib
FBS	fetal bovine serum
FDA	Food and Drug Administration
FVD	functional vascular density
FITC-Dextran	fluorescein isothiocyanate - Dextran
G-418	geneticin
GBM	glioblastoma Multiforme
GPI	glycosylphosphatidylinositol
HEK	human embryonic kidney
HNSCC	head and neck squamous cell carcinoma
IDH	isocitrat-Dehydrogenase
JNKs	c-Jun NH(2)-terminal kinases
MGMT	O6-methylguanine DNA methyltransferase
MMP-2	matrix metalloproteinase 2
MoMuLV	Moloney murine leukemia virus
MoMuSV	Moloney murine sarcoma virus
MRI	magnetic resonance imaging
NOS	not other specified
OS	overall survival

PBS	phosphate-buffered saline
PCR	polymerase chain reaction p
PD	progressive disease
PDGF	platelet-derived growth factor
PFS	progression free survival
Phoenix-ECO	reporter cells
PI	perfusion index
PLC-γ1	phospholipase C - γ1
pLXSN	control tumors
pLXSN + Sun	control tumors + Sunitinib
p.o.	postoperative
PTEN	phosphatase and tensin homolog
Q_v	volumetrical blood flow
ROI	region of interest
RTK	receptor tyrosine kinase
SF126	human glioma cells
TMZ	Temozolomide
TUNEL	Terminal deoxynucleotidyl transferase dUTP nick end labeling
TVD	total vascular density
VD	vessel diameter
VEGF	vascular endothelial growth factor

8 Declaration of Authorship

Eidesstattliche Versicherung

„Ich, Christian Uhl, versichere an Eides statt durch meine eigenhändige Unterschrift, dass ich die vorgelegte Dissertation mit dem Thema „Die Rolle des ephrinB2-EphB4 Signalweges bei der Vermittlung vaskulärer Resistenzmechanismen unter antiangiogener Therapie“ selbstständig und ohne nicht offengelegte Hilfe Dritter verfasst und keine anderen als die angegebenen Quellen und Hilfsmittel genutzt habe.
Alle Stellen, die wörtlich oder dem Sinne nach auf Publikationen oder Vorträgen anderer Autoren beruhen, sind als solche in korrekter Zitierung kenntlich gemacht. Die Abschnitte zu Methodik (insbesondere praktische Arbeiten, Laborbestimmungen, statistische Aufarbeitung) und Resultaten (insbesondere Abbildungen, Graphiken und Tabellen werden von mir verantwortet.

Meine Anteile an etwaigen Publikationen zu dieser Dissertation entsprechen denen, die in der untenstehenden gemeinsamen Erklärung mit dem/der Betreuer/in, angegeben sind. Für sämtliche im Rahmen der Dissertation entstandenen Publikationen wurden die Richtlinien des ICMJE (International Committee of Medical Journal Editors; www.icmje.og) zur Autorenschaft eingehalten. Ich erkläre ferner, dass mir die Satzung der Charité – Universitätsmedizin Berlin zur Sicherung Guter Wissenschaftlicher Praxis bekannt ist und ich mich zur Einhaltung dieser Satzung verpflichte.

Die Bedeutung dieser eidesstattlichen Versicherung und die strafrechtlichen Folgen einer unwahren eidesstattlichen Versicherung (§156,161 des Strafgesetzbuches) sind mir bekannt und bewusst.“

Datum Unterschrift

Anteilserklärung an etwaigen erfolgten Publikationen

Christian Uhl hatte folgenden Anteil an den folgenden Publikationen:

Uhl, C., Markel, M., Broggini, T., Nieminen, M., Kremenetskaia, I., Vajkoczy, P. and Czabanka, M., *EphB4 mediates resistance to antiangiogenic therapy in experimental glioma.* Angiogenesis, 2018.

Herr Uhl führte im experimentellen Bereich der oben genannten Publikation alle Untersuchungen bezüglich der orthotopen Implantationen durch, sowie die anschließenden histologischen Untersuchungen und die statistische Auswertung der orthotopen Implantationen, ebenso wie die Experimente und die Auswertung der Daten der Schädelfensteroperationen. Darüber hinaus trug er maßgeblich zur schriftlichen Verfassung der Publikation bei. Die Experimente, die Datenauswertung und die Visualisierung der Figures 1B, C sowie 3 und 4 C, D, G, H, K, L wurden ausschließlich von Herrn Uhl angefertigt, ohne Inanspruchnahme der Hilfe weiterer Personen. Herr Uhl teilt sich die Erstautorenschaft der Publikation mit Herrn Dr. Moritz Markel.

_____

Unterschrift, Datum und Stempel des betreuenden Hochschullehrers/der betreuenden Hochschullehrerin

_____

Unterschrift des Doktoranden/der Doktorandin

9 Curriculum Vitae

Mein Lebenslauf wird aus datenschutzrechtlichen Gründen in der elektronischen Version meiner Arbeit nicht veröffentlicht.

10 Publications

Uhl, C., Markel, M., Broggini, T., Nieminen, M., Kremenetskaia, I., Vajkoczy, P. and Czabanka, M., *EphB4 mediates resistance to antiangiogenic therapy in experimental glioma.* Angiogenesis, 2018.

11 Acknowledgment

Hereby I would like to thank first and foremost my advisor PD Dr. Marcus Czabanka, who guided me through this whole journey, which took more than four years, with a lot of patience and a good sense of humor and who was always available, when I needed council. Subsequently I would like to thank my second advisor Prof. Dr. Vajkoczy, who gave me the possibility to work in his renowned laboratory for experimental research and who supported the publication of the work in an international peer-reviewed journal. Also my advisor in the laboratory, Thomas Broggini took big part in teaching me all the necessary techniques for this thesis, including orthotopic implantations, chronic cranial window operations, intravital microscopy, immunohistology and statistical evaluation.

I would also like to thank my friends and family, above all my parents, who always supported me and encouraged me to keep on going, especially at times, when it seemed, like this work would never come to an end.

And last, but by far not least, I would like to thank Oliver Kahn. Without his phrase “Weiter, immer weiter!” this thesis would not have been finished.